7

Continuous Wave Mode Locking for the Determination of the Acoustic Nonlinearity Parameter B/A

by
Jevon Raymond Davies

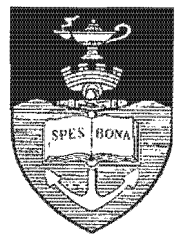

Thesis Presented for the Degree of
DOCTOR OF PHILOSOPHY
in the Department of Electrical Engineering
UNIVERSITY OF CAPE TOWN
September 2001

Declaration

This thesis is being submitted for the degree of Doctor of Philosophy in the Department of Electrical Engineering at the University of Cape Town. It has not been submitted before for any degree or examination at this or any other university. The author confirms that it is his own original work. Portions of the work have been published in condensed form in the journals of Ultrasonics and the Journal of the Acoustic Society of America. The author confirms in accordance with University rule GP7(3) that he was the primary researcher in all instances where work described in this thesis was published under joint authorship.

.....

J.R. Davies

30th September 2001

Acknowledgments

I would like to thank my advisors, Professor Jonathan Tapson and Professor Bruce Mortimer for their invaluable advice and guidance throughout this research work. I am also indebted to Professor John Bell for his discussions and insight into the behaviour of tube resonators and to Victor Balden for his help with finite element modelling. I must extend my thanks to Dr. Ian de Vries, Irshad Khan and Mr. S. Shrire for their many helpful and entertaining discussions, and finally my gratitude goes to my mother and Kerry for their constant encouragement throughout this study.

This work was supported financially by the Foundation for Research Development (F.R.D.) and the National Research Foundation (N.R.F.).

CONTINUOUS WAVE MODE LOCKING FOR THE DETERMINATION OF THE ACOUSTIC NONLINEARITY PARAMETER B/A

by

Jevon Raymond Davies

Submitted to the Department of Electrical Engineering
on April 29, 2002, in partial fulfillment of the
requirements for the degree of
Doctor of Philosophy

Abstract

The acoustic nonlinearity parameter B/A is a measure of the nonlinearity of the equation of state for a fluid. Its significance can be found in numerous fields including shockwaves, biochemistry and medicine. Recent studies in the field of biomedical ultrasound have necessitated a simple and accurate means of measuring B/A *in vitro*. Two novel techniques based on continuous wave mode locking are presented in this thesis as an alternative to existing pulsed techniques. Both techniques utilise the isentropic phase method of measuring the change in sound velocity accompanying a prescribed change in ambient pressure under constant entropy. The first technique was designed to use existing interferometer cavities to phase lock the driving and receiving transducers in quadrature. Any variation in sound velocity is interpreted by a change in lock-in frequency. This technique was used successfully in measuring four test liquids including two slow sound speed fluorocarbons. Results indicated good comparison with literature and achieved measurement uncertainty of less than 0.5%. An artefact of continuous wave measurement was observed with liquid modes locked adjacent to, or in the vicinity of a disc resonance. B/A values for these modes were inflated due to a frequency dependant phase contribution associated with coupled transducer-liquid systems. This phenomenon is described as frequency pulling. In an attempt to quantify this behaviour, a tube transducer was investigated, sealed at one end to form a cup. Through a wetting phenomenon, an unique acoustic resonant series was uncovered. This series appears undocumented in the literature and was carefully characterised using equivalent transmission line theory. As a result, a new 'acoustic' extension to Masons transmission line model is proposed, showing excellent agreement between simulation and measurement. Using this model, frequency pulling was unravelled and is explained, defining boundary conditions for which mode locking can be used. Building a cavity resonator for the cup transducer, a resonant locked loop was developed. The loop phase locks transducer current to voltage, ensuring the resonant trapping of radial modes inside the cavity. B/A was measured following isentropic constraints for the four test liquids. Results indicate good agreement with literature and previously measured values. We conclude that continuous wave measurement of B/A is a viable and accurate method for measuring B/A, and is simpler in implementation than similar pulsed systems.

Thesis Supervisor: Jonathan Tapson
Title: Professor of Electrical Engineering (University of Cape Town)

Thesis Supervisor: Bruce Mortimer
Title: Professor of Instrumentation Research (Cape Technikon)

Contents

Abbreviations and Symbols

Anglicised spelling has been used throughout this dissertation.

Abbreviations

c.w.	Continuous wave
F.A.M.	Finite amplitude method
TPL	Transmission phase locking
RPL	Resonant phase locking
PZT	Lead-Zirconate-Titanate
PRF	Pulse repetition frequency
CWPL	Continuous wave phase locking
VCO	Voltage controlled oscillator
Tx	Transmitter
Rx	Receiver
GPIB	Hewlett-Packard data bus (IEEE-488, HPIB)
BS	British standard
HP	Hewlett Packard
LED	light emitting diode
HPVEE	Hewlett-Packard visual programming language
DMA	Direct memory access
RTD	Resistance temperature detector
PLL	Phase locked loop
TPL	Transmission phase locking
RPL	Resonant phase locking
FM	Frequency Modulated

AGC	Automatic gain control
p.e.	Piezoelectric
FEM	Finite element methods
SNR	Signal to noise ratio

Symbols

L	Inductance
C	Capacitance
R	Resistance
κ	Bulk modulus
χ	Sheer viscosity
η	Compressional viscosity
x	Acoustic path length
S	Entropy
P	Pressure
c	Velocity
T	Temperature
ξ	Stiffness
γ	Compressibility
β	Coefficient of nonlinearity
u	Particle velocity
ψ	Condensation
l	Discontinuity distance
σ	Shock parameter
σ_g	Uncertainty in the gradient
g	Gradient
B/A	The nonlinearity parameter
ρ	Density
f_o	Static frequency
f_r	The fundamental resonant frequency of the piezoelectric transducer

θ, ϕ	Phase
RC	A resonant circuit consisting of a capacitor and resistor connected in series or parallel
f_{in}	Input frequency to a phase locked loop
f_{out}	Driving frequency from the output of the VCO
λ	wavelength
S_{12}	Transfer gain characteristic
I	Current
V	Voltage
Z	Impedance
ω	Frequency in radians
Q	Quality factor
K	Loop gain element
τ	Time constant
Φ	Transformer turns ratio
M	Equivalent mechanical mass
$\frac{1}{K}$	Equivalent mechanical compliance
Z_r	Mechanical Impedance
Z_o	Characteristic Impedance for a transmission line
X	Electrical Reactance (units ohms Ω)
Y	Electrical Admittance (units siemens)
k_{eff}	effective coupling coefficient
S	Susceptance (units siemens)
G	Conductance (units siemens)
N	Mode number
ξ	Displacement
Γ	Propagation coefficient
α	Attenuation coefficient
r	Inside radius of the cylinder
ϑ	Material stiffness
γ	Adiabatic compressibility
C_p	Specific heat capacity
k_t	Thermal conductivity
Q_t	Internal energy

Chapter 1

Introduction

"Would I had phrases that are not known, utterances that are strange, in new language that has not been used, free from repetition, not an utterance which has grown stale, which men of old have spoken"

Khakheperresenb, an Egyptian scribe (circa 2000 B.C.)

The development after World War 1 of the tuneable ultrasonic transducer made possible the production of high frequency sound on a practical basis [56]. This development provided a means of harnessing ultrasound for non-invasively examining objects, and has since provided numerous ultrasonic applications in both the biomedical and engineering fields. In fact, the use of ultrasound has become so diverse that its applications range from complex instruments such as scanning acoustic microscopes, to the well-known movement detectors found in most motor vehicle alarm systems.

Applied research in ultrasonics has generally based its understanding of acoustics on linear wave theory, more commonly referred to as 'infinitesimal wave theory' [13]. This branch of linear physics refers to the fact that the intensity of sound within a system is sufficiently low so as to consider the waves propagating within the system to have infinitesimal amplitude. This analogy has long been considered useful, and is acceptable in many low powered applications [62]. However, because of the inherent nonlinear nature of both the wave and state equations, several elastic wave phenomena exist that linear wave theory cannot describe [93]. These nonlinear phenomena can be found in numerous finite amplitude wave applications, exhibiting such properties as accelerated acoustic absorption, cavitation, streaming and the classical harmonic distortion typically associated with shock waves. Many of these effects have been observed in commercial ultrasonic instruments particularly within the medical and biomedical fields [86]

[23] [27]. With the development of high powered acoustic devices such as the EMAS (used in lithotriptors) [84], the issue of nonlinear acoustics has become an important aspect of understanding and managing nonlinear phenomena typically accompanying the presence of finite amplitude sound.

This growing need to understand the behaviour of finite amplitude waves, and the way in which they deviate from linear theory, has led to much research in the field of nonlinear acoustics [13]. An essential result of this has been the derivation of the nonlinearity parameter B/A. This parameter, initially described by Robert Beyer in 1960 [11], provides a distinct relationship between nonlinear sound propagation of finite amplitude waves, and linear wave theory. The coefficients A and B provide the necessary mechanical and thermodynamic information to the equation of state in order for a medium to be fully characterised. This information not only describes the nonlinear characteristics of the medium, but can also be used as a tool to investigate several properties of the medium [15] [5]. This concept has been the topic of much research particularly in the medical field where B/A has been used for anatomical diagnosis and subsequent investigation of pathology diagnosis [58] is being examined.

With the exception of ideal gasses and liquids, the ratio B/A has to be determined experimentally. Although several inventive techniques [13] have been developed over the years to determine B/A, there is no consensus as to an optimum method. It has been the effort of this study to review previous measurement techniques in order to identify aspects of instrumentation which merit improvement, and ultimately to introduce two unique methods for determining B/A based on *continuous wave phase locking*. It will be shown that a 'continuous wave platform' can be used as an effective alternative to pulsed systems, providing a simpler and more efficient means of measuring B/A in vitro.

1.1 Formulation of the Nonlinearity Parameter B/A

Before reviewing previous measurement systems, it is important to understand where the *nonlinearity parameter* B/A comes from, and how it relates to the nonlinear distortion found in finite amplitude waves. The following discussion provides simple insight into the origins of B/A and explains its function in characterising fluids. The nonlinear contribution that B/A makes to the equation of state is demonstrated together with the correlation between B/A and harmonic distortion.

The equation of state in its simplest form can be expressed as the thermodynamic relation-

ship between pressure, density and entropy [93]. This can be described as the following simple adiabatic relationship.

$$\frac{P}{P_0} = \left(\frac{\rho}{\rho_0}\right)^{\zeta} \tag{1.1}$$

with P defined as the instantaneous pressure, P_o the hydrostatic pressure (under zero velocity conditions), ρ the instantaneous density and ρ_0 the equilibrium density. The exponent ζ is a constant that depends on the nature of the medium. For ideal gasses it is simply equal to the ratio of specific heats C_p/C_v. This is however not true for liquids [12] and the equation must be modified by expanding $P = P(\rho, S)$ as a Taylor series for the isentropic case (where the entropy, S, is constant)

$$P = P_0 + (\rho - \rho_0)\left(\frac{\partial P}{\partial \rho}\right)_{S,\rho=\rho_0} + \frac{(\rho-\rho_0)^2}{2!}\left(\frac{\partial^2 P}{\partial \rho^2}\right)_{S,\rho=\rho_0} + \frac{(\rho-\rho_0)^3}{3!}\left(\frac{\partial^3 P}{\partial \rho^3}\right)_{S,\rho=\rho_0} + \cdots \tag{1.2}$$

The above expression can be rewritten with thermodynamic coefficients A, B and C as follows [11]:

$$P = P_0 + A\left(\frac{\rho-\rho_0}{\rho_0}\right) + \frac{B}{2!}\left(\frac{\rho-\rho_0}{\rho_0}\right)^2 + \frac{C}{3!}\left(\frac{\rho-\rho_0}{\rho_0}\right)^3 + \cdots \tag{1.3}$$

Additionally by defining the fractional change in density within the fluid as the *condensation* ψ or:

$$\psi = \frac{\rho-\rho_0}{\rho_0} \tag{1.4}$$

we obtain

$$P - P_0 = A\psi + \frac{B}{2!}\psi^2 + \frac{C}{3!}\psi^3 + \cdots \tag{1.5}$$

On inspection of the above derivation, it can be seen that the first derivative in equation 1.2 is simply the square of the infinitesimal sound velocity c_0 ($c_0 = \sqrt{\frac{\partial P}{\partial \rho}}$) and hence the coefficients

A, B and C of equation 1.5 may be expressed as follows:

$$A = \rho_0 \left(\frac{\partial P}{\partial \rho}\right)_S = \rho_0 c_0^2 \tag{1.6}$$

$$B = \rho_0^2 \left(\frac{\partial^2 P}{\partial \rho^2}\right)_S \tag{1.7}$$

$$C = \rho_0^3 \left(\frac{\partial^3 P}{\partial \rho^3}\right)_S \tag{1.8}$$

The physical significance of these constants (A, B, C etc.) can be seen if we apply linear wave theory, where the condensation is assumed to be infinitesimal. In this case, the higher order terms B and C quickly tend to zero defining a simple linear relationship between acoustic pressure $P - P_0$, density ρ and the velocity of sound c_0, thus defining a case where the propagation of the wave remains constant. If on the other hand we consider the effect of finite amplitude waves, the higher order terms B and C become increasingly more important, introducing a deviation from the local sound speed c_0 with increasing pressure. This can be seen from the following manipulation of equations 1.6 and 1.5 to obtain an expression for c^2

$$c^2 = \left(\frac{\partial P}{\partial \rho}\right)_S = \left(\frac{\partial P}{\partial \psi}\frac{\partial \psi}{\partial \rho}\right) = \frac{1}{\rho_0}\left(\frac{\partial P}{\partial \psi}\right) \tag{1.9}$$

$$If \quad \frac{\partial P}{\partial \psi} = A + B\psi + \frac{C\psi^2}{2} + \cdots \quad then \tag{1.10}$$

$$c^2 = c_0^2\left(1 + \frac{B\psi}{A} + \frac{C\psi^2}{2A} + \cdots\right) \tag{1.11}$$

From equation 1.11 it can be seen that the change in sound velocity within a liquid is a function of its nonlinearity ratios (B/A, C/A etc.) and the condensation; hence for liquids with large values for B/A, the local sound velocity will differ considerably from c_0 under increasing pressure. The parameter B/A is therefore simply the ratio of the quadratic term in the equation of state to the linear term, hence the definition of B/A as the *acoustic nonlinearity parameter* [11]. The higher order terms beyond the quadratic in equation 1.5 are typically truncated as their contribution is in most cases considered negligible[1].

[1]For the case of water at 20°C and excess pressure of 6 atmospheres; the relative size of the terms B and C to that of A is typically $6.75\text{x}10^{-4}$ and $4.56\text{x}10^{-7}$ respectively. (Beyer - Nonlinear Acoustics[13])

1.1.1 The Usefulness of B/A in Describing Fluids

Recent studies have shown that B/A may be used to describe several properties of fluids including thermodynamic [25], mechanical [37, pgs 2-9] and molecular information [82] [47], which have been used in several mixture laws to successfully determine biological tissue compositions [5].

By manipulating the coefficients A and B in equation 1.6 it is possible to extract both thermodynamic and mechanical relationships. In particular the ratio of B/A can be expressed as the change in sound velocity with hydrostatic pressure (under constant entropy) as follows:

$$\frac{B}{A} = \frac{\rho_0}{c_0^2}\left(\frac{\partial^2 P}{\partial \rho^2}\right)_{S,\rho=\rho_0} = \frac{\rho_0}{c_0^2}\left(\frac{\partial}{\partial \rho}\left[\frac{\partial P}{\partial \rho}\right]\right)_{S,\rho=\rho_0} \tag{1.12}$$

$$= \frac{\rho_0}{c_0^2}\left(\frac{\partial c^2}{\partial \rho}\right)_{S,\rho=\rho_0} = \left(\frac{2\rho_0}{c_0}\left[\frac{\partial c}{\partial \rho}\right]\right)_{S,\rho=\rho_0} \tag{1.13}$$

$$= 2\rho_0 c_0\left(\frac{\partial c}{\partial P}\right)_{S,\rho=\rho_0} \tag{1.14}$$

Equation 1.14 can then be rewritten in terms of its isobaric and isothermal components [95] namely:

$$\frac{B}{A} = 2\rho_0 c_0\left(\frac{\partial c}{\partial P}\right)_T + \frac{2T\varphi c_0}{C_p}\left(\frac{\partial c}{\partial T}\right)_P \tag{1.15}$$

where C_p is the specific heat at constant pressure, T is temperature and φ is the *isobaric volume coefficient of thermal expansion* of the medium $\varphi = \frac{1}{V}\left(\frac{\partial V}{\partial T}\right)_P$, with V as the volume. This equation is often used for evaluating B/A experimentally, by measuring the fractional change in phase velocity accompanying an isothermal change in pressure $\left[\frac{\Delta c}{\Delta P}\right]_T$ and isobaric change in temperature $\left[\frac{\Delta c}{\Delta T}\right]_P$. A drawback to this method (detailed in chapter 2) is the necessity for prior knowledge of both thermodynamic constants of specific heat and thermal expansion in order for B/A to be fully evaluated.

An example of the mechanical property of B/A can best be described in the expression that relates B/A to the compressibility or stiffness of a fluid undergoing an isentropic pressure change. This may be defined (see Eq A.3, Appendix 1) as

$$\frac{B}{A} = \left(\frac{\partial \vartheta}{\partial P}\right)_S - 1 \tag{1.16}$$

where $\vartheta = \frac{1}{\gamma}$ is known as the stiffness or reciprocal of the compressibility $\gamma = [\rho c^2]^{-1}$. This

equation infers that a material undergoing large changes of stiffness under an isentropic pressure change, will accordingly have a large value for B/A.

1.2 Harmonic Distortion of Finite Amplitude Waves

A direct consequences of nonlinear wave theory is the "steepening" or distortion associated with large amplitude waves as they propagate through a fluid. This harmonic distortion ultimately evolves into what is commonly recognised as a saw-tooth or shock wave. Various types of shock waves have been reported over the years, dating back to the early acoustic investigations of Poisson[94], Stokes[101] and Lord Rayleigh[103], but have not received the attention of a rigorous analysis. Although such analysis is beyond the scope of this study, it is intuitive to formulate the underlying relationship between B/A and the cause of harmonic distortion within plane waves. For this reason a brief description of nonlinear distortion is provided together with its relationship to B/A.

An axiom of linear wave theory is that the velocity of a planar wave remains constant i.e.

$$\frac{dx}{dt} = c \tag{1.17}$$

where x is the propagation displacement and t is the time of propagation. In addition, it is well known that the total wave velocity of a wave travelling in a moving medium is the vector sum of the velocity of the wave relative to the medium and the velocity of the medium relative to a fixed point. For a simple planar acoustic wave, the propagation velocity can thus be expressed as:

$$\frac{dx}{dt} = c + u \tag{1.18}$$

where u is the particle velocity of the wave. This expression obeys linear wave theory provided $u << c$; however a consequence of nonlinear acoustics is that this assumption is known to be incorrect and equation 1.11 is provided as a better approximation of c. This nonlinear relationship for c contributes to a more rigorous derivation, namely

$$\frac{dx}{dt} = c_0 + \beta u \tag{1.19}$$

where β is defined as the *coefficient of nonlinearity* and expressed as $\beta \simeq 1 + \frac{B}{2A}$. This relation-

ship describes the propagation velocity $\frac{dx}{dt}$ of the wave as a function of acoustic wave amplitude u. This dependence of propagation velocity on acoustic amplitude eventually results in the distortion of the waveform. A simple demonstration of this fact was well described by Earnshaw [32] [12] .in his solution of a harmonic wave with the boundary condition $u(0,t) = u_0 \sin(\omega t)$ propagating in the x direction. The rate of propagation of the wave can be expressed as a function of particle velocity, with the general form :

$$u(x,t) = u_0 \sin[\omega t - \frac{\omega x}{c_0}(\beta \frac{u}{c_o})^{-\frac{2A}{B}-1}] \tag{1.20}$$

A plot of this solution as a function of x, for specific values of u, (see Fig 1-1) demonstrates how particles of higher acoustic amplitude travel at faster particle velocities, thereby increasing the distortion of the original wave with distance. It should be noted that Earnshaw's solution is only valid for the interval leading up to the shock. Beyond this point the acoustic wave literally falls over itself thereby inducing the well known 'N' wave associated with the formulation of shock fronts. The derivative of solution 1.20 with respect to x and evaluated at u=0 results in

$$\frac{\partial u}{\partial x} = \frac{\frac{-w}{c_0}}{\frac{1}{u_0} - \frac{wx}{c_0^2}\beta} \tag{1.21}$$

This equation defines the point at which $\frac{\partial u}{\partial x}$ becomes increasingly negative with increasing x, resulting in a distance l at which the waveform becomes negatively infinite. This point, which is the distance at which a shock wave is formed is known as the *discontinuity distance* [13] and is defined for the ideal case of zero viscosity as follows:

$$l = \frac{c_0^2}{\beta w u_0} \tag{1.22}$$

The discontinuity distance l is often represented by the reduced distance σ known as the shock parameter, given by :

$$\sigma = \frac{x}{l} \tag{1.23}$$

The detailed formulation of the explicit solution to equation 1.20 is beyond the scope of this study, notwithstanding that a brief description is given for completeness. The solution to the Earnshaw equation can be attributed to the individual efforts of Fubini [41], Fay [40] and Blackstock [16].

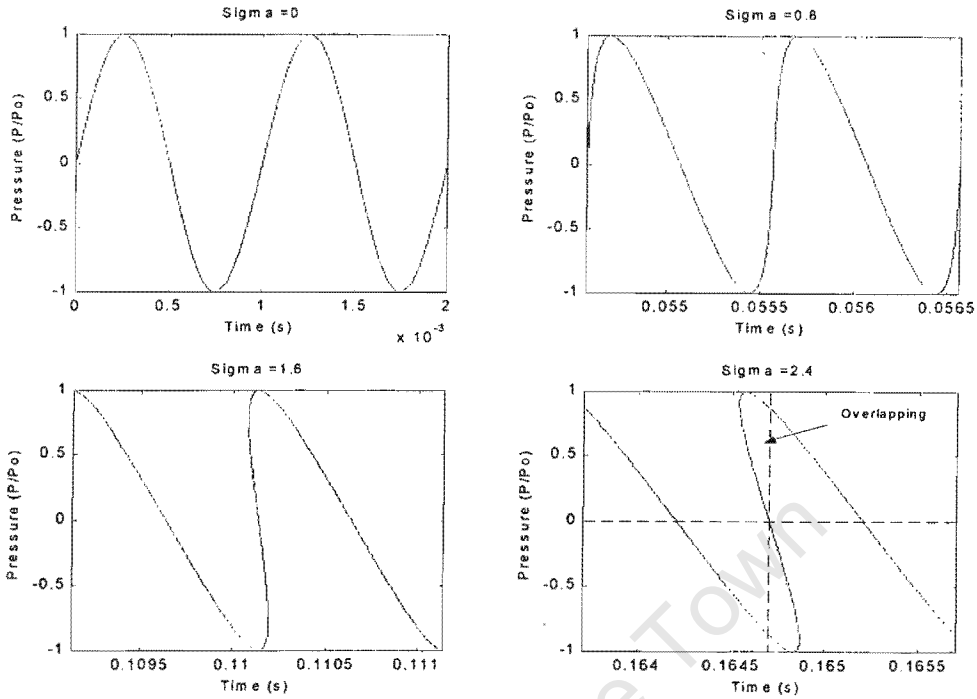

Figure 1-1: A demonstration of the distortion of a sinusoid wave with time. Particles of higher acoustic pressure have faster particle velocities, causing the wave to become increasingly distorted. Notice the deviation of Earnshaw's solution past σ =1, developing into an invalid pressure front at $\sigma = 2.4$ with distinct 'overlapping'.

Fubini's solution (specifically for the region $\sigma \leq 1$) is obtained by expanding equation 1.20 in terms of the Fourier series :

$$\frac{u}{u_0} = 2\sum_{n=1}^{\infty} \frac{J_n(\frac{nx}{l})}{\frac{nx}{l}} \sin n(wt - kx) \tag{1.24}$$

where J_n is a Bessel function of the order n.

Fay on the other hand developed a solution based on the nearly stable periodic shock wave (the region $\sigma \geq 3$) in a viscous perfect liquid [40], with the following Fourier series :

$$\frac{u}{u_0} = \sum_{n=1}^{\infty} \frac{\frac{2}{\Gamma}}{\sinh(n\frac{1+\sigma}{\Gamma})} \sin n(wt - kx) \tag{1.25}$$

where Γ defines a group of constants characterizing the importance of the nonlinearity relative to that of dissipation. This however still left the region $3 > \sigma > 1$ which was eventually solved by Blackstock [16] using a bridging of the Fubini-Fay functions. The solution provided

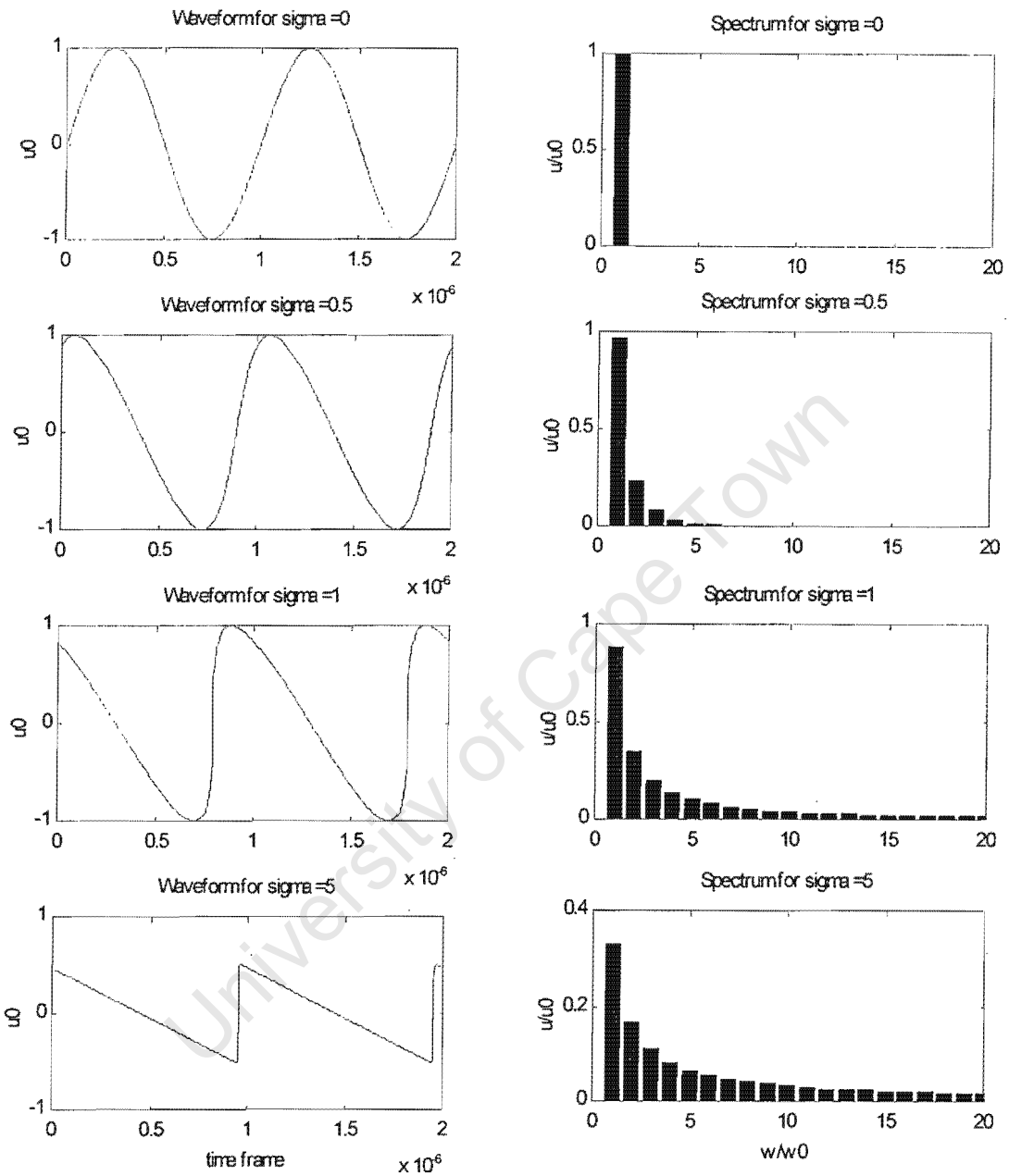

Figure 1-2: A simulation of the Blackstock bridging function for a 1Mhz sinusoid waveform travelling through water (B/A=5). It can be seen that the waveform develops a shock front at $\sigma = 1$, at which point the waveform becomes discontinuous with a notable increase in amplitude of higher order spectral components. At $\sigma = 5$, the absorption and dispersion of these components causes an attenuation in amplitude of the shock wave.

by Blackstock can be seen as the harmonic transition from equation 1.24 to equation 1.25. This solution was used to generate the waveforms in Fig 1-2 and their corresponding frequency spectra.

1.3 Purpose and Scope

Measuring the nonlinearity parameter *in vitro* has previously been an involved and arduous experimental process, often requiring complex electronic instrumentation coupled with difficult time of flight calculations. Such techniques have used pulsed time of flight systems to measure B/A, by determining the fractional change in phase velocity with pressure. It is an objective of this study to develop a continuous wave (c.w.) lock-in system using a simple and accurate alternative method for measuring the B/A of any liquid [29]. Furthermore, to accommodate small sample volume liquids such as biological preparations, a novel acoustic cell was engineered which deviates from traditional double disk interferometry.

A review of previous experimental methods is given in Chapter 2. Each method is described and analysed in terms of its complexity, accuracy and usefulness in measuring B/A. As a consequence of this survey, several aspects of instrumentation are identified and discussed, laying a foundation for the design and development of a simple isentropic measurement system.

Chapter 3 debates the pros and cons of existing time-of-flight systems with that of c.w. systems. An overview of individual techniques is summarised together with the difficulties and inaccuracies associated with each technique. The need for an alternative mode locking solution is argued, comparing previously used control instrumentation with the novel technology proposed in this study, and showing the inherent application of phase locking to B/A measurement

The sample cell, designed in Chapter 5, was based on a double-disk interferometer and used as a generic investigative tool for exploring and identifying problems associated with B/A interferometry. The concept of phase locking was implemented as a lock-in approach to measuring deviations in phase velocity [28]. The scope of this initial investigation covers several aspects of isentropic phase measurement including aspects of disk nonlinearities, pressure variations, and the importance of temperature control, leading to the design of a small volume interferometer.

An outcome of the initial interferometer experimentation was the need for a compound resonant cavity. At first, the double disk interferometer was used as a dual disk resonant

cavity, driving both transducers at the same time and phase locking current to voltage. Once again this technique worked adequately to determine fractional changes in phase velocity; however differences in transducer characteristics introduced unwanted effects. For this reason the classical double disk interferometer was abandoned for a single transducer resonator.

An investigation of PZT (Lead-Zirconate-Titanate) tubes lead to the uncovering of a set of loosely coupled acoustic modes which occur as a result of cylindrical modes forming within the liquid cylinder. This discovery led to an extensive investigation of these modes using equivalent transmission lines and finite element analysis to provide a coupled circuit analogue. Using this model, a new acoustic cell was designed and developed for the measurement of B/A.

This single element cell was used, together with several new lock-in techniques, to measure the nonlinearity parameter of different fluids. The range of lock-in methods explored were limited to transmission and resonant phase locking with each method described in detail and evaluated in terms of its ability to measure B/A accurately. The extent of this work was to provide the experimentalists with an opportunity to use c.w. phase locking in existing interferometers; or, to adopt the new single element resonant cavity and implement resonant phase locking.

Chapter 2

A Review of Empirical Methods used in Determining B/A

Numerous experimental techniques for measuring B/A are described in the literature [22] [49] [44] [38] [71, pg 38-79], several of which follow directly from the fundamental definition of B/A (as explained in Chapter 1). This chapter serves as a review of these 'direct' methods viz. the *thermodynamic* and *isentropic phase* methods, together with various indirect approaches for determining B/A. The indirect methods base their evaluation of B/A on the harmonic distortion of finite amplitude waves. Such methods use resourceful techniques such as *finite amplitude absorption* and *optical diffraction* as a means of measuring harmonic growth (Fig 1-2, chapter 1) typically found in finite amplitude waves. Each method is described with emphasis placed on the simplicity in implementation coupled with its accuracy in determining B/A. A comparison of methods shows the isentropic phase method as the most suitable for measuring B/A *in vitro*, providing an ideal platform on which to base continuous wave technology.

2.1 Indirect Methods

2.1.1 Finite Amplitude Absorption

The Finite Amplitude Method (F.A.M.) for measuring the parameter B/A involves the measurement of the second harmonic, which is generated as a result of a purely sinusoidal wave distorting under large acoustic amplitudes. A qualitative description of this distortion is given in Chapter 1. This method relies on the ability of the experimental determination of the second harmonic to be used as an indication of B/A by comparing theory with experiment [22]. It can

be shown that the acoustic pressure amplitude of the second harmonic is proportional to the nonlinearity parameter B/A, as follows

$$P_2(x) = P_1^2(0)\frac{\pi f x\left(\frac{B}{A}+2\right)}{2\rho_0 c_0^3} Diff(x) e^{(\alpha_1+\frac{\alpha_2}{2})x} \tag{2.1}$$

where $Diff(x)$ is a diffraction correction function [110, pgs 24-27] [71, pgs 32-37] [87] determined for specific transducer geometries and $P_1(0)$ is the acoustic pressure output from the transmitter at the driving frequency. The subscripts 1 and 2 refer to the fundamental and second harmonics respectively, whilst α refers to the attenuation coefficients at each frequency f, and x is the acoustic pathlength. This equation only holds true under the following conditions:

- Energy cannot be transferred from any harmonic component to other higher order harmonics.
- The medium under examination must have a near linear frequency dependence of absorption i.e. $\alpha_1 \simeq 2\alpha_2$.
- The diffraction correction function should be an exact model for the particular experiment.
- The loss mechanism for the medium must be fully characterised.

By using plane-wave theory, both thermal [67] and piezoelectric sensors [96] have been used successfully in measuring the amplitude of the second harmonic as a function of its distance from the radiating source. In terms of providing an accurate value for B/A however, the F.A.M, is beset with disadvantages. These are listed as follows:

1. The theory used for extracting B/A from experimental data must be an exact model of the experiment used. This is often not the case, as pointed out by W. Cobb[22]. He argues that Fubini's solution relies on a nondissipative plane wave, which cannot be accurately reproduced experimentally. Many experiments rely on piezoelectric transducers as 'piston' transmitters and receivers, but it is well-known[87] that because of diffraction, these ultrasonic transducers cannot be modelled as plane wave sources even in the near field. Consequently the accuracy of the F.A.M. is determined largely by the accuracy of $Diff(z)$.
2. A major disadvantage of this technique is the fact that Fubini's solution[41] is presented for the non-dissipative wave, which does not provide for small signal attenuation. This

means that unless the loss mechanism is fully characterised, the finite amplitude method cannot be used with highly attenuating liquid sources.

3. Finally the problem of measuring the second harmonic is both difficult and complicated since it has to be separated from spurious harmonics typically generated by the source transducer. Furthermore, a wide bandwidth detector is a necessity for this measurement technique since any attenuation due to the bandwidth of the detector could distort harmonic amplitude measurements.

For these reasons the F.A.M. has relatively inferior results for measuring B/A, with a typical inaccuracy of 5% or more for fluids[112].

Alternatively, the F.A.M. is advantageous in the fact that measurements can be performed *in vivo* using only a small quantity of the sample material. Large pressure and temperature variations are not required, nor is there a need for isothermal conditions as specified by other thermodynamic methods. Notwithstanding this, the F.A.M.'s inadequacy in establishing an accurate value for B/A without the detailed modelling of acoustic wave propagation and interaction, render this method ineffective as a useful measurement tool in most applications.

2.1.2 Optical Diffraction

The theory of optical diffraction by sound waves has a rich history and is well known in literature [56]. The diffraction phenomenon is often employed to visualise the propagation of a wave in a liquid by using the "schlieren" or striation method discussed by Toepler in 1866 [48]. This method uses a coherent light source, which is sent normal to the propagating vector of the ultrasonic wave. The resulting diffraction pattern caused by the phase grating in the liquid in response to the sound pressure field is related to the wave profile.

Early researchers employing this method often noted a slight asymmetry between the intensity of the positive and negative diffraction order [97]. This was ignored and it was suggested that the second harmonic signal was present in the source. Twenty years later Hiedemann et al [49] suggested that the asymmetry lay in the presence of a distortion of the medium, and thus finite amplitude distortion was first characterised. Experimentally it has been shown that the light intensity in any diffraction order can be related to B/A. This is done by averaging continuous measurements of light intensity as a function of sound amplitude, and relating the derived data to theory to obtain the quantity B/A. A typical example of characterising light intensity as a function of sound amplitude is shown in Fig. 2-1.

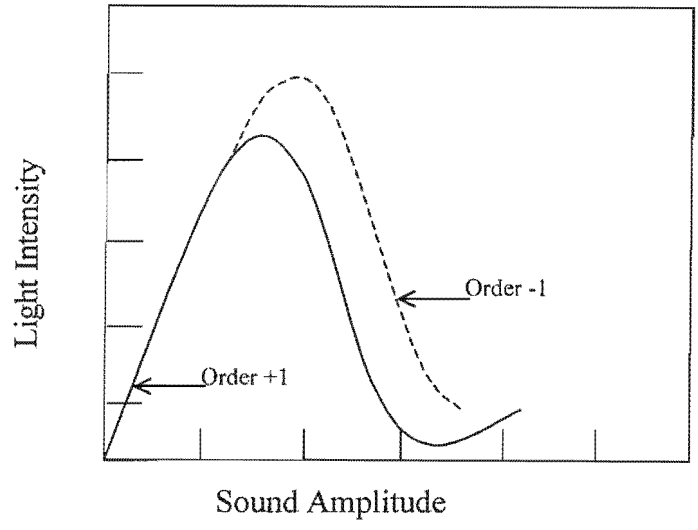

Figure 2-1: A demonstration of light intensity as a function of sound amplitude for diffraction orders +1 and -1 in an arbitrary liquid. On observation it can be seen that the intensity is not symmetric with the zeroeth order. This phenomenon, is a direct result of the distortion associated with finite amplitude waves, and is shown to vary with distance from the sound source.

It is obvious from Fig. 2-1, that the positive and negative diffraction orders are not symmetric with the zeroeth order, clarifying the expected consequences of the distortion of the wave profile. Heidemann and Zankel [49] resolved the theoretical problem of finding diffraction intensity data for all orders with one B/A value by resolving the distorted wave in terms of its Fourier components. The diffraction effect of each of these components is then combined to obtain the total result. Using this theory, the experimentalist has to obtain a value for all diffraction orders to generate a reliable quantity for B/A.

The Optical Diffraction Method is significantly more accurate than the F.A.M. A comparison done by Kashkooli *et al* [60] quotes "an internal consistency of 8% for the Finite Amplitude Method and 4% for the Optical Diffraction Method". The reason for this difference can be attributed to the optical method making use of all the diffraction orders present in the distorted wave, as opposed to using just a single second harmonic, as is the case with the F.A.M.

The optical diffraction method however is far more complicated in both the range of technologies employed, and the experimental alignment requirements, resulting in the following fundamental problems :

1. The optical method is limited to transparent liquids; consequently liquids such as biological fluids and commercially important polymers and gels are impossible to characterise.

2. Igneto and Cook [57] have shown that by changing the shape of the transducers (from circular to square) a better result is obtained for B/A. An explanation for this can be attributed to diffraction effects similar to that found in the Finite Amplitude Method, but this still remains to be proved.

2.2 Direct Methods

2.2.1 Thermodynamic Method

Coppens *et al* [25] developed the thermodynamic method as an experimental procedure for measuring B/A of several liquids *in vitro*. The method is simply a direct application of the definition of B/A previously described by equation 1.15. Specifically, if the sound velocity is a function of pressure amplitude, it follows directly that an isentropic pressure variation will induce a change in sound velocity directly proportionate to the nonlinearity parameter of the medium. Therefore, careful measurement of the change in sound velocity with pressure should be sufficient to determine B/A, provided the measurement procedure remains isentropic. In order to avoid the difficulties associated with isentropic measurements, Coppens adopted a technique proposed by Rudnick [95], which permits B/A to be expressed as the sum of two thermodynamic terms namely:

$$\frac{B'}{A} = 2\rho_0 c_0 \left(\frac{\partial c}{\partial P}\right)_T \tag{2.2}$$

and

$$\frac{B''}{A} = \frac{2T\varphi c_0}{C_p} \left(\frac{\partial c}{\partial T}\right)_P \tag{2.3}$$

where B/A is expressed in the form :

$$\frac{B}{A} = \frac{B'}{A} + \frac{B''}{A} \tag{2.4}$$

From this analysis, Rudnick suggests that $\frac{B'}{A}$ is the isothermal increase in phase velocity brought about by a change in pressure, whilst $\frac{B''}{A}$ provides the isobaric increase in phase velocity caused by a change in temperature. It should be noted that $\frac{B''}{A}$ is in most cases only 5% as large as

$\frac{B'}{A}$ and is often neglected[1] in thermodynamic measurements of B/A [73].

The thermodynamic method provides an easier approach for measuring B/A in comparison with the F.A.M., where transducer characteristics and complex theoretical models are required. B/A is determined primarily by the change in sound velocity associated with changes in pressure and temperature. Since temperature and pressure are relatively simple quantities to measure, the measurement accuracy of B/A relies primarily on the ability of the experimentalist to provide accurate sound velocity information.

Techniques for measuring the velocity of sound are widely available and accuracies of less than 0.001m/s [30] have been reported. Based on these measurements it should be possible to measure B/A with an error of less than 1%.

The foremost disadvantage of the thermodynamic method is the fact that large pressure (10000 kg/cm^2) and temperature changes (0 - 80°C) are necessary [46] to resolve the term $\frac{B'}{A}$ and $\frac{B''}{A}$ in order to obtain an accurate measure of B/A. These large fluctuations have often resulted in irreversible damage to the sample fluid [23] particularly in biological preparations. Secondly, it is often difficult to measure the thermodynamic constants of specific heat and volume expansibility within small volume biological preparations. These additional measurements often introduce measurement uncertainties which add to the inaccuracy of the overall B/A measurement. It is for this reason that measurements of B/A using the thermodynamic method have only achieved accuracies of around 3% [112].

The thermodynamic method provides a simple alternative to the F.A.M.; however its inability to resolve B/A using small pressure and temperature changes, coupled with the prerequisite of accurate values for thermodynamic constants, makes this method difficult to adopt as a generic approach for measuring B/A in liquids.

2.2.2 Isentropic Phase Method

The isentropic phase method is a derivative of the thermodynamic technique. It is the direct application of equation 1.14, eliminating the need for thermodynamic liquid properties. B/A is typically determined using pulsed interferometry to measure the change in phase velocity associated with a stepped adiabatic change in pressure (pressure jump) [63] [51] through the

[1]The term 'isentropic' refers to a process of equal entropy. Such a process is said to be thermodynamically reversible, implying no increase to the overall entropy of the system. The second term in equation 2.4 exclusively accounts for such a change in entropy[95], and varies greatly with different sample liquids. Neglecting this term greatly affects the accuracy with which B/A can be measured.

relation

$$\frac{B}{A} \approx 2\rho_0 c_0 \left[\frac{\Delta c}{\Delta p}\right]_{S_q} \tag{2.5}$$

where Δp is a pre-determined pressure jump and S_q refers to a quasi-isentropic system. Since it is impractical to accomplish theoretically isentropic conditions, the so-called isentropic method relies exclusively on two features to allow it to claim quasi-isentropic stability:

- The first is the fact that the predetermined pressure jump occurs within a small time frame (typically 5 seconds). This is usually done through electronic automation, whereby many independent measurements can be carried out within the small time frame. This ensures that any additional entropy engendered can be assumed to be negligible within the time frame in question (see Appendix: A) .

- The second feature is *isothermal stability*: It is critical to keep the sample and its surroundings in an isothermal environment, since any additional fluctuation in temperature will result in a more pronounced fluctuation in phase velocity. To achieve this in practice, it is common to place the sample in a temperature-controlled bath with temperature fluctuations of less than 0.01°C.

This technique, which is relatively new to the field of nonlinear measurements, has produced outstanding results with reported accuracies of 1% and less [38] [111]. The difficulty in using this measurement technique is that meticulous attention must be applied to ensure minimal change in entropy. This measurement technique provides a uniquely simple approach for determining B/A and is often accomplished with overpressures of less than 200KPa.

2.3 Conclusions

A survey of existing B/A measurement methods clearly shows two trends in determining the nonlinearity parameter of a medium. If the medium under investigation is to be measured *in vivo*, the indirect methods are more suitable, since no external pressure and temperature variations of the sample medium are required for the measurement. However, for small volume sample liquids, B/A is usually measured using one of the indirect thermodynamic approaches. The isentropic phase method is generally preferred over the thermodynamic method since the prerequisite knowledge of thermodynamic constants are not required. This method has the

additional advantage of providing accurate sound velocity data using only small changes in ambient pressure. This makes the isentropic phase method ideal for measuring sensitive biological samples, where such changes could cause irreversible damage. On reviewing these methods it is evident that the isentropic phase method lends itself as a generic approach to measuring the nonlinearity parameter of liquids *in vitro*. Since it is the ambition of this study to provide a generic solution to measuring B/A *in vitro*, the isentropic phase method was adopted as the foundation on which continuous wave mode locking shall be developed.

Chapter 3

A New Approach to B/A Measurement

The success of measuring B/A isentropically is principally determined by the ability with which a fractional change in sound velocity can be measured on a real time basis.

Several methods exist for determining the velocity of sound in a liquid. The more common approaches employ pulsed systems utilising the concept of 'time of flight'. Reviewing these methods it is apparent that although the time of flight approach is accurate for measuring absolute sound velocity, it falls short in determining fractional changes in sound velocity. Therefore pulsed systems have used phase measurement and locking (over existing time of flight techniques) as an alternative for measuring B/A isentropically. In this chapter we conduct a survey of two such methods which have shown a remarkable improvement in B/A measurement with accuracies in differential velocimetry of typically 1 part in 10^7 being reported. Closer inspection however reveals aspects of phase nonlinearities inherent in both systems. These nonlinear phase contributions manifest themselves as a function of frequency, causing seemingly stable measurements of B/A to be incorrect. Such phase contributions are shown to be a nonlinear function of the pulse envelope and amplitude.

As an alternative to pulsed systems we present a new approach to B/A based on a continuous wave method. This technique applies traditional aspects of phase locking to continuous wave interferometry, removing the phase nonlinearities and complex electronic instrumentation typically associated with pulsed systems.

3.1 'Time of Flight' Velocimetry and Traditional Pulsed Systems

The earliest recorded measure of the velocity of sound in a liquid was made by J. Colladon at Lake Geneva in 1826 [24]. Colladon recorded the time taken for an acoustic pulse (a bell) to traverse a section of liquid (two points on Lake Geneva). He then calculated the sound velocity c using the well known formula $c = \frac{s}{t}$, where s is displacement and t is time, to obtain a value of 1435 m/s for water[1] at 8°C. Since 1826, the velocimetry field has grown to include many diverse methodologies; however Colladon's underlying principle of calculating a 'time of flight' still remains popular in literature today. A typical implementation of such a system usually involves an acoustic cell as described by Pethrick [91] [34], where one or two piezoelectric discs are coupled to a fluid which is under investigation. A single sinusoidal pulse is applied to a piezoelectric transducer which then converts electrical to mechanical energy and launches the pulse into the liquid. The pulse, after traversing the column of liquid, is normally received by a second transducer which conversely transforms the acoustical energy into electrical energy. In order for the velocity of sound in the liquid to be calculated precisely, both the path length and the time of flight of the pulse need to be measured with suitable accuracy. Today it is relatively easy to measure a fixed path length to within 1 part in 10^6 using laser interferometry [42]. The problem however remains in precisely determining the time of flight of the travelling acoustic pulse. The reason for this has been the discussion of many journal papers and can be explained as follows:-

A single pulse applied to a column of liquid does not have a simple harmonic frequency spectrum because the square envelope of the pulse is effectively an amplitude modulation of the carrier frequency. This concept is well known in the field of telecommunications [102], with the combined Fourier spectrum being a simple addition of both the modulation (the square pulse) and carrier frequency components. The problem with launching this combined frequency spectrum into a liquid medium, is that the liquid acts as an acoustic filter [77] attributed mainly to the absorption and dispersion of the medium. It is well known that the attenuation coefficient of a liquid is frequency dependent [77], resulting in most cases with the rate of attenuation of high frequencies being greater than that of low frequencies. This 'low pass' filter characteristic [13] [83] can best be described by the equivalent circuit [77] shown in

[1]The present accepted value for the velocity of sound in pure water at 8°C is given by Del Grosso[30] as 1439.132m/s.

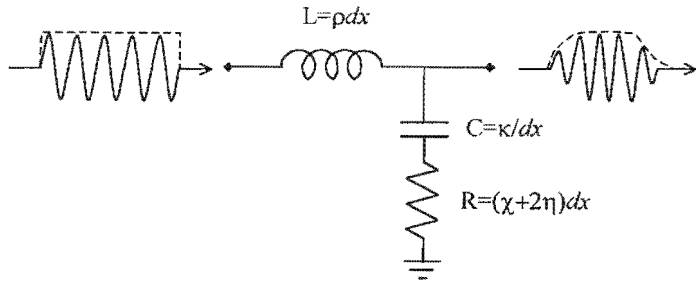

Figure 3-1: An equivalent 'transmission line' circuit [77] for an adiabatic liquid. The series branch is an inductance 'L', determined by the density 'ρ', of the liquid, whilst the shunt branch is a capacitance 'C', defining bulk modulus, 'κ', in series with a resistance 'R', composed from shear viscosity 'χ', and compressional viscosity 'η'. The LC reactive components indicate a low pass filter attenuating the higher frequency components of the input pulse as a function of distance 'dx'

Fig 3-1.

For a pulse propagating in a liquid medium, the distortion of the envelope will be both a function of the liquid properties and the acoustic path length. For the received pulse, the distortion of the envelope introduces an uncertainty in the measurement of time of flight principally caused by an uncertainty in the envelope threshold. This 'threshold ambiguity' is translated into an uncertainty [111] in sound velocity.

This topic has been the cause for much debate [107, pp 81-105] in the literature, offering several interesting solutions. A review of the more popular time of flight methods are described in abbreviated form below:

- *Pulse Superposition Method*

  This technique uses a single transmitter-receiver transducer pair. The pulse repetition frequency (P.R.F.) of the transmitter is adjusted so that the time between pulses is equal to an integer multiple of the round trip transit time. This causes an integer number of pulses to be present within the sample at any time. If the P.R.F. is critically adjusted so that successive echoes are superposed, the round trip transit time can be established. This method adopts superposition as a way of avoiding threshold uncertainties and has achieved claims of a typical accuracy of 0.006% [79] for absolute velocity measurement.

- *Pulse Echo Overlap Method*

  The echo overlap technique uses the same analogy as the superposition method, however no superposition of the waveforms occurs within the sample vessel. Only a single pulse

is present in the sample fluid at any time. An oscilloscope is triggered using the audio carrier frequency of the pulse. The frequency is adjusted so that the sweep time is an integer multiple of the round trip transit time. The P.R.F. is typically generated by the same carrier frequency using a divide by 1000 circuit. By critically adjusting the carrier frequency it is possible to superpose any two echoes on the oscilloscope screen. Once this is done, the carrier frequency determines the time of flight [90] [88].

- *Sing-Around System*

  The sing-around method uses the received pulse to retrigger the transmitter. This causes the P.R.F to be periodic with a frequency equal to the reciprocal of the time of flight. The problem with this self-oscillator type setup is that the electronics used in regenerating the signal add time delays, which are additive to the overall time of flight. Accuracy in determining phase velocity is typically 0.01% [19] [45].

Although many of the techniques described above provide sufficient accuracy for absolute measurement of sound velocity, most lack the extreme sensitivity necessary for accurate B/A measurement. Such a system is concerned primarily with the determination of a small change in phase velocity associated with pressure or temperature variations. This change in phase velocity is typically of the order of 1.7×10^{-6}m/s/Pa for pure water at 30°C, meaning that a pressure change of 1 atmosphere would result in a velocity change of 0.17 m/s. In order to resolve B/A to within 1%, it is necessary to be able to measure a fractional change in sound speed of 0.001 m/s. This requires a system capable of resolving a differential change in sound velocity of typically 1 part in 10^7 [38].

The requirement to measure fractional changes in phase velocity can be achieved with time of flight, using autocorrelation techniques [111], but a more commonly employed method is pulse phase-comparison [112] and pulse phase-locking [37, pgs 89-92] [109] from which estimates of sensitivity are reported to be of the order of parts in 10^8.

3.2 B/A Measurement Using Phase Methods

In order to accomplish real-time velocity information, pulsed systems have implemented the technique of phase-locking [109] [42] as a means of accurately maintaining an integer number of pulses within a sample vessel. Such systems have been effectively employed in both elasticity and spectrometry calculations. The principle idea behind pulsed phase locking is to adjust

the drive frequency so as to maintain quadrature between the received signal and a comparison signal derived from the drive oscillator. In a liquid filled interferometer the loop becomes locked once quadrature conditions are met, with any variation in phase velocity or path length tracked precisely by a change in oscillator frequency.

The technique of phase measurement [7] and its counterpart phase locking, have been adapted by several investigators for measuring B/A using both thermodynamic and isentropic phase methods. A comparison between the measured results of both methods show that B/A can be determined with a resolution of ±3% for direct phase measurement [112] and less than 1% for phase locked measurement [38]. This improvement in accuracy is a direct consequence of the inherent noise rejection and phase sensitivity accompanying the flywheel action of a phase locked loop.

A review of two such isentropic-phase methods in the following section, identifies uncertainties relating to each technique and phase measurement in general. The topic of frequency dependent phase variations, arising from extraneous sources and electronic instrumentation, is investigated alongside prescribed solutions.

3.2.1 Pulsed Phase Measurement

Zhu [112] and Gong *et al* [44] describe a method of measuring B/A by relating phase information between the driving and receiving pulses, to that of sound velocity. For a prescribed change in pressure, the measured phase is a linear function of B/A. Fig 3-2 shows a block diagram of this technique, in which a pulse is launched into a column of liquid at the transducer resonance frequency. Once the pulse is received at the opposite end, the two signals (being the transmitted and received pulse pairs) are multiplied together using an analogue multiplier. The multiplier combined with a low pass filter produces an output proportional to the cosine of the phase difference between both pulses. A variable delay is then used to nullify this output, defining quadrature between the transmit and receive signal paths. Following the isentropic phase method, a predetermined pressure jump produces a variation in sound velocity proportional to the B/A of the liquid. This change in sound velocity is measured at the output of the low pass filter as a change in phase. B/A is then determined by the equation [44]

$$\frac{B}{A} = -\frac{2\rho_o c_o^3}{l\omega_o}\left(\frac{\Delta\phi}{\Delta p}\right) \tag{3.1}$$

where l is the pathlength, ϕ the phase and ω_o the driving frequency.

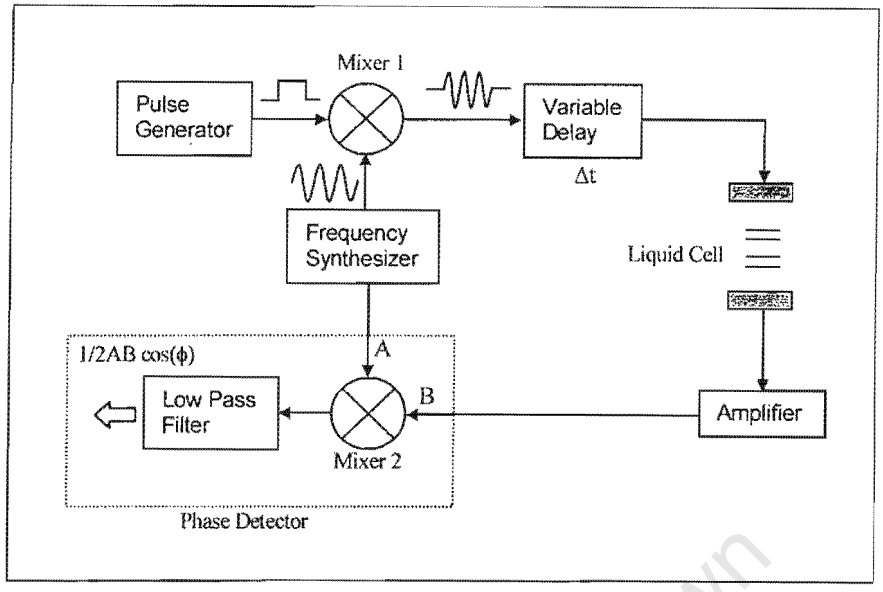

Figure 3-2: A simplified block diagram showing pulsed phase measurement. The sample and hold circuitry following the phase detector is not shown. Note that phase is described in terms of a cosine function and the individual pulse amplitudes.

Although pulsed phase measurement appears to provide a simple solution to isentropic phase measurement of B/A, there are several spurious phase contributions which may be interpreted incorrectly as changes in sound velocity. These effects are listed in point form below.

- The phase detector is nonlinear, but can be assumed to be linear in a narrow range.
- Depending on the liquid sample, a distortion of the pulse envelope occurs at the receiving transducer [83]. This distortion, which is a function of B/A, causes the RMS amplitude of the carrier (shown in Fig 3-2 as B) to change together with sound velocity. Therefore the resulting output from the phase detector is a phase combination of velocity and amplitude information, both a function of B/A.
- For liquids with large B/A values, (such as bubbly media [69] [39]), there is a large change in velocity accompanying a change in pressure, causing the phase output from the multiplier to operate in a nonlinear region. This results in a nonlinear relationship between phase and sound velocity.
- Should the pulse repetition frequency excite a liquid resonant mode, the system will behave as a liquid interferometer, introducing an unwanted phase contribution [98] to

the output of the phase detector. This behaviour can be described in terms of coupled resonances and is closely examined in Chapter 6.

3.2.2 Pulsed Phase Locking

Everbach *et al* [38] make use of a commercial[2], pulsed phase-locked loop to measure the change in sound velocity as a change in resonance frequency. Figure 3-3 shows a timing diagram of the received pulse for three instances during an isentropic pressure jump. A t=0, the microprocessor is instructed to sample the received pulse, calibrating the sampled voltage V_s to an internal reference voltage V_{ref} (the sample time, t_{smp} is manually determined by the operator). Once the sampled voltage is established, any deviation is used in feedback for phase correction.

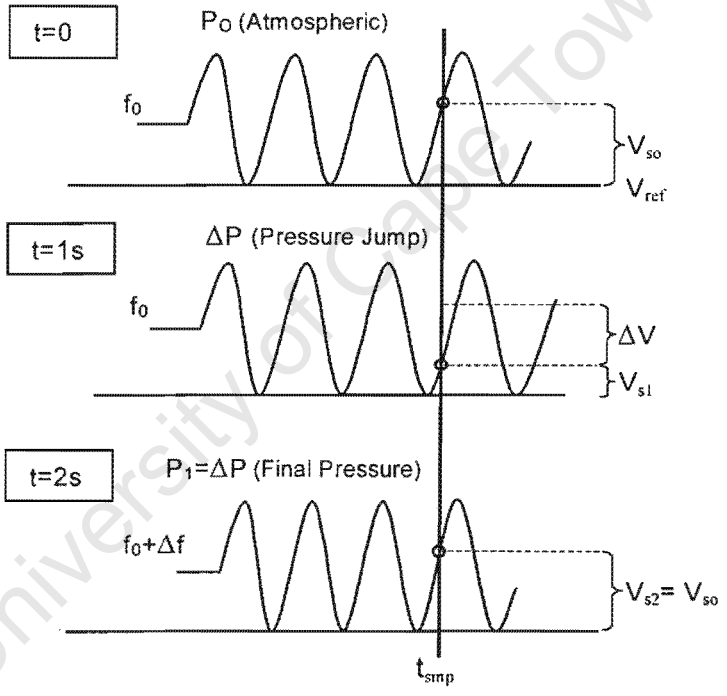

Figure 3-3: A timing diagram showing the received pulse being phase locked. At t=0, the sample voltage V_{s0} is calibrated to the reference voltage V_{ref}. At t=1s the system is pressurised causing the phase of the pulse to change. This causes a change in the sampled voltage V_{s1}, which is used as feedback to adjust the carrier frequency f_0. At t=2s, the frequency change causes the sampled voltage V_{s2} to match the value V_{s0}.

For an isentropic pressure jump (see t=1s), a phase change resulting from a change in sound velocity causes the sampled voltage to change (ΔV). This change is suitably compensated by

[2]The PLR-1000 from Micro Ultrasonics (Everbach et al[38]).

the microprocessor by adjusting the carrier frequency f_o in a direction to eliminate the phase offset, thus returning the sampled voltage to its referenced position. This technique permits changes in sound velocity to be determined by a change in carrier frequency. B/A is then calculated by the change in frequency with pressure as follows

$$\frac{B}{A} = \frac{2\rho c_0^2}{f_0}\left[\frac{\Delta f}{\Delta p}\right]_{Sq} \tag{3.2}$$

where Δf is the change in frequency and f_0 the steady state frequency.

The process of phase locking provides an ideal platform from which phase sensitivity may be captured for the purpose of measuring B/A. However, the pulsed technique above, although sufficiently sensitive to be able to determine B/A to 1%, is still subject to a variety of spurious phase errors, viz.

- Liquid attenuation is known to be frequency dependent [77] ($\approx \frac{\alpha}{f^2}$). This means that a change in the carrier frequency of the pulse will cause a change in amplitude of the pulse, resulting in a differential change in the sample voltage. This will be interpreted as a phase offset[3], and corrected in frequency resulting in a nonlinear phase addition to B/A measurement.

- For a differential change in frequency, the driving crystal is no longer operating at the same point in its resonance curve, causing a change in the amplitude of the driving pulse proportional to the Q of the transducer. This is a function of PZT filter characteristics and can be somewhat reduced by parallel inductive tuning; however a differential change in amplitude (as shown before) will manifest itself as a change in phase.

- Different cell lengths require different PRF. If the PRF is set up near or at a liquid resonance, interferometer effects will apply as previously described. It is critical for the pulse to dissipate completely in the cell for these effects to be avoided.[98]

3.3 A Continuous-Wave Alternative

As an alternative to pulsed systems we consider continuous wave (c.w.) methods for measuring B/A, thereby abandoning existing techniques of time of flight for that of real-time phase locking.

[3]The phase offset is a function of V_s. If V_s is set to zero, amplitude contributions will be independent of phase.

Sehgal *et al* [98] have shown that c.w. measurement of B/A is feasible, claiming a resolution of 1% with published data, using a direct phase measurement approach. From the methods of Everbach [38] and Zhu [112], we can conclude that phase locking improves the sensitivity of phase measurement by providing real-time velocity information as a function of frequency. In this study we pursue a new concept involving continuous wave phase locking (CWPL) for the purpose of measuring B/A isentropically without the errors or complexity of the pulsed methods.

The principle behind CWPL is to lock an integer number of half wavelengths within an interferometer cell. This is achieved (much the same as pulsed phase locking), by adjusting the drive frequency such that the drive and receive signals are in quadrature. In order to implement this condition, the phase difference between the driving and receiving transducers is measured using a phase detector (see Fig 3-4). The output from the phase detector is then used in feedback to drive the input of a voltage controlled oscillator (VCO).

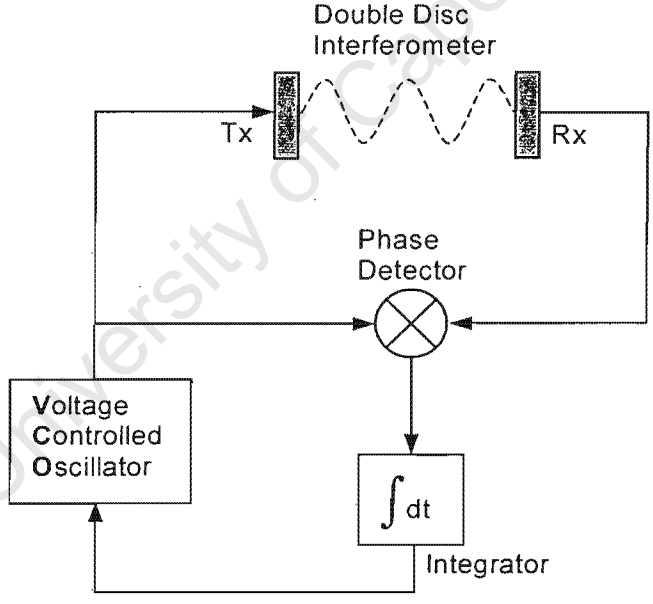

Figure 3-4: The principle of CWPL is demonstrated here using a block diagram. The phase difference between the transmitting (Tx) and receiving (Rx) transducers is integrated, and used in feedback to adjust the control voltage to the VCO. Any change in sound velocity will be interpreted by the loop as a change in phase, and instantaneously corrected by changing the drive frequency.

For an adiabatic pressure jump, the sound velocity of the liquid will vary, causing a change

in phase which is immediately corrected by the VCO with a corresponding change in frequency. The relationship between change in frequency and sound velocity may be represented by

$$\Delta f = \frac{\Delta c f_0}{c_0} \tag{3.3}$$

with f_0 and c_0 as the initial frequency and velocity respectively.

Using equation 2.5 the term $\frac{\Delta c}{\Delta p}$ may be rewritten with equation 3.3 as follows:

$$\frac{\Delta c}{\Delta p} = \frac{c_0 \Delta f}{f_0 \Delta p} \tag{3.4}$$

resulting in the isentropic expression used by Everbach in equation 3.2.

Since the technique of CWPL follows an interferometer approach to velocimetry, liquid resonant modes are excited within an interferometer cavity introducing the problem of coupled acoustic resonances. This unwanted effect, associated with frequency pulling and nonlinear phase contributions, is the topic of discussion in future chapters showing that the phase contribution is only applicable to liquid modes adjacent to the fundamental thickness resonance of the driving transducer. Further investigation of acoustic cells will show a novel cavity resonator based on a tube which demonstrates this continuous phase lock measurement principle convincingly.

3.4 Conclusions

Pulsed systems, although common to the field of velocimetry, are shown to be difficult to use to accomplish accurate B/A measurements. They require complex electronic systems and secondary calculations of time of flight, which are masked with uncertainties including pulse thresholds and diffraction effects. As a result, traditional time of flight systems have been abandoned for pulsed phase lock methods. A review of two such techniques has shown the need for complex instrumentation, with pulses subject to phase nonlinearities which are attributable in part to the pulse envelope becoming distorted. Other phase contributions are shown to be a function of the individual phase technologies employed.

As an alternative to pulsed systems we have proposed a continuous wave solution to isentropic measurement of B/A. The solution, based on a novel continuous-wave phase locked loop approach, entails a simple electronic control circuit capable of tracking extremely small changes in phase velocity. The discussion of continuous wave phase locking and its ability to

overcome inherent problems associated with pulsed systems will be the subject of discussion for the remainder of this study.

Chapter 4

General Instrumentation and Measurement Procedures

This chapter will provide some insight into the practical design problems encountered with developing instrumentation necessary for isentropic phase measurement of B/A. This requires a comprehensive understanding of how each component module, including the acoustic cell, integrates to form a cohesive measurement system. The instrumentation has been categorised into component modules, each of which are discussed in detail, covering aspects of design, calibration, modularity and tolerance with the purpose of establishing a generic blueprint for future use.

Albeit that relatively little of this section is original to this study, it is the intention to evoke a broader understanding of the measurement process associated with B/A. Several of the design techniques mentioned offer effective remedies to obstacles typically encountered with isentropic phase measurements. Furthermore, an explanation of the measurement procedures and statistical post processing is included, together with measurement approaches used to determine absolute sound velocity and density. Functional design considerations such as modularity and automation are addressed, summarising the prerequisites for isentropic phase measurement.

4.1 Design Criteria

Before we begin a discussing of the measurement system, the following design considerations are summarised, providing an overview of the constraints imposed by isentropic measurement.

- *Pressure Constraints*: Thermodynamic methods have previously used large overpressures

[46] in measuring B/A. These large pressure variations have caused, in biological cases, damage to the sample liquid [71, pg 1]. As an alternative, the isentropic phase method offers overpressures of less than a few bars provided the change in sound velocity can be measured adequately. Adopting this approach, the pressure instrumentation should be designed for overpressures of no greater than 200kPa.

- *Isentropic Considerations*: The isentropic phase method stipulates minimal entropy gain (see Appendix A). To achieve this, the measurement procedure should be confined to a small time period. A conservative time delay, used in previous studies and considered appropriate herein, is 2 seconds or less.

- *Thermal Stability*: Thermal fluctuations within the sample liquid introduce significant fluctuations in sound velocity[1], which subsequently reduce the overall accuracy with which B/A can be measured. To achieve an uncertainty error of less than 1% for B/A, requires the temperature of the sample liquid to be stable to within 0.001°C.

- *Cell Volume*: It is often necessary to measure B/A for liquid samples of particularly small volume. Such samples are often the result of biological preparations and impose a physical constraint on the volume of the acoustic cell. This restriction has been overcome in the literature through the use of small volume interferometers [111]; however a more elegant and novel approach will be demonstrated in chapter 7 with the use of tube resonators.

- *Instrument Modularity*: A prerequisite for this study is modularity in instrumentation. By using a modular approach to component design, a variety of test scenarios are possible without possible conflict between component modules. Each piece of apparatus should be independently calibrated and work without the need for external, shared resources.

- *Necessity for Computerisation*: Automation of the measurement system through the use of a computer enables increased experimental reproducibility and measurement speed. By automating the measurement procedure, measurements can be taken within seconds ensuring minimal changes in entropy and hence reliable data for B/A evaluation.

[1] A change in temperature of 0.0024°C will result in a change of sound speed in water by 0.001m/s[37].

4.2 Measurement Apparatus

The measurement apparatus consists of a combination of instrumentation and control modules. These modules, coupled together, form the complete B/A measurement system. It is the intention of this section to provide both micro and macro understanding of this system, detailing the design and development of individual modules together with a functional understanding of the effect that each module has on the final B/A measurement. For instance, the error introduced by any single instrument provides a weighted contribution to the ultimate inaccuracy of B/A. Based on this understanding, it is possible to allocate error tolerances to the design of each measurement module, thereby efficiently reducing the error contribution to B/A.

4.2.1 Description of the Measurement System

Figure 4-1 shows a block diagram schematic of the measurement system, detailing the interaction between measurement modules and the test cell. The focal point in this diagram is the test cell, whose primary function is both to hold and excite the sample liquid. Since isothermal stability is critical to B/A measurement, the cell also acts as a thermal buffer (or low pass filter) to extraneous fluctuations in temperature from the outside. To minimise these fluctuations the test cell was immersed in an 'isothermal water bath'. This water bath was designed with two 500W heaters together with a PI (proportional-integrator) control system to maintain the water temperature to within $\pm 0.015°C$ of its set temperature. The absolute temperature of the sample liquid was measured using a platinum resistive temperature sensor. This sensor was capable of measuring both absolute and dynamic changes in temperature of less than 0.001°C. The pressure system stipulated in the design criteria, is to have an excess pressure of no greater than 200KPa with a pressurisation time constant of no longer than 2 seconds. To accommodate this prerequisite, a 220bar nitrogen cylinder was used in conjunction with a 220-2 bar regulator. The time delay was introduced by using a needle valve and a small diameter helix-shaped pipe. Two solenoid valves connected in series provided the necessary control of pressurisation and depressurisation. Figure 4-1 shows the interconnection of this pressure circuit together with the pressure control system. By means of the laboratory computer (shown), the pressure system opens valve 2 to pressurise the test cell and polls the pressure sensor until the required pressure has been reached. Once this occurs, the computer closes valve 2 to fix the pressure, and observes the temperature of the sample liquid until thermal stability has been reached, at which time valve 1 is opened thus depressurising the test cell. The mode locking system not

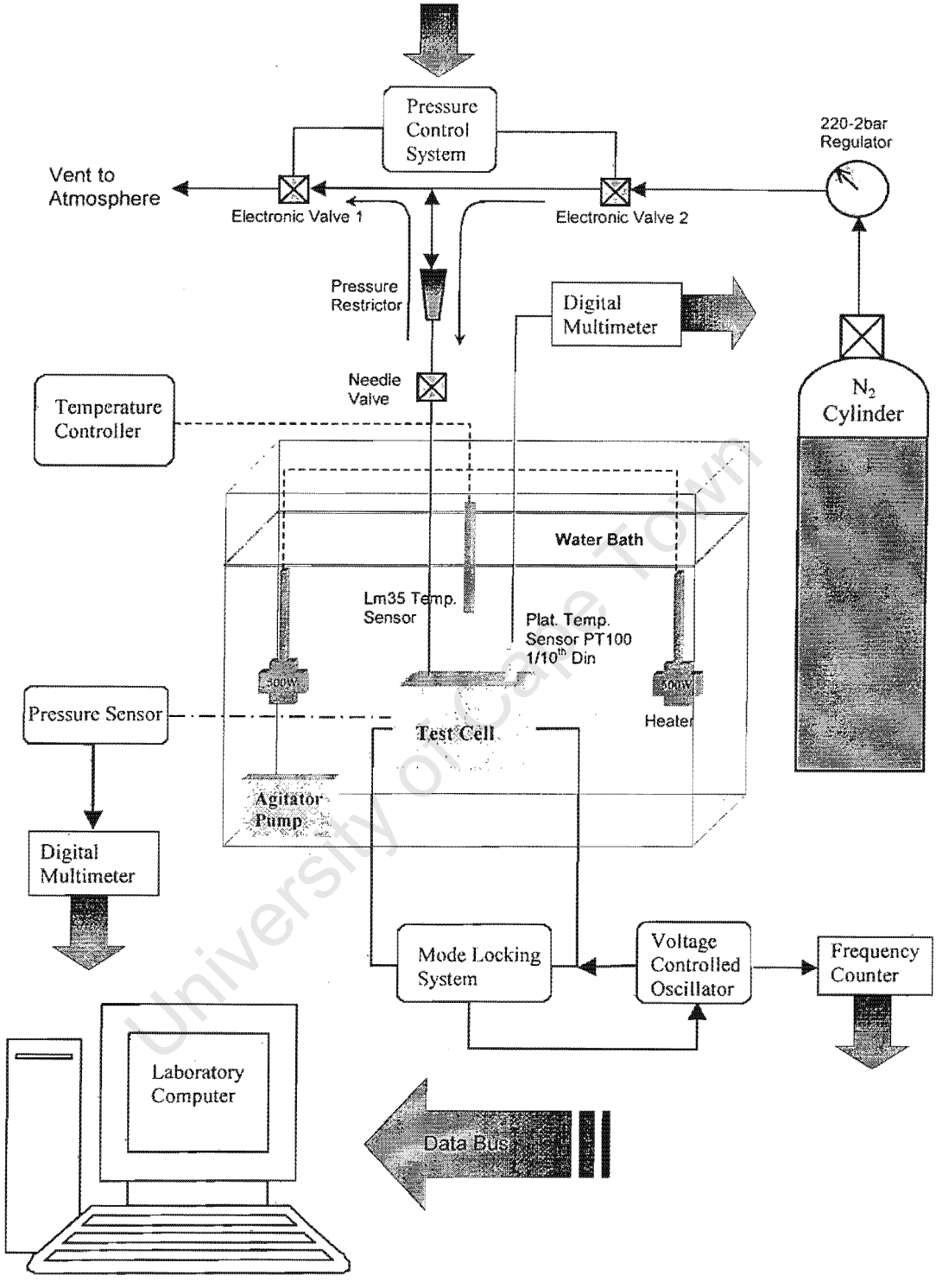

Figure 4-1: A block diagram showing the interconnection of individual instruments to form the complete measurement system. Each component communicates to the laboratory computer via a GPIB or Analogue Data Bus (depicted here by thick shaded arrows).

only tracks the necessary change in velocity required for B/A measurement, but can be used as a measure of the thermal stability of the sample liquid. Once depressurisation has been activated, the laboratory computer samples the frequency counter to acquire the necessary data within the 2 second time window.

4.2.2 Temperature Control

Temperature control of the sample liquid is of paramount importance for the precise measurement of B/A. This is achieved through the stable temperature control of the environment surrounding the sample liquid. Such an environment is typically established by immersing the test cell within a temperature controlled water bath. The test cell should be designed to act as a thermal buffer between the sample liquid and the water bath, thereby filtering external thermal fluctuations to the sample liquid.

The water bath was constructed using 5mm thick glass to form a rectangular tank capable of holding 40 litres of water. The tank was then insulated on all sides with 2.5cm thick polystyrene foam (of low thermal conductivity). Once filled, the surface of the water was covered with polystyrene chips to further reduce thermal conduction/convection and to reduce the unwanted effect of evaporation.

The temperature control system was designed for elevated ambient temperatures only. Since cooling systems are costly and neither contribute nor detract from the focus of this study, they were deemed unnecessary. In order to heat 30 litres of water from a typical ambient temperature of 20°C to 30°C requires approximately 1.2MJ of energy ($E = mc_p\Delta t$). To do this in a time of ±20 minutes (neglecting all thermal and electrical losses) requires a heating source of typically 1kW.

The final temperature bath shown in Fig 4-1, was filled with 30 litres of water and consists of two 500W (220V) immersion heaters together with an LM35A temperature sensor, used as feedback to the temperature controller. The first control system developed was based on a bang-bang[2] [89] approach. This system was inadequate for B/A measurements, with set point temperatures only stable to ±0.5°C. The final control system is based on a standard proportional-integrator approach, which angle modulates the 50Hz AC voltage to the heaters by using a combination of triac and diac devices.

[2]A bang-bang approach is a simple control system that operates in two states; either fully "on" or "off". This technique was applied to temperature control using a single comparator to switch the immersion heaters either on or off depending on the set point temperature.

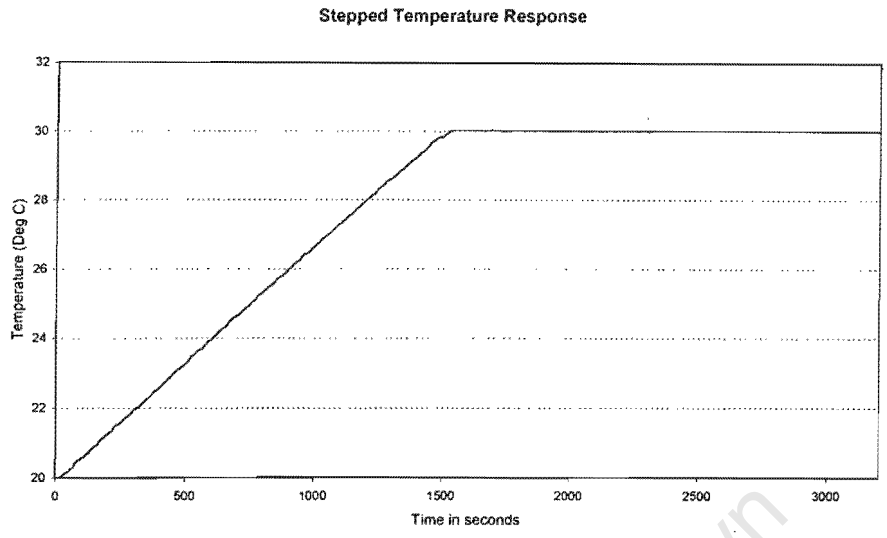

Figure 4-2: A step response of the temperature controlled water bath over a temperature range of 10°C. The measured slope indicates a heating time of 2.5 minutes per degree. (Ambient temperature was 16°C). The step input was at time t=0s.

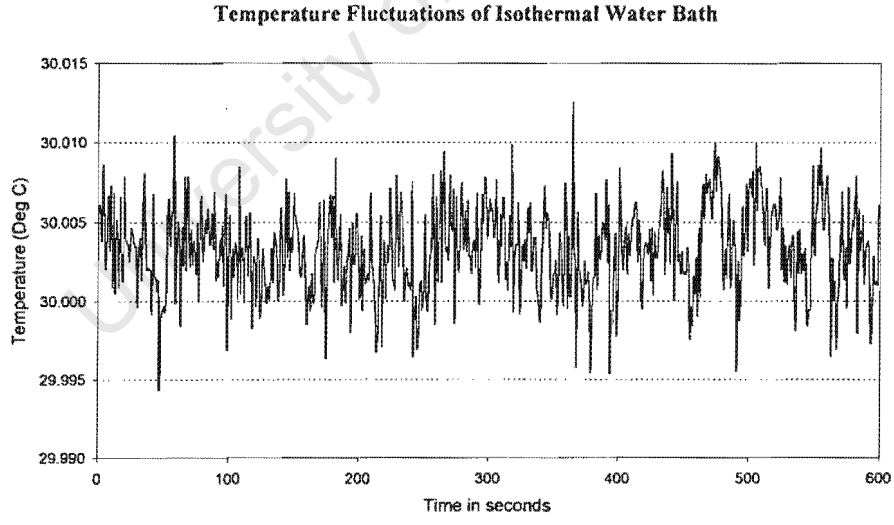

Figure 4-3: The above graph shows a ten minute data sampling of temperature using a calibrated platinum RTD. The control thermostat was set at 30°C. The mean temperature calculated is 30.0032°C, with a standard deviation of ±0.0028°C. The maximum and minimum residuals are 30.0125°C and 29.9943°C, resulting in a point spread of 0.0181°C which is a conservative resolution of thermal stability for the bath.

This system provides sufficient control sensitivity to maintain a set point temperature of $\pm 0.018°C$ in the external bath (see Fig ??). A measured step response for the control bath can be seen in Fig.?? below. The circuit diagram of the controller itself is shown in Appendix B.

To reduce thermal hotspots within the bath, a stirring action was performed by an EHEIM water pump, capable of recycling the water at a rate of 10 litres /minute. The temperature of the sample liquid is constantly measured by means of a platinum PT100 $\frac{1}{10}$th Din temperature sensor [106]. This sensor makes use of a 99.999% pure platinum element whose resistance changes as a function of temperature. The element is placed in a thin walled, stainless steel sleeve (filled with thermal conductive paste) which was epoxied into the test cell, exposing just the active surface to the sample liquid. This arrangement secured temperature measurement with minimal acoustic wave disruption. The sensor was designed and calibrated according to the British Standard BS 1904:1984 (IEC 751:1983), which specifies a second order polynomial relating temperature to resistance together with a thermal time constant of 0.8ms. By capturing the resistance of the sensor on a laboratory computer, it is simple to accomplish a final temperature calculation.

The fundamental difficulty in designing an electronic system capable of resolving 0.001°C for any electrical temperature sensor, is providing a stable, low noise, current source capable of determining such resolution. Any electrical noise or power fluctuation is inevitably transferred to the sensor and is misconstrued as thermal noise. To overcome this problem a Hewlett-Packard (H.P.) HP34401A digital multimeter was used in 4 wire mode to measure the resistance of the platinum element. Two well-shielded wires were connected to the multimeter, which sourced a stable current of 1mA to the platinum sensor. A further set of wires was used for high impedance voltage sensing [54], resolving the potential developed across the platinum resistor to within 100nV. Using this technique, the resistance of the platinum element was resolved to within $100\mu\Omega$, which corresponds to a temperature resolution of 0.000258°C. The H.P. multimeter is microcontrolled, which enables remote interface to the laboratory computer through an IEEE-488 (HPIB) Bus structure. SCPI[3] commands embedded within an HPVEE computer program enabled remote triggering and data communication to the multimeter.

[3]Standard Commands for Programmable Instruments

4.2.3 Pressure System

A readily available cylinder of compressed nitrogen was used as a pressure source for this study. The cylinder, normally compressed to 220bar, was attached to an Afrox series 9500, multi-stage, nitrogen regulator capable of converting a pressure head of 300bar to a variable 0-10bar output. From this regulator, 3.1mm copper tubing was used to assemble the pressure circuit displayed in Fig. 4-1. This circuit includes two (normally closed), Burkett solenoid valves which were responsible for the pressurisation and depressurisation process. Each valve was interfaced to a laboratory computer, thereby enabling the pressure system to be automated. For this to be accomplished, an electronic driving circuit was designed. This circuit (shown in Appendix B), uses a standard 24 volt, regulated, DC power supply to drive both solenoid valves. Each valve was switched open and closed using NPN power transistors. The base current for each transistor was supplied by an opto-coupler unit, which includes an LED and optotransistor on a single chip. This ensures electrical isolation between the computer and the driving circuit. A standard 5 volt digital output from the computer port was used to drive the LED of the optocoupler. In addition, override buttons were implemented for user intervention to enable manual opening of each valve. Both valves were designed to blow open for gauge pressure exceeding 4 bar. This safety feature prevented over pressurisation of the test cell and destruction of the pressure sensor.

In order for the pressure automation to be controlled, the gauge pressure of the test cell had to be measured. This was accomplished by designing a pressure transducer module which could communicate to a laboratory computer through a data acquisition card. For the design to be generic, both pressure transducer and calibration electronics were combined outside the water bath, connecting to the test cell through a 30cm piece of 1.6mm teflon tubing. The Motorola MPX2200 pressure transducer makes use of four strain gages placed over a thin diaphragm of silicon. The wheatstone bridge configuration of the strain gages, results in a highly accurate and linear relationship between pressure and resistance (typically $\pm 0.25\%$ nonlinearity). A double regulated voltage source (see Appendix B) was used to excite the transducer. This ensured the supply of a stable voltage (± 0.1mV) to the strain gauge bridge, thereby minimising any stray voltage fluctuations which could be misinterpreted as pressure offsets or variations. Temperature compensation of the transducer is achieved through a built in, laser trimmed, resistive network, which enables operating temperatures between 0°C and +85°C.

The change in phase velocity experienced with excess pressure is typically 1.8×10^{-3}m/s/kPa

for water at 30°C. Based on this understanding, an error budget of ±0.5 kPa will introduce an error of ± 0.0009m/s, which is well within the tolerance for measuring B/A to 1%. In order to achieve a transducer accuracy of ±0.5 kPa, careful electronic shielding was utilised together with high precision opamps. Calibration was done using a mercury manometer before each measurement run, allowing calibration constants to be calculated and incorporated within a computer program.

A design prerequisite set out earlier defines a time period of two seconds in which all measurement data is to be acquired. For this to be practically implemented, the design and development of a variable pressure delay system is required. To facilitate such a design requires the detailed understanding of both linear and nonlinear dynamic fluid flow. Since this analysis was beyond the scope of this study, a less formal and simplistic approach was adopted. By assuming laminar flow (i.e. a Reynolds No. below 2000), an electrical analogy using capacitance and resistance was derived to describe the transient nature with which a pressure delay could be designed [89, (pg 126-132)]. Since a typical electrical RC filter exhibits the same exponential decay as observed in fluid flow, it is possible to correlate the mathematical model used in filter design to that necessary in fluid flow design. For example, a typical pressure constriction such as a needle valve can be considered a variable resistance, whilst the volume of the container being pressurised, may be considered analogous to electrical capacitance being charged. The time to pressurise the container through the needle valve is defined by the RC time constant of the pressure circuit.

With this electrical analogy in mind, it is obvious that any time delay can be constructed with the correct 'RC' values. The type of test cells used in this study fall into two categories, each with its own capacitance, thereby necessitating two individual delay systems. The first cell developed (see Chapter 5), was based on the design of a standard double disc interferometer. The sample liquid was contained within a cylindrical cavity, enclosed on both ends by piezoelectric transducers. The volume of the tubing used to pressurise the cavity determines the necessary capacitance, which in the case of 3.1mm tubing is negligible. The second cell was designed as a thermal jacket for a tube resonator (see Chapter 7) which contains the sample liquid. The jacket was designed with a small air volume, providing the necessary capacitance for the delay system.

For the first test cell, a liquid gas interface tube was utilized to facilitate filling of the test cell. The volume of this perspex 'viewing tube' was sufficient to create a reasonable maximum capacitance for the delay system. This in series with a variable flow needle valve creates an

adequate time constant which can be coarsely adjusted by changing the level of sample fluid in the viewing tube, or finely adjusted through the needle valve. The second test cell required a constriction in series with the needle valve to create sufficient resistance. This constriction (based on similar systems [37, pg 85]) was determined experimentally using the filter analogue mentioned earlier. A standard piece of 30cm long 1.6mm copper tubing was wound in a helix shape with a diameter of 3cm to create a fixed flow resistance. This constrictor in series with a constant flow needle valve was sufficient to create the two second time delay required. Coarse adjustment of the delay was possible by changing the internal diameter of the helix whilst fine adjustment was again obtained using the needle valve.

By implementing the pressure delay system in series and directly before the test cell, it was possible to establish a time delay for both the pressurisation and depressurisation processes. This permitted a two second pressurisation of the test cell, minimising any entropy changes to the sample liquid and allowing sufficient time for the laboratory computer to observe the event.

4.2.4 Absolute Density and Velocity Measurement

To measure the nonlinearity parameter of any liquid, using the isentropic phase method, requires the pre-determination of two liquid properties; namely, absolute velocity and absolute density. Given that both of these constants are familiar entries in many chemistry textbooks, the task of measuring standard liquids is assumed redundant. Nevertheless, poorly characterised liquids (such as fluorocarbons FC43 and FC75) necessitate an accurate means for evaluating these properties. Although numerous methodologies and instruments exist to accomplish these measurements, a formal discussion of these techniques falls beyond the scope of this study. However, two measurement techniques were implemented for the determination of absolute velocity and density and are described below.

Picnometry is a standard means for determining the density of a fluid. The technique makes use of a glass vessel known as a picnometer. This vessel is designed to hold an accurately defined volume of liquid. Once the prescribed volume of sample liquid is placed within the picnometer, the picnometer is weighed. The combined mass of the picnometer vessel and sample liquid is subtracted from the mass of the empty picnometer vessel thereby determining the mass of a known volume of liquid. Two independent scales where utilized for this procedure in order to statistically reduce instrumentation error. Once mass and volume were determined, density could finally be calculated using $\rho = m/v$. The measurement of densities for both fluorocarbon liquids are shown in tabled form in Chapters 5 and 7. Standard error analysis of this technique

revealed a density accuracy of less than 0.01%, comparing favourably with published data [73].

Absolute phase velocity has been discussed in detail in Chapter 3, and is therefore briefly examined here. Although copious sound velocity instruments have been developed in the past, the most common and accurate methods still involve pulsed time of flight. Using the interferometer cell developed for continuous wave locking, an existing pulse echo overlap method became an obvious means to determine absolute sound velocity. This technique was used to confirm measurements reported in the literature and values for the fluorocarbon liquids are tabled in Chapter 5 and 7. The average measurement uncertainty calculated for this technique was 0.013%.

4.2.5 Computer Programming and Data Acquisition

The computer used for data acquisition and statistical post processing was an Intel based 150Mhz Pentium with 16Mb of Ram. Although a slower computer would have sufficed, the Pentium processor proved expedient in statistical post processing, and was capable of multi-tasking during the data capture process. The computer was also used as a post processing terminal for all finite element analysis used in this study. The open architecture of the laboratory computer facilitated the addition of two ISA cards, namely a HPIB interface card and a PC30B data acquisition card.

All the commercial measurement instruments used in this study are manufactured by Hewlett Packard, and support the IEEE-488 communication protocol. By implementing the HP82341D, HPIB[4] interface card together with the visual programming language HPVEE [50], it was possible to access and control each instrument, exchange data and automate the measurement procedure. The interface card combines high speed, 16 bit data transfer together with a built in buffer which provides I/O and system performance that is superior to direct memory access (DMA). The instrument network included: a digital multimeter, frequency counter, VCO (voltage controlled oscillator), oscilloscope and network analyser. Each of these instruments was networked in parallel to the computer using standard GPIB cables. The address for each instrument was defined in the software to enable simple identification and communication. The speed of communication proved more than adequate with a data rate of up to 750KB/s.

In addition to the digital bus described above, an analogue bus was utilized to communicate

[4]HPIB stands for Hewlett-Packard Information Bus. This communication protocol developed by Hewlett-Packard was adopted by other instrumentation vendors and labelled GPIB (General Purpose Information Bus). The protocol is now endorsed as an IEEE standard and is described as IEEE-488.

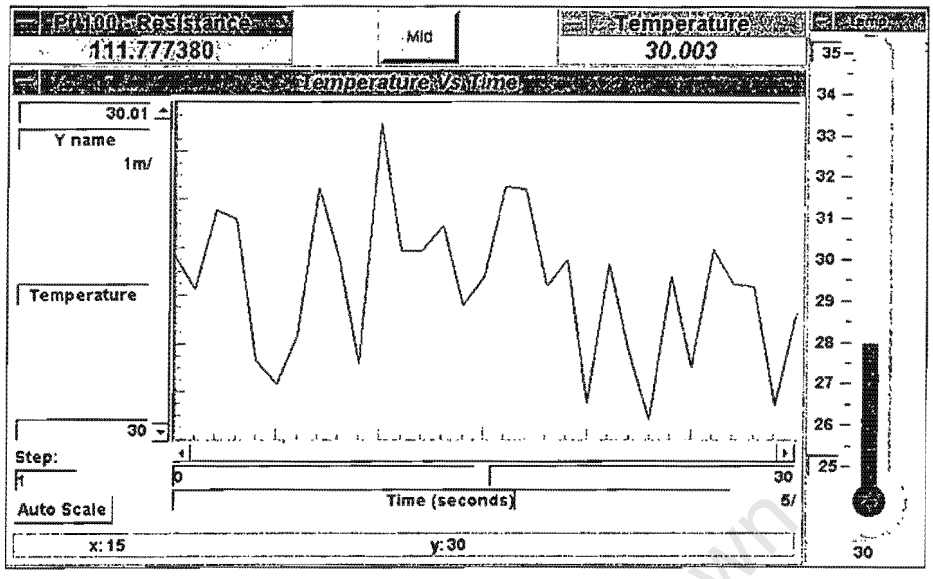

Figure 4-4: A typical visual interface using HPVEE. The temperature panel provides real time information of temperature within the isothermal water bath by measuring the resistance of a platinum RTD and converting it using calibration data into temperature. This is then plotted on a strip chart and stored to a file.

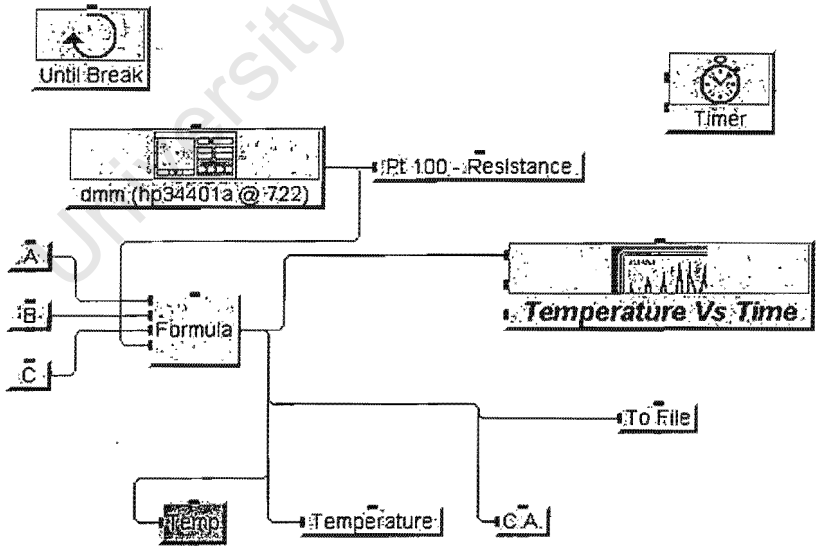

Figure 4-5: The simplicity in programming the application in Fig 4-4 is shown above. Each object represents an algorithm, variable or interface. The interconnecting lines represent program execution and data flow.

analogue pressure data and to permit automatic triggering of the pressure valves. The multi-purpose data card used was an Eagle Technology PC30B which supports 16 channels of 12-bit analogue to digital inputs together with 24 programmable digital I/O lines. Although the PC30B card proved more than adequate for data acquisition in this study, its integration to the HPVEE visual language was tedious due to the fact that an embedded C++ DLL library had to be written and incorporated within the HPVEE code. Notwithstanding this, the PC 30B provides a cost effective means of data acquisition with a sustainable sampling rate of 30kHz.

Pressure data was transferred from the pressure module through a line driver using a shielded twisted pair cable. Two analogue inputs were used in differential mode in order to reject any common mode noise developed during data transfer. The solenoid valves were activated through the driving circuit (described previously) by implementing two of the programmable I/O lines. Each line was used to drive the LED of the optocoupler, sinking less than 1mA of current.

The HPVEE programming language forms the foundation of the automation procedure, providing an extremely simple visual structure which compliments the goal of this study in maintaining simplicity in measuring B/A. HPVEE was chosen over similar visual languages such as LabView due to its availability and uniformity with existing Hewlett-Packard measurement equipment. Since the language is designed with a high speed compiler, data acquisition and instrument I/O were easily achieved within the two second time frame stipulated. The visual environment using the 'control panel' enables real-time analysis of data such as temperature and pressure. Furthermore, calibration constants are easily incorporated within the program enabling simplicity in data acquisition. A typical programming example in Fig. 4-5 shows the data acquisition of temperature within the thermal bath using a platinum resistance temperature sensor. A snapshot of the control panel (Fig.4-4) indicates the resistance of the sensor together with a real-time calculated value for temperature which was extracted from the calibration equation supplied by the sensor manufacturers. The sampling rate for this procedure was set at one sample per second.

4.3 Measurement Procedure

A generic measurement procedure is described in this section for determining B/A *in vitro*. This procedure was used as an investigative tool for examining the performance of various continuous wave (c.w.) lock-in systems and test cells developed in the course of this study. Although adapted for continuous wave measurement, the procedure described herein is simply

an adaption of the technique adopted for measuring B/A using the isentropic phase method [37, pgs 21-23]. Whilst the isentropic phase method typically involves the use of a double disc interferometer for pulsed velocimetry, the continuous wave method facilitates various approaches to differential phase velocimetry. These approaches include the use of different test cells, each requiring a unique procedure for pressurisation, liquid filling and mode locking. These procedures together with the individual design of the test cell will be discussed in Chapters 5 and 8.

Prior to measurement, the isothermal bath was filled with water and the temperature control system set to a pre-determined temperature (usually 30°C). The test cell was then immersed in the bath to allow it to reach thermal equilibrium. During this period, the pressure transducer was calibrated and liquid constants of absolute density and velocity were established, either from published measurements or through experiments (see Appendix D). An HPVEE computer program was activated to monitor the temperature of the water bath using a platinum RTD sensor. The program was designed with an audible alarm to indicate when the bath had reached set point temperature.

Once thermal equilibrium had been reached, the sample fluid was introduced to the test cell. Given that gas saturated liquids typically exhibit larger B/A values than degassed liquids, it was critical to keep the sample liquid degassed, therefore the liquid was dispensed carefully (under laminar flow) into the test cell. After the liquid had been transferred, the computer was again utilized for temperature observation, this time monitoring the absolute temperature of the sample liquid. During this period (usually 1 to 2 hours) the continuous wave lock-in system was initiated, trapping an acoustic mode within the cell. As soon as the mode was locked, the change in frequency (monitored using a 10-digit frequency counter), indicated the relative isothermal stability of the sample liquid. Observation of this frequency indicated a small increase in temperature due the thermal contribution of the piezoelectric transducer/s. This thermal contribution was kept to a bare minimum by providing minimal power to the transducers.

After checking that all instrumentation modules were functioning correctly, the N_2 cylinder valve was opened and the HPVEE data acquisition program was executed. This program automates the data capture of 10000 data points per sample run. A flow diagram of the program execution is given in Fig.4-6. The following list of events narrates the measurement procedure performed by the computer:

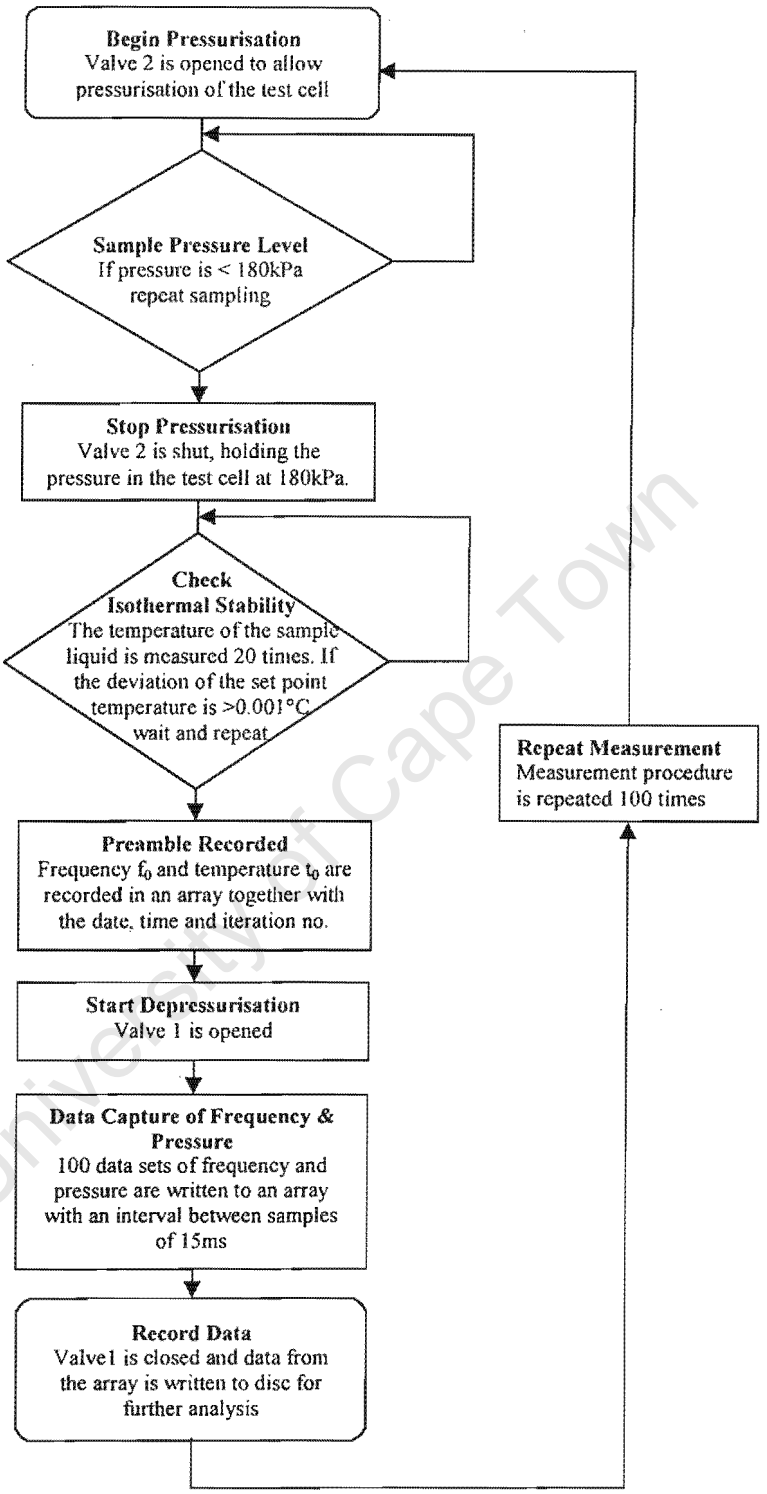

Figure 4-6: A flow diagram showing the automatic control and data capture performed by the laboratory computer using the visual programming language HPVEE.

1. Firstly, pressure valve 2 (shown in Fig.4-1) was opened using the digital I/O on the data acquisition card. This enabled an approximate 200kPa pressure head to be supplied to the test cell by means of a time delay constriction.

2. During this two second time delay the computer repetitively polled the data acquisition card for pressure readings. Each reading was compared to a pre-determined, maximum pressure value (typically 180kPa), which indicated to the computer when to shut valve 2.

3. Once the prescribed pressure had been reached, the temperature of the sample liquid was carefully monitored using a platinum temperature sensor. The sample liquid was observed for any increase or fluctuation of temperature as a result of the pressurisation process. This was accomplished by sampling the temperature repetitively in data sets of 20. For each data set acquired, a standard deviation was calculated. This deviation from the set point was compared to $\pm 0.001°C$. If the result exceeded this tolerance, the procedure was repeated. As soon as isothermal conditions were satisfied the program launched the data capture routine.

4. The first algorithm of the data capture routine acquired some parameters, which it wrote to a header array. The following were typically included:

   - The absolute temperature of the sample liquid, t_0
   - The initial lock-in frequency, f_0
   - The iteration number
   - The date and time

5. After these parameters were acquired, valve 1 was opened allowing a 2 second depressurisation of the sample cell in which 100 data sets of pressure and frequency were acquired. Each data set was obtained by simultaneous polling of the data acquisition card and the frequency counter. Since both systems utilize individual data buses, multiprocessing of this kind was possible. The estimated time between data acquisition of frequency and pressure was considered negligible.

6. This data capture routine was executed 100 times, storing each data set repetitively in an array. The time required to capture and store a single data set was estimated as 15ms.

7. Once depressurisation was complete and 100 data sets were acquired, the data block was transferred to a file and valve 1 was closed.

Following this, a counter was incremented and the entire data capture program was repeated for a total of 100 iterations. This recursive measurement enabled statistically significant data to be acquired, which was further analysed using Matlab to determine a single value for B/A.

4.4 Statistical Analysis

Having finished its measurement cycle, the HPVEE capture program exits, leaving 100 text based data files for analysis. Each file represents a single data set or iteration, containing 100 samples of pressure vs frequency. This provides an ensemble of 10000 data points from which B/A can be determined. In order for the data to be assembled in a more manageable form, a Matlab script was written to read recursively in each text file and write the data to a suitable matrix, saving the result as a binary '.mat' file.

In addition to the read script, two statistical programs were written using Matlab. The first was written primarily as a checking utility, enabling a user to read in and perform a statistical analysis on any one of the 100 data iterations. As shown in Fig. 4-7, an isolated data set (wtr 5) was chosen and plotted with pressure as the abscissa and frequency the ordinate. A linear least-square regression is performed, providing a measure of the gradient g, an estimate of the uncertainty in the gradient $\sigma_{\bar{g}}$ and the linear correlation coefficient R. The calculated gradient is then used together with the starting frequency and user defined values for velocity and density in an initial calculation of B/A. As data sets are stored as individual files, the user can inspect any captured iteration during the measurement process for instrumentation errors, systematic uncertainty, and a provisional value for B/A.

The second script that was written uses the binary file described earlier for a more comprehensive statistical evaluation of B/A. Before reviewing this script, it is important to understand that true 'isentropic measurement' is improbable, since by definition it prescribes no change in entropy during or between a measurement process or iteration thereof. We therefore expect (even though every effort has been taken to minimise entropy change), that a small random uncertainty will manifest itself in our measurements, attributable in part to thermal and electrical noise. This is the reason for multiple iterations, enabling us to quantify this uncertainty and provide a more realistic value for B/A. Figure 4-8 shows a cluster plot of all 10000 data points. The width of the positively correlated line is an indication of the measurement uncertainty, which under true isentropic conditions should tend to zero. In order for B/A to be evaluated from Fig 4-8, we require a best estimate of the gradient $\bar{g} = \frac{\Delta f}{\Delta P}$ together with the starting

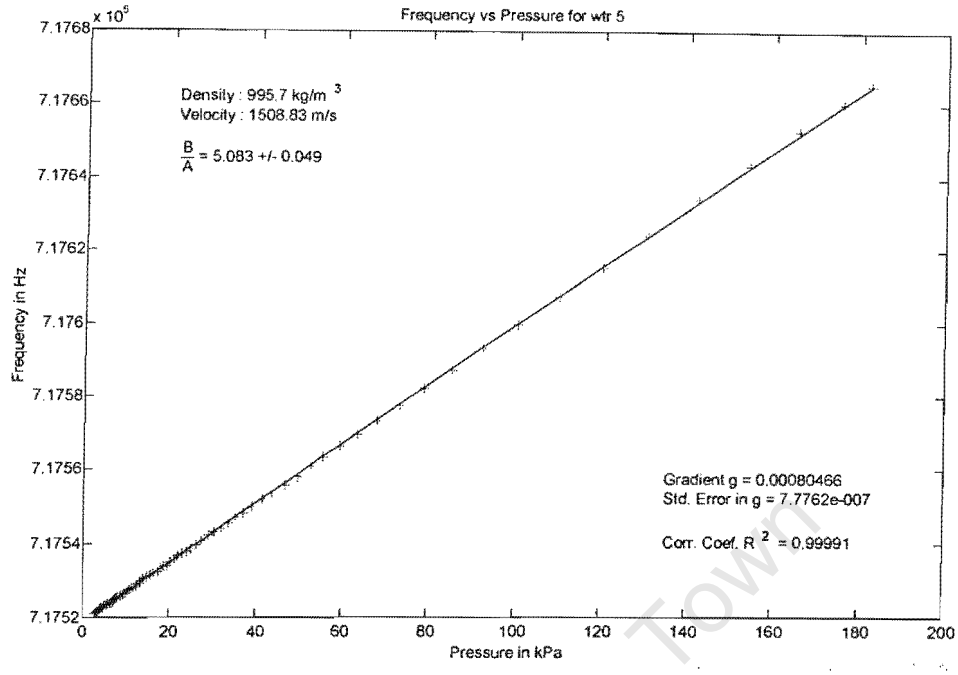

Figure 4-7: A single data block representing iteration number 5/100. 100 points of pressure versus frequency are used to determine B/A. Values for density and velocity are provided to evaluate B/A from the graph at a temperature of 30°C

frequency f_o. Having acquired these values, B/A may be determined from the simplified form of equation 3.2 given here as

$$\frac{B}{A} = \frac{2\rho c_o^2}{f_o}\bar{g} \tag{4.1}$$

Remembering that each measurement iteration contributes information of both gradient and uncertainty, we have adopted a weighted averages approach to calculating the mean gradient [37, pgs 108-117] $\frac{\Delta f}{\Delta P}$. This method follows the principle of *maximum likelihood* [105] estimating a true value for the gradient by considering the uncertainties described earlier as zero mean random variables governed by a normal distribution. Following Taylor [105], the weighted mean is given by

$$\bar{g}_w = \frac{\sum_{i=1}^{N} w_i \bar{g}_i}{\sum_{i=1}^{N} w_i} \tag{4.2}$$

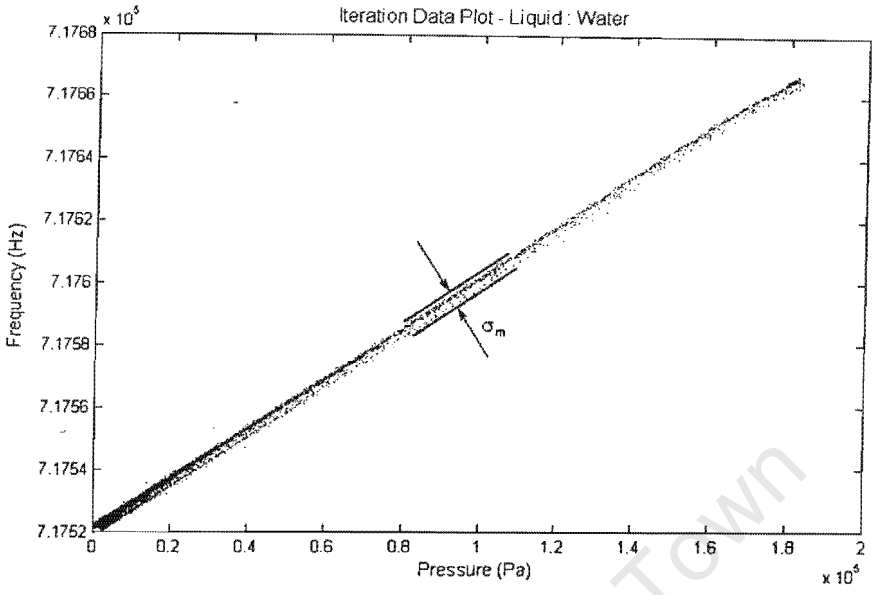

Figure 4-8: A cluster plot of 10000 data points derived from a single measurement of B/A. The uncertainty in the slope is represented by the width of the line.

where the weighting function w_i is defined by the inverse variance of the slope $w_i = \frac{1}{\sigma_i^2}$ and $\bar{g}_i$ is the best estimate of the gradient for iterations i = 1,2,...,N.

Having calculated the weighted mean of the slope $\bar{g}_w$ it is now necessary to quantify the uncertainty in this calculation. Since the weighted mean gradient is simply a function of the original calculated values $\bar{g}_i$ for each iteration, it is elementary to calculate the uncertainty in $\bar{g}_w$ using error propagation, defined by Taylor [105] as:

$$\sigma_{\bar{g}w} = \frac{1}{\sqrt{\sum_{i=1}^{N} w_i}} \tag{4.3}$$

A plot of the gradient and standard deviation associated with each iteration is given in Fig 4-9. From the plot it is interesting to note that the standard error of the gradient is typically constant throughout the measurement process, whilst the uncertainty of the slope between measurement is often greater than the standard error. A broader examination of individual points reveals the possibility of memory or trends within the data; further examination reveals a correlation coefficient of -0.353 indicating some anticorrelation. This subtle trend in the data is most probably the result of random thermal fluctuations (<0.001°C), being within the error budget of this study. We may therefore conclude, (following similar observations [37, pg 115])

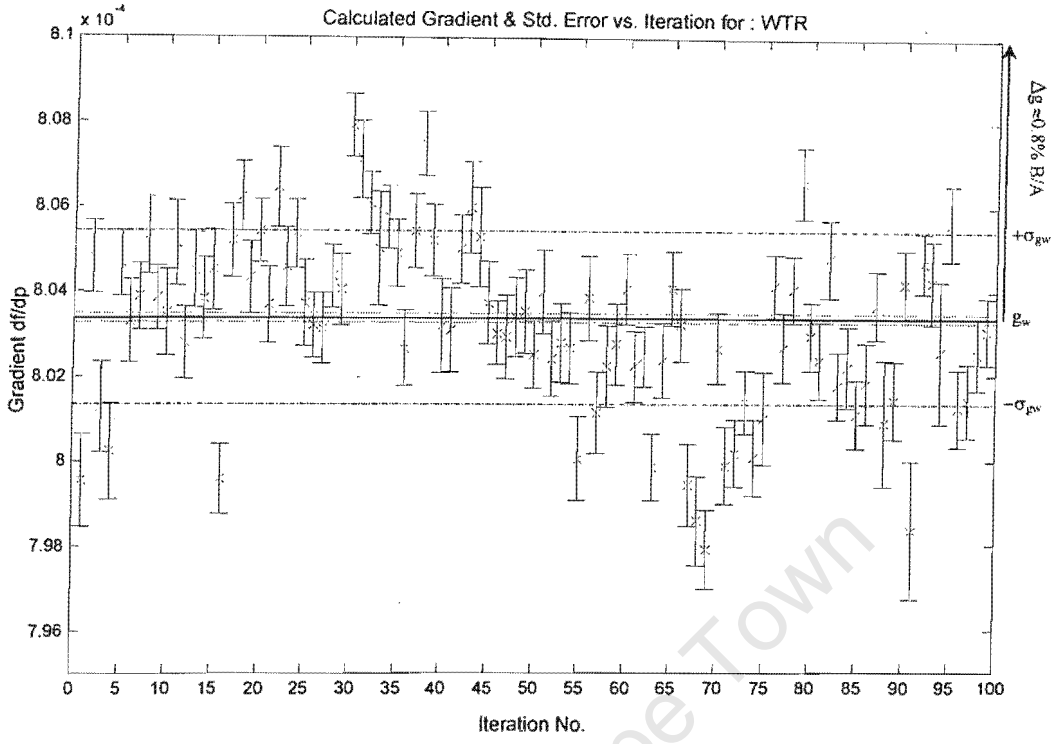

Figure 4-9: A plot of gradient and standard error versus frequency. Each cross represents a least square estimate of the gradient for an isolated data set. The error bars are an indication of associated standard error. The weighted mean for the data is given by the solid line with standard deviations of the mean represented by the dashed lines.

that a more conservative approach to measurement uncertainty can be obtained by treating each gradient point $\bar{g}_i$ as an independent measurement with the uncertainty in the gradient points $\sigma_{\bar{g}w}$ defined by the familiar expression:

$$\sigma_{\bar{g}w} = \sqrt{\frac{1}{N-1}\sum_{i=1}^{N}(\bar{g}_i - \bar{g}_w)^2} \tag{4.4}$$

This expression for uncertainty in gradient has been adopted throughout this study as a means of estimating B/A.

4.4.1 Accuracy in Method and Propagation of Uncertainties

We have established in the previous section a statistical procedure that enables us to estimate a conservative value for the gradient $\frac{\Delta f}{\Delta P}$, based upon 10000 independent measurements. The uncertainty in this value is the standard error of the mean, defined within a 68% confidence

interval.

In order to quantify the overall uncertainty in B/A, we need to re-examine equation 4.1, defining the uncertainties accumulated from individual experimental methods and instrumentation modules. The first quantity to be evaluated is f_o, being the starting frequency for each data set. Although the measurement uncertainty in frequency is based on the absolute accuracy of the frequency counter, we consider this contribution to be negligible, since the frequency counter claims an accuracy of typically 1 part in 10^8. However an estimate of the overall frequency f_o can be defined by calculating the mean frequency associated with each of the 100 data iterations and calculating the standard deviation, resulting in $f_o \pm \sigma_{fo}$.

Following the error budgets and modular design criteria set out earlier, we have summarised the experimental uncertainties together with instrumentation uncertainties in the following table.

Variable	Measurement Uncertainty σ
Density ρ	$\pm$0.01%
Velocity c_o	$\pm$0.013%
Pressure	$\pm$0.5 Pa
Frequency	$\pm$1 Hz in 1Mhz
Temperature	$\pm$0.018°C

Table 4.1: A summary of the individual uncertainties associated with the experimentation and instrumentation used for B/A measurement.

Examining Table 4.1, we see that the experimental methods used to determine density (picnometry) and sound velocity (pulse-echo method) have both experimental uncertainties of approximately 0.01% falling well within the uncertainty budget previously defined. The uncertainty in pressure measurement is an estimate based on systematic and random errors associated with the pressure transducer and calibration electronics. The frequency error is a conservative estimate based on the lock-in system used. The temperature error is the thermal fluctuation from the setpoint within the temperature bath. Each test cell provides a thermal low pass filter to this fluctuation together with insulation, resulting in most cases with an isothermal uncertainty of $\pm$0.001°C. As a measure of the overall uncertainty in B/A, we combine these errors in the familiar fractional uncertainty formula, derived for B/A as follows

$$\sigma_{\frac{B}{A}} = \frac{B}{A}\sqrt{\left(\frac{\sigma_\rho}{\rho}\right)^2 + \left(2\frac{\sigma_{c_o}}{c_o}\right)^2 + \left(\frac{\sigma_{f_o}}{f_o}\right)^2 + \left(\frac{\sigma_{\bar{g}w}}{\bar{g}_w}\right)^2} \tag{4.5}$$

resulting in the final calculated value for B/A as

$$\frac{B}{A} = \frac{2\rho c_o^2}{f_o}\bar{g} \pm \sigma_{\frac{B}{A}} \tag{4.6}$$

Chapter 5

Aspects of Phase Locked Interferometry

The focus of this chapter is to investigate a continuous-wave (c.w.) approach to measuring B/A based on existing interferometer techniques. This was achieved by developing a novel mode locking scheme based on phase-lock technology to capture liquid modes within an interferometer cavity. The implementation of this scheme is discussed in two parts. The first part investigates the design and construction techniques required to build a double disc interferometer. This begins by formulating a practical design approach for developing the interferometer cell based on a consolidation of literature reports and experimental observations. Investigation of prototype cells resulted in the modular design and construction of a small volume interferometer. The second part of this chapter details the design of a c.w. phase locked loop electronic lock-in system. The novel ability for phase lock to track changes in sound velocity is analytically examined and a theoretical study of the system behaviour is expressed using linear frequency analysis. Classic control theory was adopted to synthesise practical electronic systems and identify loop response characteristics.

Having built the interferometer cell and lock-in instrumentation, B/A was measured using water as a test liquid for several acoustic modes spanning the fundamental PZT resonance. Fluctuations in B/A were carefully examined and aspects of experimental error considered. A phenomenon involving frequency pulling was identified and is discussed in detail, defining frequency boundary limits under which continuous wave mode locking may operate. Using liquid modes within this constraint, several test liquids were measured and are tabled together with similar measurements reported in the literature.

5.1 Developing an Acoustic Interferometer

The double disc acoustic interferometer has been used to measure characteristics of fluids for more than a century. The Kundt tube [68] (first developed in 1874), is recognised as the first important predecessor of the acoustic interferometer, laying the foundation for many interferometer designs described in the literature today. Since 1874, the underlying principle of the interferometer has remained the same, being to 'fold' or convolute the path of propagation via multiple reflections, as a means to increasing the effective acoustic propagation distance. The interferometer cavity, which shapes the sonic field, has received much analysis in the literature [103] [66] [55] [36], with several geometries being explored including those designed for plane [18], cylindrical [61] and spherical waves [35]. However, present needs for liquid studies have led to the shaping of cylindrical acoustic cavities to accommodate longitudinal modes [35]. The reason for this is the simplified interferometer geometry and the elementary theory accompanying quasi-planar waves. This style of interferometer has found popularity in many instruments related to B/A measurement, and was subsequently adopted in this study as a test cell for evaluating continuous wave phase locking.

5.1.1 Design Requirements

The conventional acoustic interferometer resembles an electromechanical system composed of a vibrating 'source' transducer, coupled to a column of liquid. A second 'receiving' transducer is located parallel, and coaxial to the first but at the opposite end of the liquid column, facilitating a means of measuring the reflected wave. These transducers are commonly fabricated from piezoelectric materials such as quartz or PZT (Lead Zirconate Titanate), because of the simplicity in their implementation, their ready availability and their customised fabrication.

Before building an interferometer, it is insightful to consider all of the design requirements pertaining to the experiment for which it is to be implemented. Fortunately, the literature is characterised by several reports documenting numerous aspects of cell design. An examination of these reports, in context with the isentropic phase method of measuring B/A, reveals the following design considerations.

1. The piezoelectric transducer should be attached rigidly to its mounting, but not so that the quality of the resonance is appreciably reduced by undue mechanical damping [56] [91].

2. Electrical contacts should be made to the front and rear surfaces of the piezoceramic without introducing significant contact resistance or mechanical damping. Such contacts should not interfere with the propagating acoustic wave [91].

3. The sample vessel should be designed so that parallelism is maintained between the transmitter and receiver; this reduces unwanted satellite resonances [8] and added diffraction effects [35].

4. The interferometer cell should be impermeable, yet permit effortless pressurisation of the sample liquid [37, pgs 71-81].

5. Interchanging of piezoceramic transducers of varying thicknesses should be permitted. This allows the user to establish which frequency is optimal for the liquid under investigation, minimising effects such as attenuation, dispersion and diffraction.

6. The test cell should act as a 'thermal jacket' insulating the sample liquid [110, pgs 34-41] [38] [70], whilst filtering any thermal fluctuations present in the temperature bath.

7. The interferometer should be designed to accommodate measurements of pressure and temperature of the sample liquid.

5.1.2 Early Experimental Investigations

As a preliminary means of understanding interferometry, an existing test cell was utilised for investigative purposes. The test cell, designed by J.F.W. Bell [9] was originally developed for Sonar research. Although the nature of the design precluded its implementation for B/A measurement, it proved exceedingly useful as an investigative tool for exploring fundamental concepts and problems associated with interferometer design.

The cell (shown in Fig 5-1) was made from a 0.5m piece of glass tubing (80mm diameter), acting as a sample vessel, enclosed by an aluminium framework. The equicrural framework consisted of three identical aluminium bars affixed equidistant from one another to two aluminium annuli. Each annulus served as a clamping structure for a 0.7mm aluminium diaphragm. The diaphragm was built by gluing [21] one face of a 15mm diameter, 700kHz (thickness resonance) PZT[1] transducer to the centre of a 100mm diameter aluminium disc. The result of this was a radially symmetric ultrasonic transducer whose resonance frequency was defined by the thickness of the PZT disc and diaphragm. Once assembled, this 'test' interferometer was filled with

[1]The piezoceramic transducers used were PZT 5, developed by MATTEK, CSIR[26]

various liquids and driven by a stable frequency synthesiser. Variations in magnitude and phase between transmitted and received acoustic signals were observed on a digital oscilloscope, and changes in frequency between resonances noted. A circle diagram plotter was used together with admittance instrumentation to evaluate transducer characteristics such as conductance and susceptance.

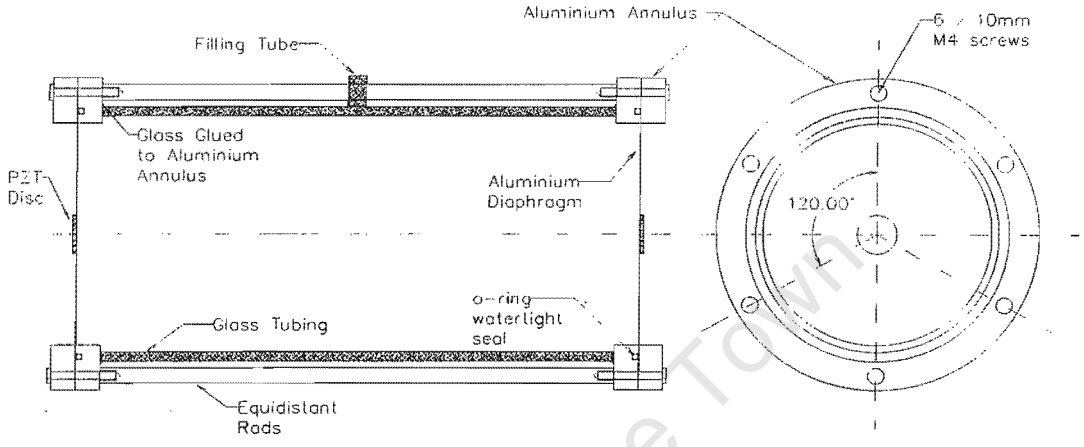

Figure 5-1: This cross sectional diagram shows the original arrangement designed by J.F.W. Bell (used for sonar analysis). Although inadequate for B/A measurement, this test cell proved invaluable in exploring interferometer concepts.

Observations of this early experimental study indicated the following :

- Parallelism between transducer faces was critical in providing a clean resonance spectrum. Misalignment between transducers manifests spurious satellite resonances as shown by Bell *et al* [8]. To compensate for this, a fine adjustment mechanism is necessary.

- Small thermal variations from ambient temperature introduced large dynamic changes in phase between the driving and receiving transducers. These thermal variations indicated the sensitivity of phase velocity to temperature and reiterated the necessity for accurate temperature control.

- The composite nature of the aluminium-PZT diaphragm revealed unique mechanical modes, which couple to existing resonant modes of both the PZT and water, producing a complex admittance and phase spectra. The task of isolating acoustic modes from mechanical modes proved arduous, signifying the need for a simple transducer mechanism.

- The sample vessel required an excessive 7.5 litres to fill. The weight of the liquid caused

the transducer diaphragm to bend resulting in an increase in path length. Velocimetry measurements of different density liquids resulted in a re-calibration of path length with each new liquid. By using solid transducers (i.e. no diaphragm) and reducing the size of the sample volume, this problem could be alleviated. A smaller sample volume would also reach thermal equilibrium quicker and facilitate measurement of small volume biological mixtures [111].

- The test cell required careful filling. Any turbulence in the filling process caused air bubbles to be infused in the liquid, resulting in a change in phase velocity [14]. In addition trapped bubbles interacted with the sound field causing a complex acoustic spectrum.

- Certain sample liquids exhibit large acoustic absorption, resulting in an almost unidentifiable acoustic signal being observed at the receiving transducer. This effect is more pronounced at acoustic modes further away from the PZT fundamental resonance. A smaller (volume) interferometer is necessary to accommodate for liquids with large acoustic absorption.

5.1.3 A Prototype Interferometer

Based on early experimental findings and design techniques set out in the literature [35] a three compartment interferometer cell was developed. This prototype cell is shown schematically in Fig 5-2. An observation of this schematic shows that compartments 1 and 3 are air filled, leaving compartment 2 as the 'sample vessel' holding the liquid under investigation. Two PZT discs were used, each was 50mm in diameter and fully electroded on both surfaces. Both had an approximate thickness resonance of 700 kHz. The discs, which were glued between the relevant compartments, form a water-tight seal. Pressurisation of the rig was achieved through the simultaneous pressurisation of each compartment with the intention of eliminating any pressure gradient across the disc. Electrical excitation was attained with minimal mechanical interference, by utilizing a 'hook' shaped platinum contact attached to a BNC connector. The radiating face for the transducer was electrically grounded to the brass housing of the rig. Air backing of each disc facilitated a reduction in backside radiation, whilst maximising the electroacoustic coupling of the transducer [77].

The physical design of the rig was modular, promoting a means of dismantling (for cleaning purposes) without the need to remove transducers. The benefits of such a design include the simplicity in substituting modules (e.g. different length sample vessels) and the flexibility in

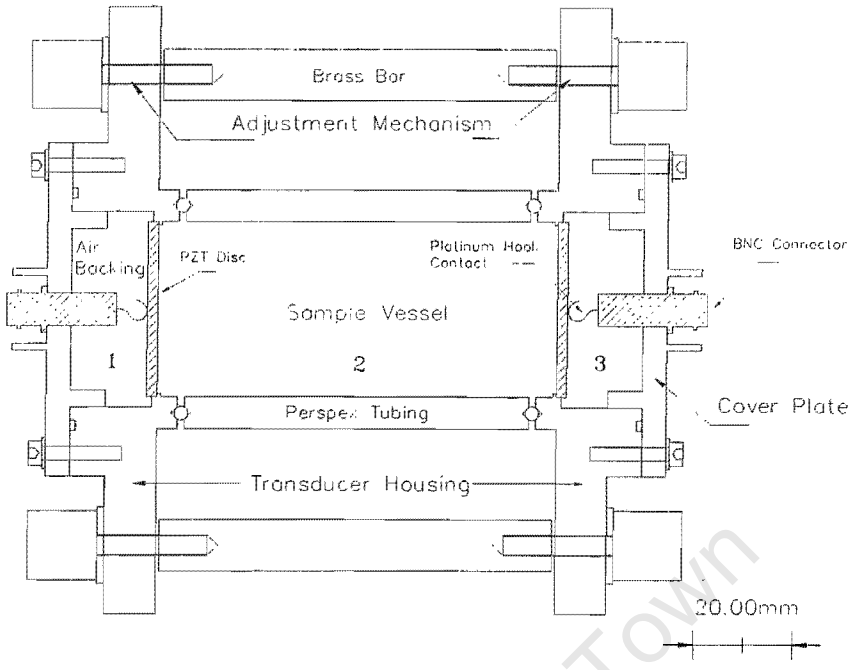

Figure 5-2: A cross section schematic of the second prototype interferometer (scale shown). From the schematic the three compartment modules are visible, together with the two glued PZT transducers. The acoustic path length equals 8 cm and the liquid volume is 157 cm^3

redesign (section 5.1.4). Four modular components were used in the design (Fig 5-2), each of which is described in detail below.

1. *Sample Vessel* : Constructed from a single piece of perspex tubing (10mm thick), this cylindrical vessel provided a housing for the sample liquid and was capable of withstanding an excess pressure of ±800kPa. Perspex was chosen for its translucent and thermal insulation properties, enabling visual inspection for bubbles once the vessel was filled. Variations in length of this module permitted experimentation of different sample volumes. Three holes were drilled into the vessel permitting pressurisation, pressure sensing and temperature sensing.

2. *Transducer Housing* : The transducer housing was designed to hold a 50mm diameter PZT disc. Each disc was glued in place using two part conductive epoxy resin. The housing provided a watertight electrical feedthrough for the transducers, enabling both transducers to be air backed.

3. *Cover Plates :* A circular brass cover plate was used to seal the transducer housing. The function of this plate was to provide an electrical feedthrough to the transducer which

would be both water and pressure tight. A tapped hole retaining a male BNC connector was used for this purpose. A length of silicon tubing was attached to the outside of the plate extending outside the water bath. This tubing provided a water tight connection to the interferometer. Each cover plate had a pressure connector enabling compartments 1 and 3 (see Fig 5-2) to be uniformly pressurised.

4. *Adjustment Mechanism* : A similar clamping mechanism to that used by Bell (section 5.1.2), was implemented in this design. Three equidistant brass bars were employed to maintain parallelism between transducer housings. Fine parallel adjustment was achieved by using three micrometer-threaded bolts. These bolts provided the necessary compression of the o-rings between the sample vessel and the transducer housing, holding the cell together whilst facilitating these adjustments.

   Once assembled, the interferometer was filled with a sample liquid and immersed in the temperature controlled water bath (outlined in Chapter 4), providing an isothermal system on which c.w. mode locking could be developed.

   Fine parallel adjustment was achieved by driving the transmitter with a pulse train and recording the received signal on an oscilloscope. The signal amplitude of the driving signal was sufficiently weak so as not to excite standing waves. Parallel adjustment was achieved by maximising the signal amplitude at the receiver through fine adjustment of the three bolts. Parallelism was assumed at maximum receiver signal amplitude.

Experimental Observations and Results

Although many of the experimental observations cannot all be included in this document, the following investigations with bearing on B/A measurement are discussed briefly below.

- A network analyser was used to examine the resonance behaviour of each of the 50mm diameter PZT 4 discs purchased from the CSIR [26]. Fifty discs were examined, revealing only a few pairs with co-incident resonant frequencies. In addition it was found that individual discs exhibited a multitude of spurious resonances, possibly associated with poling anomalies[2]. Two similar discs were used for this study; however attempts at measuring B/A proved unsatisfactory, with liquid modes interacting with spurious PZT

[2]Variations in admittance of the PZT discs are most commonly a result of inaccurate poling techniques implemented by the manufacturer. As a result of this, tighter tolerance discs produced by PI Ceramics were used in the final interferometer design.

modes causing a nonlinear phase interaction. It is evident that the spectral purity of transducers is of paramount importance to measuring B/A.

- A pulse-superposition method (detailed in Chapter 3) was implemented to measure the absolute sound velocity for FC43 and FC75. Water was used as a calibration liquid to define precisely the path length between transducers. The pulsed chirps were generated using an arbitrary function generator. This instrument allows a user to accurately dial in the burst and carrier frequency to within a fraction of a Hertz. The transmit and received pulse pairs were superimposed using a 10MHz digital oscilloscope, facilitating an accurate determination of the time of flight.

- A simple phase locked system was designed, enabling a predefined acoustic mode to be locked within the interferometer cell. A detailed discussion of this will follow; however it should be noted that attempts at measuring B/A using the prototype interferometer were unsuccessful on two accounts. The first was directly related to the PZT discs, with liquid modes being excited and pulled by spurious 'satellite' resonances introduced by the transducer. The second was a design flaw in the interferometer, with a pressure instability encountered within the cell during the isentropic pressure jump process.

- A technique exploring collocated control[31] was adopted as a means of cancelling the spurious effects caused by the transducers. By utilising self excitation of the driving disc, it was hoped that nonlinearities of the discs could be cancelled; however this proved inadequate and was eventually abandoned.

- The phase locked loop was successful in mode locking, achieving an extremely fine resolution of differential phase velocity (see results). Fluctuations in temperature within the sample liquid could be easily tracked by the loop as a function of frequency. It was found that a good indication of isothermal conditions could be achieved by observing the fluctuation in frequency of the VCO.

- Inductance tuning was examined by exploring series and parallel methods of tuning out the electrical capacitance associated with a PZT transducer. It was found that careful tuning increases transducer bandwidth and efficiency, but is not essential to the measurement of B/A. Additionally, parallel tuning of any kind introduces a filter response to the phase locked loop, injecting a frequency dependent phase offset which contributes to the uncertainty in measuring B/A.

Conclusions

The experiments performed on the prototype interferometer indicated the validity of phase locking as a means of measuring B/A; however, disc nonlinearities coupled with a fundamental design flaw precluded the accurate evaluations of B/A in the final experiment. The reason for this can be attributed to the depressurisation process. Although each of the three compartments of the test cell were pressurised simultaneously so as to eliminate a pressure difference across the PZT disc, the depressurisation of each compartment did not occur at the same rate. The reason for this can be explained by the same concept used for generating a pressure delay (see Chapter 4). The volume or 'capacitance' of compartments 1 and 3 are the same, but compartment 2 has a capacitance relative to the volume of air in the perspex viewing tube. Since the depressurisation occurs more quickly in compartment 2 than in compartments 1 and 3, the transducers bend inward and then slowly outward during the depressurisation process. This slight change in path length is largely visible in the measurement of B/A where changes in sound velocity are typically resolved to 1 part in 10^6. Although a fine needle valve resolved this equalisation problem by introducing a variable pressure resistance to the capacitance of compartment 2, the measurement of B/A became a function of the accuracy with which the pressure delay systems could be matched, providing an inadequate solution for this study.

5.1.4 A Small Volume Interferometer

The prototype interferometer had to be completely redesigned in order for B/A to be measured with any degree of certainty. A result of this redesign process was the conception of a 'small volume interferometer'; a scaled-down version of the prototype cell, capable of overcoming prior difficulties whilst adhering to previously determined design constraints. Fig 5-3 shows a photograph of the complete measurement rig following the redesign process. This final rig was developed using the existing shell of the prototype interferometer acting as both an isothermal jacket and uniform pressurisation vessel for the small volume interferometer held within. The interferometer was configured on the same modular principles used for designing the prototype. Notwithstanding this, the interferometer was designed without air backing, resulting in backside radiation from both transducers, coupled with damping from the surrounding fluid. The trade off for this was the fact that the interferometer, including the sample liquid, could be uniformly pressurised and depressurised. This was achieved by immersing the interferometer into a pressure vessel containing silicon oil. The silicon oil was chosen for its electrical insulation

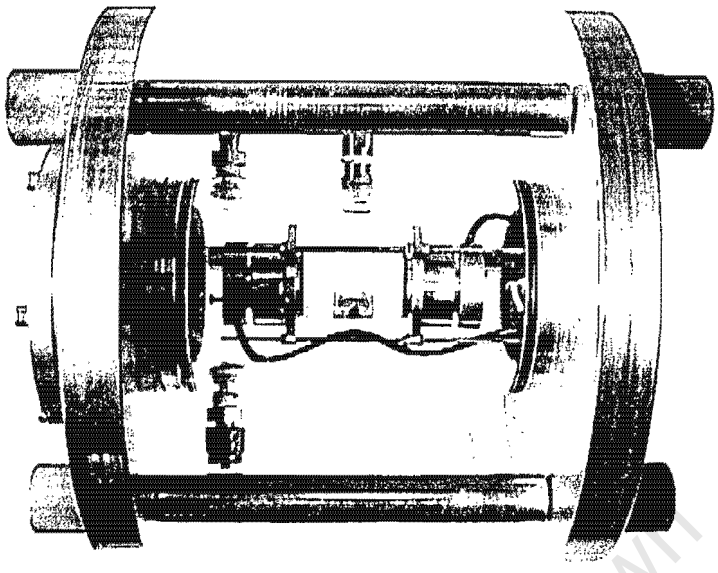

Figure 5-3: A photograph of the complete measurement rig, consisting of both interferometer and pressure vessel (The scale of this photograph is not 1:1).

and thermal conduction properties. Pressurisation of the sample liquid was performed by pressurising the silicon oil, which in turn pressurised the interferometer unit. Any pressure difference across the PZT discs was eliminated by two thin teflon diaphragms which were used as pressure diaphragms enabling the sample fluid to be effortlessly pressurised. Following the designs of Law [71, pgs 65-79] and Everbach [37, pgs 75-81], this concept of creating equal pressurisation whilst maintaining isothermal stability proved to be an effective remedy to the problem of measuring B/A experienced in previous sections. Any backside radiation was reduced by including glass wool at both ends of the interferometer, whilst the small path length of the interferometer facilitated measurement of high attenuation liquids.

Figures 5-5 and 5-4 show both a schematic cross section and a photograph of the interferometer cell. From these figures it can be seen that the cell was designed in various component modules, a functional description of which is detailed below.

Transducers

The transducers used were sintered PZT 5 discs, 20mm in diameter, obtained from PI Ceramics [92]. Each one of these disc pairs was designed with wrap around electrodes and an active centre spot of 12mm. Three pairs of transducers were examined in this study for effects of

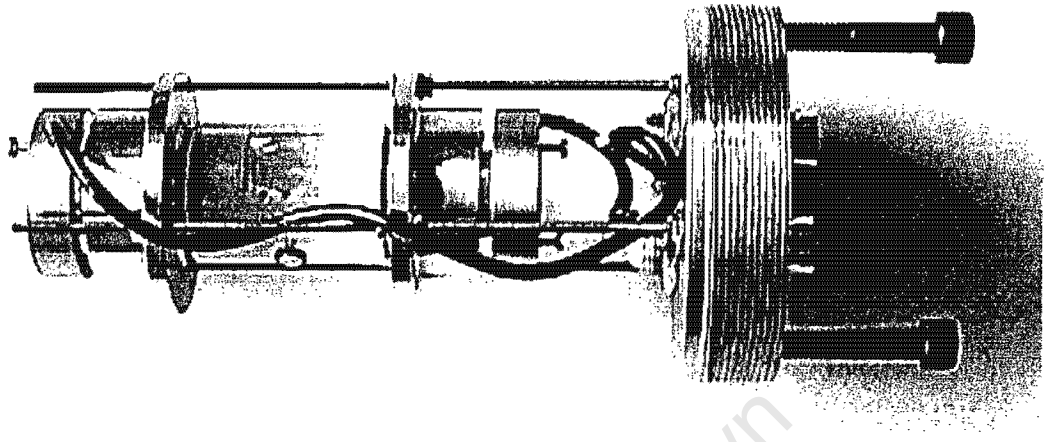

Figure 5-4: This photograph shows the small volume interferometer attached to a threaded plate used to secure the cell inside the pressure vessel

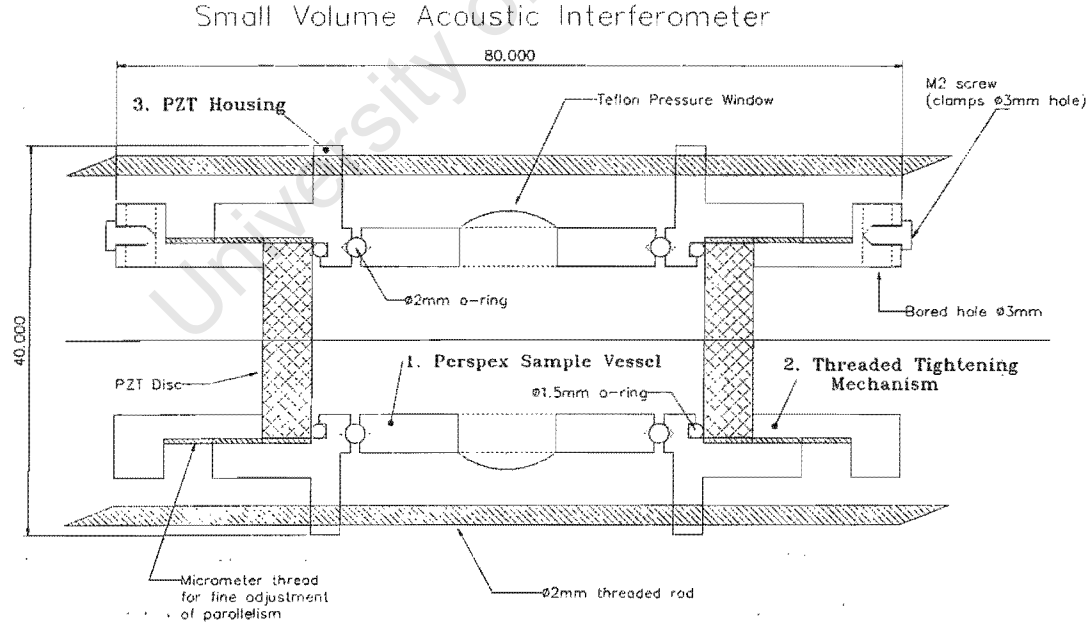

Figure 5-5: A cross section of the final small volume interferometer design. The acoustic pathlength equals 4cm and the liquid volume is 7.25 cm^3

diffraction and attenuation on mode locking. The thickness resonances used were 500kHz, 1MHz and 5MHz.

Each disc was excited using a thin hook shaped platinum electrode, providing a mechanically undamped contact whilst promoting a simple means of exchanging discs. The wrapped electrode of the PZT was electrically grounded by the clamping mechanism (Fig 5-6 'A'). By grounding the wrapped electrode the PZT disc is shorted at its perimeter, minimising mechanical coupling between the transducer housing and the disc (see collocated control[31]) and facilitating a clean production of longitudinal waves.

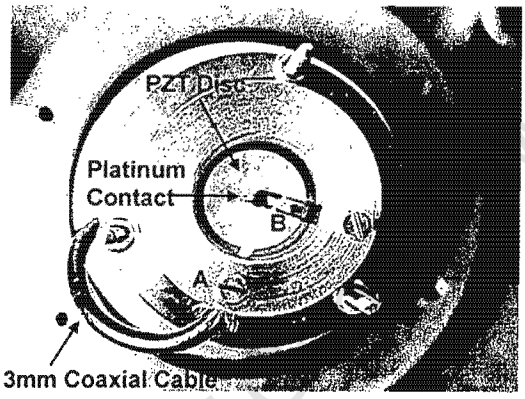

Figure 5-6: A photograph depicting the transducer housing mechanism. The active electrode of the PZT disc is excited using a thin platinum hook contact. The hook was attached to an insulated conductor which was soldered to the core of a miniature coaxial cable. The grounded braided of this cable was clamped using a 2mm screw at point 'A' forcing the brass housing to act as a ground plane. Once tightened the housing completes the circuit making contact with the wrap around electrode of the PZT.

Transducer Housing

The transducer housing was constructed using two threaded sections. Dissimalar metals were used to avoid adherance or sticksion once tightened. The first was made from 304 stainless steel and designed to house a 20mm PZT disc, providing a seal between the sample liquid and surrounding silicon oil with a 1mm o-ring. The disc once located was clamped using a second, micrometer threaded, cylindrical brass section. This section was carefully designed to secure the PZT disc with minimal mechanical damping. Electrical feedthough was achieved by boring two orthogonal 3mm holes into the end of the brass cylinder (see Fig 5-6). A miniature coaxial cable was threaded through one of the holes, enabling the section to be earthed. The second

hole was used to secure a hook shaped platinum contact (with ends insulated from the brass). Both contacts were held in place by 2mm threaded screws.

Sample Vessel

Fig 5-5 shows the cylindrical sample vessel designed with a 15.2mm diameter and 4mm wall thickness. This vessel was made from perspex tubing and provided a housing for the sample liquid. Perspex was chosen for its translucent properties, enabling visual inspection for bubbles once the vessel was filled. Variations in length of this module permitted experimentation with different sample volumes. Two 10mm holes were drilled into the vessel and sealed with a thin teflon membrane. This supported effortless pressurisation of the sample fluid. A third 2mm filling hole was drilled orthogonal to the pressure membranes enabling the vessel to be filled using a syringe. This hole was sealed using a threaded screw and an o-ring washer.

Adjustment Mechanism

The interferometer framework consists of three stainless steel 'threaded rods' attached to a threaded brass plate and spaced 120° apart (see Fig 5-4). The plate forms an end cap of the pressure vessel and enables the interferometer assembly to be securely mounted within the pressure rig.

The interferometer was assembled by clamping the sample vessel between the driving and receiving transducer housings. The driving transducer housings were securely clamped in place by six stainless steel nuts threaded onto the 'threaded rod' framework. Fine parallel adjustment was achieved by tweaking the three remaining nuts used to clamp the receiving transducer housing, which effectively compresses the two watertight o-ring seals between the three modules.

Pressure Vessel

The pressure vessel as shown in Fig 5-3 consists of the existing shell used for the prototype interferometer, with two changes made for simplifying the filling process.

A conical vault (see Fig 5-7) was designed with tapped centre hole to enclose the pressure vessel from one side, with the other side enclosed by the interferometer assembly. The centre hole was used to fill the vessel with silicon oil, whilst the conical nature of the vault ensure the removing of all air bubbles from the pressure vessel. Together with this, a new cover plate was

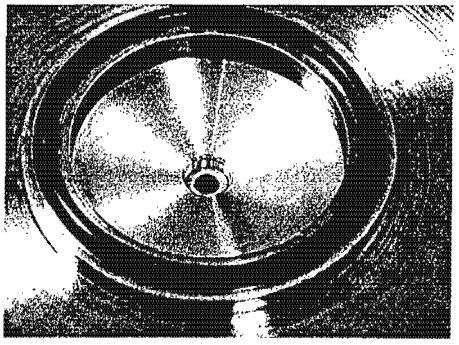

Figure 5-7: A photograph of the conical vault used to enclose the pressure vessel is shown. The cone shape was designed so that bubbles could easily be removed from the pressure chamber during the filling process. A threaded plug was used as a final seal of the vault.

built to seal the vault section. Temperature and pressure sensors were used from the existing initial prototype design.

5.2 Implementing the Nature of Phase Lock

Continuous wave phase-locking is a common element in electronic design, however its application to B/A measurement is novel and warrants formal discussion. The principle of phase locking is reviewed here, its application to continuous wave mode locking is examined, and its ability to be used as a means of tracking changes in sound velocity is explored. An analysis of the loop performance and electronic synthesis is given together with several experimental measurements of B/A.

5.2.1 Definition of a Phase Locked Loop

"A phase locked loop (PLL) is an electronic circuit that controls an oscillator so as to maintain a constant phase angle relative to a reference signal."[99]

The block diagram given by Fig 5-8 outlines the fundamental elements of a phase locked loop. From the figure, it can be seen that the output frequency f_{out}, tracks the input frequency f_{in} by using phase as a feedback mechanism. Typically, the phase difference between f_{in} and f_{out} is measured by a phase detector. The output from the phase detector θ_e is a DC voltage which is conditioned by a loop filter and applied to the control input of the voltage controlled oscillator (VCO). Once the loop is locked, the control voltage v_c maintains the output frequency of the VCO to exactly equal the average input frequency f_{in}.

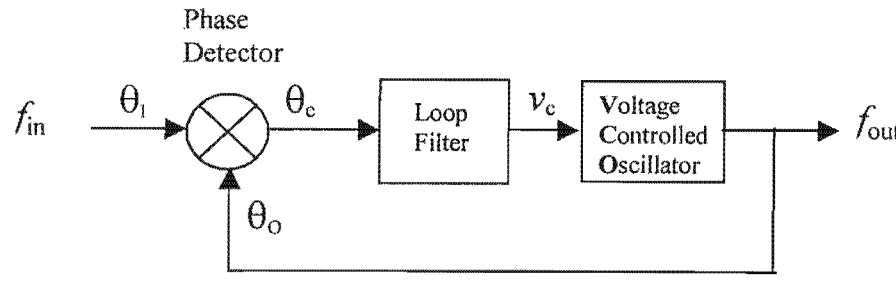

Figure 5-8: A block diagram showing the fundamental elements of a phase locked loop. The phase of the input signal, θ_i, is compared to the phase of the output signal, θ_o, by means of a phase detector. The voltage output from the phase detector, θ_e (being a DC representation of the phase error) is conditioned using a loop filter and applied to the control input of the VCO. This loop causes the input signal to be 'regenerated' by the output signal as the output frequency, f_{out}, always tracks the input frequency, f_{in}.

5.2.2 Tracking Changes in Sound Velocity with Frequency - an Examination of Transmission Phase Locking

Isentropic phase measurement of B/A demands an ability to resolve incremental change in sound velocity associated with a pre-defined step in ambient pressure. In addition, the isentropic constraint requires this measurement to be achieved as fast as possible[3]. Both pre-requisites define the ability with which B/A can be resolved, indicating the need for a control system capable of tracking incremental changes in sound velocity with negligible error and a sufficiently fast response time. The control system presented here uses the ability of an analogue phase locked loop to accomplish both of these tasks. For reference, the author has labelled this technique *Transmission Phase Locking* (TPL).

The broad concept behind TPL is similar in concept to methods used in transmission spectrometry [80], utilizing the nature of a phase locked loop to trap an acoustic mode within an interferometer cavity. Once the mode is 'locked' within the cavity, any subsequent change in sound velocity will cause a change in wavelength ($\Delta c = f\Delta\lambda$). This change in wavelength (represented as a change in phase) is then used in feedback to adjust the driving frequency in order to resume the lock condition. Following this analogy any change in sound velocity can be interpreted as a change in driving frequency.

By using the lock-in ability of a phase locked loop to maintain a constant (or zero) phase error between two signals, it is possible to trap any liquid mode within an interferometer cavity.

[3]A typical time frame of two seconds is stipulated for this study as defined in Chapter 4 and Appendix A.

The setup for such a system is shown in figure 5-9. By applying the VCO signal (V_{in}) to the

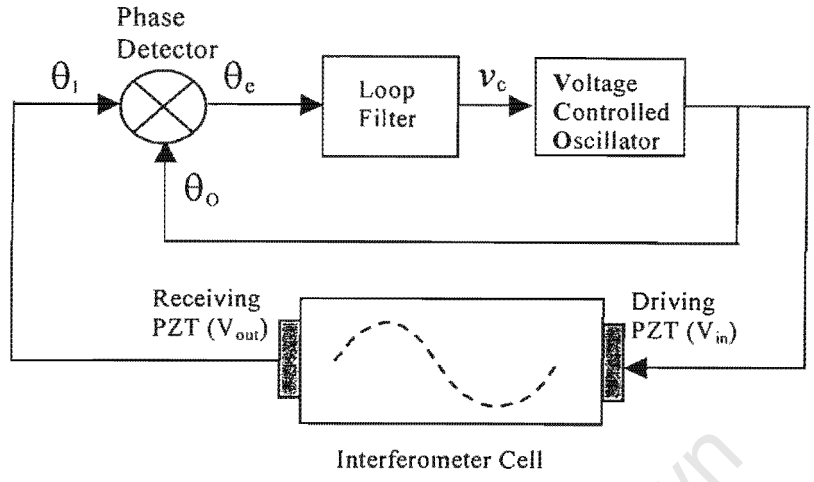

Figure 5-9: This block diagram shows how a phase locked loop may be adapted to trap an acoustic mode within an interferometer cavity. By phase locking the driving voltage V_{in} to the received voltage V_{out}, the transducer pair maintain an acoustic mode, independent of path length.

driving PZT disc and using the signal (V_{out}) developed on the receiving PZT disc as a reference signal, the phase locked loop inherently maintains the driving signal in phase with the reference signal, thereby 'mode locking' the interferometer cavity. The maximum lock-in range for the loop is typically determined by the bandwidth of the VCO.

Observation of the transmission phase locked loop (TPLL) (shown in figure 5-9) reveals a resemblance to negative feedback control. It is therefore reasonable to apply linear control theory to the design of the loop filter. A pre-condition for this is the necessity for all elements other than the loop filter to be characterised. Since both VCO and Phase Detector can be defined as active circuit elements, however the interferometer model still remains to be determined.

A review of interferometer equivalent circuits reveals numerous models which depend on interferometer design and function. A more accurate representation of this study's interferometer characteristics can therefore best be determined through experimental observation. Under this premise, a HP 4195A network/spectrum analyser was used to plot the transfer characteristics of the interferometer cell, treating the transducer pair as a two port network. The resultant S-parameter gain plot S_{12} for this system, spanning the first thickness mode of the transducers, is given in Fig 5-10.

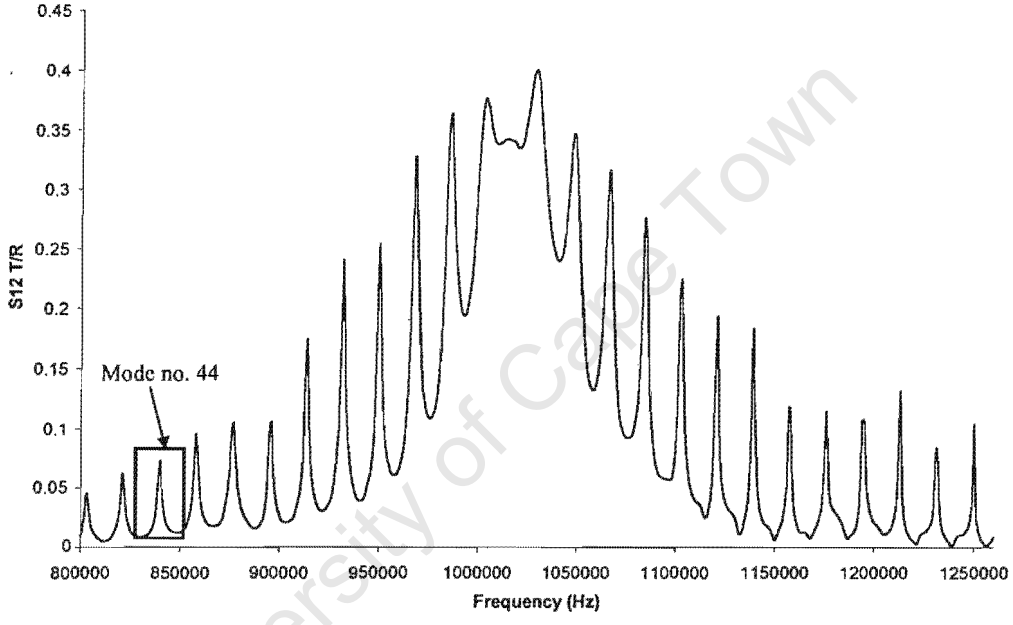

Figure 5-10: A plot of the S-parameter transfer characteristic S_{12} across the interferometer filled cavity. Each peak represents an acoustic water mode superimposed upon the piezoelectric driving mode (fundamental thickness resonance ±1Mhz). The boxed window is centred at f_{ac}=±840kHz with a width typical of the bandwidth constraint chosen for TPL.

It is evident from the gain plot that the local maxima represent acoustic modes superimposed upon the driving mode (or thickness resonance) of the PZT discs. An equivalent electromechanical circuit for this spectrum is derived from acoustic transmission line theory developed by Mason *et al* [76] [77] [75]. Based on this theory, an equivalent electrical network for the interferometer system is shown in Fig 5-11.

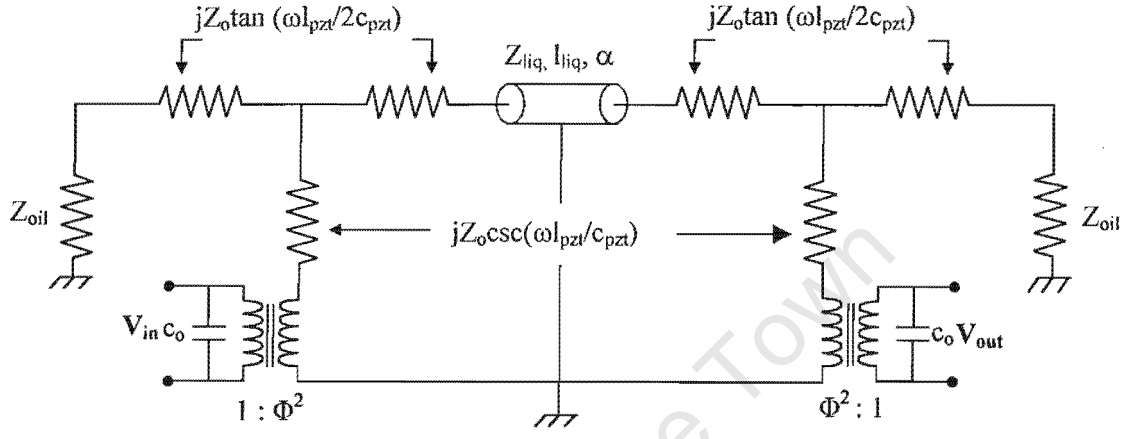

Figure 5-11: An electromechanical equivalent circuit for a liquid filled ultrasonic interferometer, based on network theory developed by W.P. Mason[76]. The liquid transmission line can be expressed as an equivalent T-network with series density impedances shunted by series viscosity and thermal conductivity elements (see Chapter 3). The voltage is coupled mechanically via the electrical capacitance to the liquid using a transformer with a turns ratio Φ defined by the electromechanical coupling factor k. Z_{oil} and Z_o represent the characteristic impedances for silicon oil and the PZT respectively.

The complex nature of this network is due to its broadband electro-acoustic analysis. If we confine the bandwidth of this model by defining boundary conditions to the control loop, the circuit shown in Fig. 5-11 can be greatly simplified. The conditions under which the bandwidth may be limited are summarised as follows:

- The resonance behaviour of the interferometer is confined to the fundamental 'thickness mode' of the PZT discs.
- Transmission phase locking is based on the phase deviation of an isolated acoustic mode. This necessitates sufficient bandwidth to enforce phase lock, yet exclude interference from neighbouring acoustic modes.
- The frequency deviation inferred by the change in ambient pressure under B/A measurement should be well within the bandwidth defined above.

The last two conditions are determined by the physical nature of the liquid under investigation and can be resolved practically through experimental observation of the transfer function S_{12}. For example, if we re-examine the transfer function S_{12} (Fig. 5-10) for an interferometer cavity filled with water, the outlined window encloses a single liquid mode representing the bandwidth constraints for the loop. This window, enlarged and shown in gain and phase form in Fig 5-12, provides both gain and phase information between the driving and receiving transducers.

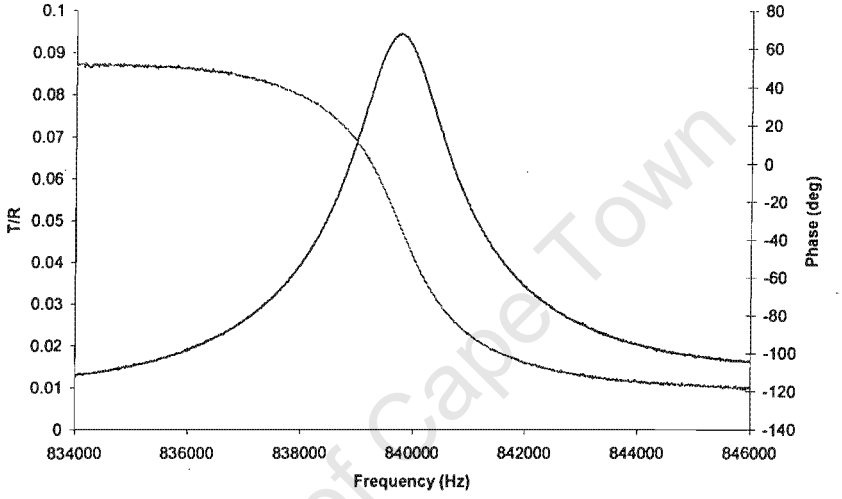

Figure 5-12: A detailed plot S_{12} of the band limited windowed area defined in Fig. 5-10. Both gain and phase are plotted to show the similarity with a series LCR circuit.

On immediate inspection of Fig 5-12, it is apparent that the response represents an electromechanical equivalence of a series tuned circuit; however a detailed examination reveals a phase offset of some 30°, attributable to the electrical nature of the PZT capacitance c_o. Mason [76] describes an effective means of eliminating this offset by tuning out the capacitance c_o with a parallel inductance. A more subtle approach is achieved by subtracting a precision offset voltage summed to the output of the phase detector (see Fig. 5-13) i.e. locking of quadrature with a defined offset. The technique eventually adopted for this study was to utilise the nature of the offset as a means of linearising the phase detector (to be discussed later).

A simplified equivalent network characterising Fig. 5-12 is given in Fig 5-13 together with the characteristic block diagram necessary for control loop calculations.

Having modelled the interferometer cavity as a simple series LCR network with the driving signal representing the voltage and the receiving signal as the current, it became possible to

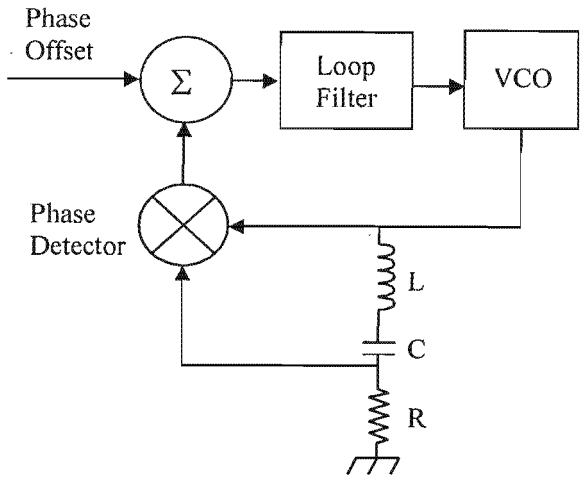

Figure 5-13: A narrow bandwidth simplified network model for the transmission phase locked loop. The LCR circuit represents the electromechanical equivalence of a single acoustic mode. The current is a measure of the received signal with applied voltage representing the driving signal. The phase lag is summed as constant offset following the phase detector.

provide a theoretical understanding of loop behaviour under various conditions and ultimately to facilitate the final circuit design.

5.2.3 A Theoretical Approach to TPL

The amplitude and phase responses for the band limited electromechanical equivalent LCR circuit corresponding to Fig. 5-12 is synthesised in Fig 5-14 using the circuit simulation program PSpice. A conventional analysis yields the following simple relationships for current, I and phase, ϕ:

$$Z = j\omega L + R - \frac{j}{\omega C} = \frac{\omega RC + j(\omega^2 LC - 1)}{\omega C} \tag{5.1}$$

$$I = \frac{V}{Z} = \frac{V\omega C}{\omega RC + j(\omega^2 LC - 1)} \tag{5.2}$$

$$\mathrm{Re}\{I\} = \frac{V\omega^2 C^2 R}{\omega^2 R^2 C^2 + (\omega^2 LC - 1)^2} \tag{5.3}$$

$$\mathrm{Im}\{I\} = -\frac{V\omega C(\omega^2 LC - 1)}{\omega^2 R^2 C^2 + (\omega^2 LC - 1)^2} \tag{5.4}$$

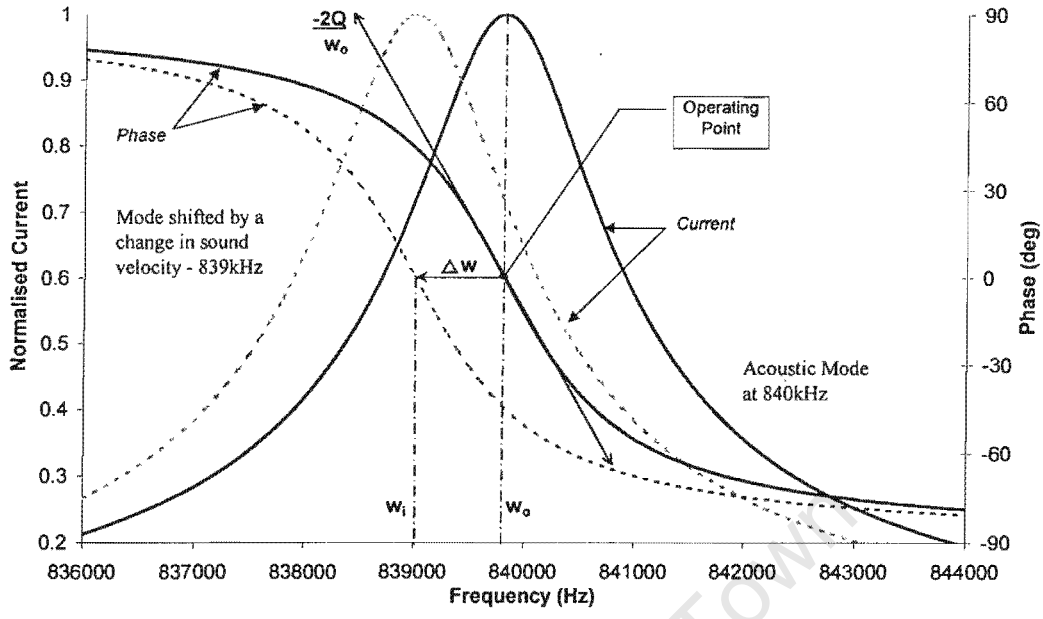

Figure 5-14: A synthesised amplitude and phase response for a series LCR circuit, both before and after a change in phase velocity. The linear region for the phase is depicted by the tangential plot of the slope at the operating point ($-\frac{2Q}{\omega_o}$). The shift in frequency from resonance, ω_o is given by ω_i with $\Delta\omega = \omega_i - \omega_o$

$$\phi = \arctan \frac{1-\omega^2 LC)}{\omega CR} \simeq \frac{1-\omega^2 LC)}{\omega CR} \tag{5.5}$$

Assuming small angle approximation for the phase [81], the slope of the phase at resonance can be determined through differentiation and substitution of $\omega_o = \frac{1}{\sqrt{LC}}$ as follows:

$$\left.\frac{\partial\phi}{\partial\omega}\right|_{\omega=\frac{1}{\sqrt{LC}}} = \left[-\frac{1}{\omega^2 CR} - \frac{L}{R}\right]_{\omega=\frac{1}{\sqrt{LC}}} \tag{5.6}$$

$$\frac{\Delta\phi}{\Delta\omega} = -\frac{2L}{R} = -\frac{2Q}{\omega_o} \tag{5.7}$$

where Q is the standard expression given for the quality factor of a series tuned resonant circuit [54]:

$$Q = \frac{\omega_o L}{R} \tag{5.8}$$

When the equivalent electromechanical circuit is driven by the loop at resonance the loop operates about a null point corresponding to the maximum slope of equation 5.6. If we consider

that a change in phase due to a change in sound velocity will be tracked immediately by the loop, it is plausible to acknowledge that the differential change in phase will always be small, and defined by the speed at which the loop can track the disturbance. This assumption both justifies the small angle approximation used in equation 5.5 and defines *ipso facto* a linear region under which TPL may be analysed.

Phase Detector

The sinusoidal output of the voltage controlled oscillator is used to generate the driving signal resulting in a similar phase shifted sinusoid at the receiving transducer. The driving signal may therefore be described as $V_d = E_i \cos(\omega_i t + \phi_i)$ and the output from the receiving transducer as $V_r = E_o \cos(\omega_i t + \phi_o)$. If a multiplier is used as a phase detector, the multiplied output of these two signals V_p will result in:

$$V_p = \frac{1}{2} K_m V_d V_r \{\cos(\phi_o - \phi_i) + \cos(2\omega_i t + \phi_o + \phi_i)\} \tag{5.9}$$

where the term K_m is used to describe the gain of the multiplier. This complex signal consists of a double frequency term added to a DC offset. The DC offset is a cosine representation of the phase difference and is usually extracted by removing the double frequency term with a low pass filter to give

$$V_p = \frac{1}{2} K_m V_d V_r \cos(\phi_o - \phi_i) \tag{5.10}$$

$$= \frac{1}{2} K_m V_d V_r \cos(\Delta\phi) \tag{5.11}$$

which may be considered linear in the region $\Delta\phi = \frac{\pi}{2} + n\pi$ for $n \in \mathbb{Z}$. Following this analogy, the output from the VCO should be phase shifted by $\frac{\pi}{2}$ to maintain an approximate linear relationship for frequencies close to the acoustic resonance. Conventional phase locking techniques synthesise a $\frac{\pi}{2}$ phase shift by using one of two approaches: either a second (fast-response) PLL is used to regenerate the VCO with a $\frac{\pi}{2}$ phase shift (quadrature phase locking), or a broad band $\frac{\pi}{2}$ phase shifting network is used. Typically the phase shifter is implemented following the VCO and directly before the phase detector. Considering the inherent phase offset observed in Fig 5-12, TPL favours the latter approach, adopting the existing electro-mechanical network (interferometer filled cavity) as part of the $\frac{\pi}{2}$ phase shift network; additional phase is summed as a DC offset to the output of the phase detector. Notwithstanding this the following should

be noted:

1. At the expense of signal power, phase lock was easily established and maintained off resonance without the need for additional phase injection.

2. The sign of the slope $\frac{\Delta v}{\Delta \phi}$ between $-\pi$ and 0 remains monotonic even though the loop is locked off resonance, therefore, provided the change in phase ($\Delta\phi$) is smaller than the phase offset, the mode locking action is not compromised by the nonlinearity of the phase detector.

By redefining the gain as $K_p = \frac{1}{2}K_m V_d V_r$ and adopting a small angle approximation[4], equation 5.10 can be redefined [54] as the following linear expression:

$$V_p = K_p \cos(\Delta\phi - \frac{\pi}{2}) = K_{ph} \sin(\Delta\phi) \quad (5.12)$$

$$\simeq K_p.\Delta\phi \quad (5.13)$$

Voltage Controlled Oscillator

The choice of VCO is typically confined to two general classes of oscillators: the relaxation oscillator (astable multivibrator) and the resonant oscillator. Both classes have been used extensively in conventional phase lock design. The selection of oscillator (VCO) to be used for TPL requires careful consideration of oscillator properties. Although linear frequency response needs to be considered for accurate loop analysis, the need for spectral purity is of paramount importance to the accuracy with which B/A can be measured. By illustration consider the acoustic mode shown in Fig 5-12, resonant at approximately 840kHz. If we wish to measure B/A for water[5] using TPL with a prescribed accuracy of less than 1% we need to be able to resolve 1.44Hz in 840kHz or conservatively 1 part in 10^6. Ideally the output frequency ω_o for a VCO (given an ideal DC input voltage) should be equivalent to a single dirac delta function at ω_o. However, in practice this frequency is typically modulated by thermal and shot noise [108] originating from within the oscillator, yielding a spectral width inversely proportional to the Q of the oscillator.

[4]For the Maclaurin series, $\sin x = \sum_{n=0}^{\infty} (-1)^n \frac{x^{2n+1}}{(2n+1)!}$, the truncation of the expansion at $\sin x = x$, introduces an error proportionate to the size of x; ie. the smaller the value for x, the quicker the series converges. By example, an error of approximately 1% is typically reached at an x value of 14°.

[5]Measurement is taken at 30°C with an excess pressure of 150KPa. Calculation based on a B/A=5.2, ρ=995.7kg/m^3 and phase velocity of 1508 m/s[38]

In order to overcompensate for this effect we used a HP 8656 RF frequency generator with an FM input as a VCO. This frequency generator provided a linear voltage to frequency response with a spectral purity of typically 1 part in 10^8 and low harmonic distortion. A centre frequency (typically set to the acoustic resonance) is programmed together with a predefined frequency bandwidth. The gain K_v for the VCO is defined by the slope of the response in the vicinity of the resonance and can be expressed as follows

$$K_v \equiv \frac{\partial}{\partial v}(\Delta\omega_o) \tag{5.14}$$

where the deviation in resonance frequency $\Delta\omega_o$ is defined as (see Fig. 5-14):

$$\Delta\omega_o = \omega_o - \omega_i \tag{5.15}$$

By rearranging equation 5.14 we define the linear transfer function for the VCO as:

$$\Delta\omega_o = K_v(v_i - v_o) \tag{5.16}$$

where v_o represents the driving voltage at resonance (VCO centre frequency) and v_i the offset voltage.

By re-examining the driving signal $V_d = E_i \cos(\omega_i t + \phi_i)$ we observe that ω_i is a constant, with dimension in radians per second, effectively implying that frequency is the time derivative of phase, with phase being the argument of the cosine function. With this understanding we rewrite the output frequency of the VCO as follows

$$\omega_o = \frac{d(\omega_i t + \phi_i)}{dt} = \omega_i + \frac{d\phi_i}{dt} \tag{5.17}$$

and substituting equation 5.15 we obtain the following definition:

$$\Delta\omega_o = \frac{d\phi_i}{dt} \tag{5.18}$$

Recalling Fig. 5-9, the feedback element from the VCO is expressed as phase, not a change in frequency. To accomplish this conversion, we simply integrate equation 5.16 with respect to

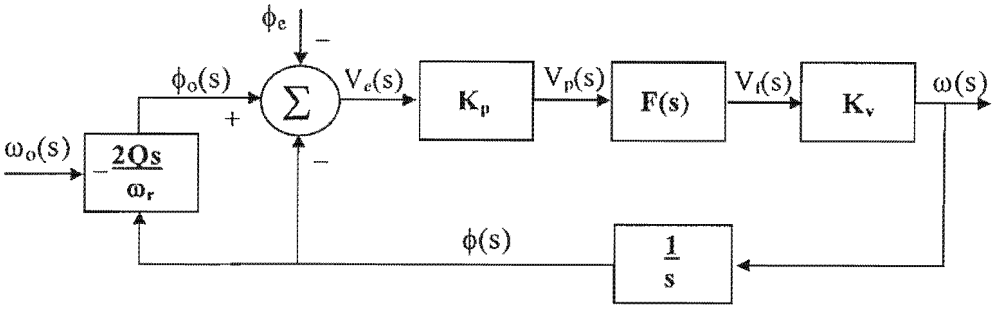

Figure 5-15: The transmission phase locked loop is depicted in the frequency domain for the purpose of linear analysis. A change in sound velocity is represented as a change in resonant frequency, defined here as $\omega_o(s)$ (the input to the loop).

time as follows.

$$\phi_i = \int \Delta\omega_o dt = \int K_v(v_i - v_o)dt \tag{5.19}$$

Linear Analysis

Having linearised the response for each element within the loop, the system may now be analysed in the frequency domain by applying the appropriate Laplace transforms (as shown in Fig 5-15). From the figure, a change in sound velocity effectively shifts the resonance frequency of the equivalent circuit from the operating point $\omega(s)$ to $\omega_o(s)$ (see Fig. 5-14). This frequency shift results in a corresponding phase shift determined by the gradient defined in equation 5.6. With the understanding that no significant change in Q occurs during this process, the gradient may be approximated as follows:

$$\Delta\phi = -\frac{2Q}{w_r}\Delta\omega \tag{5.20}$$

where $w_r \simeq \omega_o$.

From Fig 5-15, the following series of equations may be expressed in Laplace form:

$$\begin{aligned} V_e(s) &= \phi_o(s) - \phi(s) && (5.21)\\ V_p &= K_p V_e = K_p[\phi_o(s) - \phi(s)] && (5.22)\\ &= K_p\left(-\frac{2Q}{\omega_o}\right)[\omega_o(s) - \omega(s)] && (5.23)\\ V_f &= F(s)V_p && (5.24)\\ \omega(s) &= K_v V_f && (5.25) \end{aligned}$$

Combining these expressions we can formulate the loop equations for frequency error $\omega_e(s) = \omega_o(s) - \omega(s)$ and the closed loop transfer function $H(s)$ as follows:

$$\begin{aligned} \omega(s) &= K_v F(s) K_p\left(-\frac{2Q}{\omega_r}\right)[\omega_o(s) - \omega(s)] && (5.26)\\ \omega_e(s) &= \frac{\omega_r}{2QF(s)K_pK_v - \omega_r}\omega_o(s) && (5.27)\\ H(s) &= \frac{\omega(s)}{\omega_o(s)} = \frac{2QF(s)K_pK_v}{2QF(s)K_pK_v - \omega_r} && (5.28) \end{aligned}$$

Having defined $H(s)$, we need to determine the loop filter $F(s)$ to provide low pass filtering (needed for phase detection) and adequate tracking performance (for frequency coherent output). A standard circuit used in phase lock design [33] [43] is a type 1 active filter shown schematically in Fig 5-16.

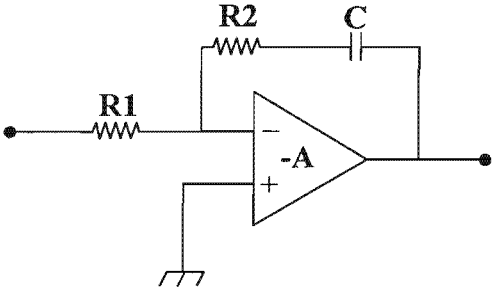

Figure 5-16: A typical lag-lead opamp filter used for loop control. The time constant for this filter is set by the respective $\tau = RC$ values, with gain defined as $A = \frac{R_2}{R_1}$. For a perfect integrator, we set $R_2 = 0$, and calculate the low pass filter time constant using $\tau_L = R_1 C$.

The transfer function for this filter is given by:

$$F(s) = \frac{-A(sR_2C + 1)}{sR_2C + sCR_1(1 + A) + 1} \tag{5.29}$$

which can be approximated [43] for large voltage gains (A) by:

$$F(s) = -\frac{s\tau_2 + 1}{s\tau_1} \tag{5.30}$$

where time constants τ_1 and τ_2 are used to represent R_1C_1 and R_2C_2 respectively.

Substituting in equation 5.29, and inverting the output to correct feedback polarity, renders the following transfer function for $H(s)$:

$$H(s) = \frac{-2Q\,(s\tau_2 + 1)\,K_pK_v}{2QK_pK_v(s\tau_2 + 1) + \omega_r s\tau_1} \tag{5.31}$$

Having established the closed loop transfer function we now need to determine the measurement bandwidth in order to calculate the filter component values. Before considering this we must examine the requirements for zero frequency error by means of the Final Value Theorem.

$$\lim_{t\to\infty} \omega_e(t) = \lim_{s\to 0} s\omega_e(s) \tag{5.32}$$

Returning briefly to the measurement process described in Chapter 4: an exponential change in ambient pressure as produced by the pressure circuit returns a similar function in sound velocity, which in turn produces an exponential change in frequency with a time constant of typically 2 seconds. It is this change in frequency that the loop must track absolutely, requiring the input frequency $\omega_o(s)$ to be expressed as the Laplace transform $\omega_o(s) = \mathcal{L}\{e^{-t/2}\} = \frac{2}{2s+1}$.

Using the loop equations 5.21 - 5.25, we calculate the following final value expression

$$\lim_{t\to\infty} \omega_e(t) = \lim_{s\to 0} \frac{s\omega_r}{2QF(s)K_pK_v - \omega_r} \frac{2}{2s + 1} \tag{5.33}$$

Implementing the active filter defined in equation 5.29, with the DC gain equal to F(0)=A, the final error value for frequency is $\omega_e(\infty) = 0$.

Having established that no final frequency error exists, we can calculate the $3dB$ bandwidth

for the loop by solving for $|H(j\omega)|^2 = 0.5$ for ω [43] as follows:

$$\omega_{3dB} = -\frac{2K_vK_pQ}{4Q^2K_p^2K_v^2\tau_2^2 - 4QK_pK_v\tau_2\omega_r\tau_1 - \omega_r^2\tau_1^2}\sqrt{(-4Q^2K_p^2K_v^2\tau_2^2 + 4QK_pK_v\tau_2\omega_r\tau_1 + \omega_r^2\tau_1^2)} \tag{5.34}$$

Assuming $\tau_1 \gg \tau_2$, and approximating $\tau_2 \approx 0$, equation 5.34 simplifies to the following more manageable solution for loop bandwidth.

$$\omega_{3dB} \simeq \frac{2K_vK_pQ}{\omega_r\tau_1} \tag{5.35}$$

In conclusion, the measurement of B/A requires the phase locked loop to track an exponential decay in frequency over two seconds. This type of loop is more robust in operation than conventional phase locked loops due to the simple fact that the input frequency is always the same as the VCO frequency, with only the phase changing. Therefore, the stringent requirement for frequency lock is not necessary and the VCO is effectively tuned by the DC signal present in the phase detector. This means that requirements for the loop filter are not stringent and the filter can therefore be optimised for measurement accuracy rather than locking efficiency. It is advantageous to utilise a high gain, second order filter (or active integrator in control terminology); this has the effect of reducing the steady state error to zero. Similar passive filters might incur some small phase error whose magnitude is inversely proportional to the loop gain (these filter types should be avoided since the tracking phase error could lead to a B/A error). A typical design of the loop filter should be to remove the double frequency term present in multiplication, but have sufficient loop bandwidth to provide accurate phase lock. Since we are only interested in tracking an exponential decay in frequency, the lock-in bandwidth can be reduced to provide extremely accurate measurements of the change in phase velocity.

A further advantage of TPL is the fact that it always operates at the null point (see Fig. 5-14) so, the system response does not in anyway deteriorate as the resonance moves due to a change in phase velocity from its initial ω_r value. Although not necessary, the loop bandwidth for this system can also be extended from DC to 1Mhz without significantly compromising the system performance.

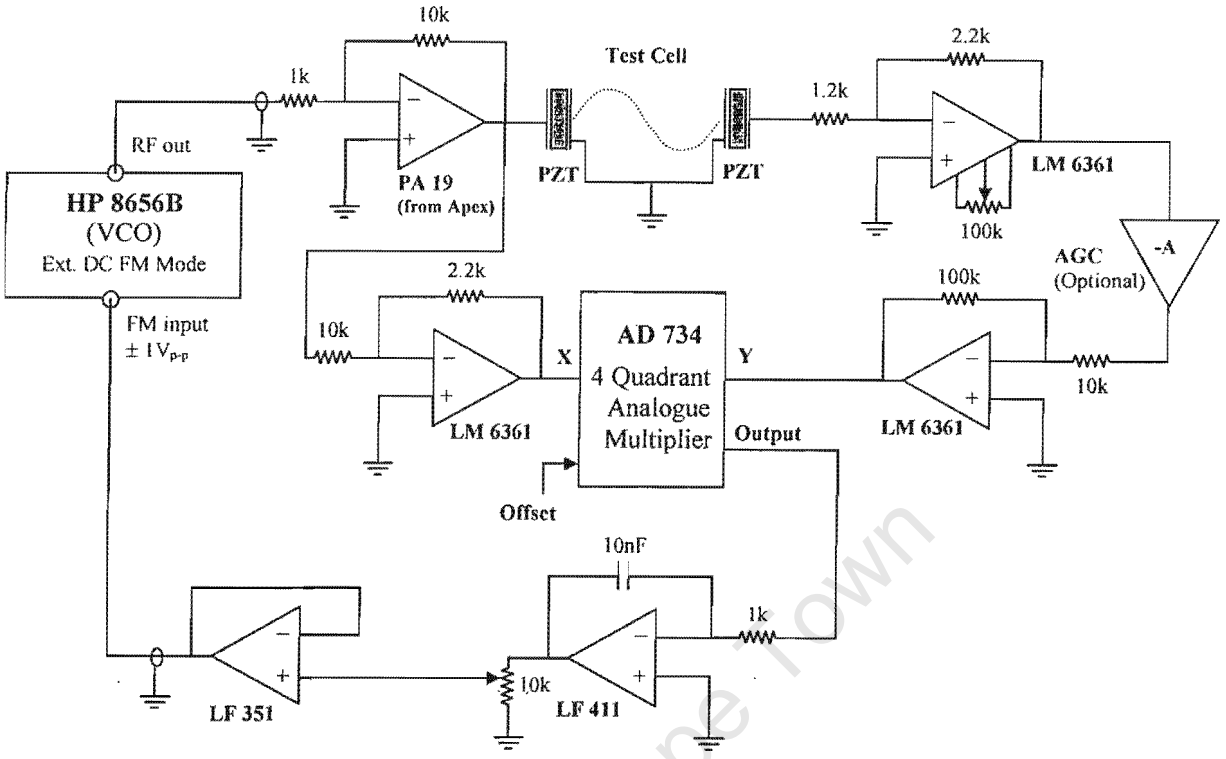

Figure 5-17: A circuit diagram showing the practical implementation of Transmission Phase Locking to lock an acoustic mode within an interferometer test cell. The bandwidth of the loop filter is set sufficiently low so as to attenuate all higher frequency components generated by the AD 734 multiplier. An automatic gain control (AGC) circuit was used to provide more stability to the loop (multiplier gain set constant) but is not critical to loop design. The operating bandwidth is set by the VCO.

5.2.4 Practical Implementation and Electronic Synthesis

Fig 5-17 shows a practical circuit used to implement transmission phase locking. This elementary opamp circuit exemplifies the simplicity with which TPL may be used to measure B/A. Other circuit combinations using both digital and hybrid components may be easily used to replace existing opamp and multiplier functions for higher frequency mode locking.

A design aspect which is not immediately apparent from the figure is that the critical phase difference between the driving and receiving transducers must be the same at both X and Y inputs to the multiplier. Since the accuracy of B/A is defined by this phase difference, any frequency dependent phase offset caused by noise filtering or opamp distortion is received as a sound velocity fluctuation. It was however found that provided the choice of filtering was symmetrical in both the driving and receiving paths, this phase difference could be effectively

subtracted.

The choice of receiver opamp used in Fig 5-17 was a high slew rate video opamp (LM6361), chosen for its high gain-bandwidth product and low phase distortion. The inverting configuration provides a fixed input impedance, without the need for biasing. This is particularly important when considering the first stage of amplification following the transducer. The PZT receiver cannot provide the necessary bias current required for a noninverting opamp without bootstrapping, which effectively introduces a phase shift into the loop.

The four quadrant analogue multiplier used in this circuit for phase detection included an offset nulling input. This provides an elegant means of injecting a predetermined (DC) phase offset into the loop.

As an alternative phase detector, it should be noted that a digital system can (and was) successfully implemented for TPL (see Appendix B). However, in debating such a design, the extreme gain change between acoustic resonance and anti-resonance must be considered (as shown in Fig 5-10). In order to realise sequential TPL using a digital phase detector, both inputs to the phase detector have to be converted from sine to square waves. This task is simply achieved in the driving path, but proves troublesome in the receiving path. The large amplitude deviations present in the received signal[6] make it difficult to set a threshold point for squaring. At anti-resonance conditions, the SNR (signal to noise ratio) is extremely low, causing jitter which can only be remedied through the use of hysteresis feedback, which introduces an undefined phase injection in the receiving path. This phase injection is a nonlinear function of the SNR and cannot be removed. Another solution might be to configure the opamps with large signal gain so as to clip the received signal. This technique proved equally disastrous, resulting in nonlinear phase offsets introduced by each opamp. A more subtle solution to this problem may be achieved by using an automatic gain control circuit or AGC (see Appendix B). This circuit provides a constant amplitude signal at its output for a $10dB$ fluctuation at its input. The AGC, although developed for digital mode locking, was also used in analogue mode locking (as depicted in Fig 5-17) as a means to stabilise the gain constant K_p. Although the inclusion of the AGC supports the linear analogy adopted earlier, its inclusion was found to be entirely optional. In fact, we postulate that the nonlinear function K_p helps the loop to find and maintain lock as it provides a large SNR at zero phase; this facilitates loop stability and creates a steady condition for lock-in. As a result the optional AGC block depicted in Fig

[6]A deviation of typically 10dB for water is shown in Fig 5-12. This deviation is a function of the liquid and the frequency separation between the acoustic mode and the transducer resonance.

5-17 may be replaced by a standard inverting amplifier (to maintain polarity).

The VCO used (as described earlier) was an HP8656B frequency generator providing excellent frequency stability with a user friendly means of adjusting both operating bandwidth and loop gain for the system.

The loop component values vary depending on the mode and liquid. Notwithstanding this, we provide the typical parameters used to synthesise the circuit in Fig 5-17:

The loop filter was an active RC integrator with infinite gain, as described in the theoretical analysis, with time constants $\tau_1 = 10\mu s$ and $\tau_2 = 0$. Although the system parameters require tuning at different acoustic modes, typical values are given here for mode number 44 (used in earlier sections). The loop parameters calculated for this mode are as follows: Q=470.2 at ω_o = 840 kHz, Kp=3.35 V.rad^{-1}, and Kv=3 kHz.V^{-1} for a driving signal of $|\omega_o| = 100mV$ (power = 0.6mW). The calculated loop bandwidth ω_{3dB} = 28 kHz.

The acoustic mode (n=44) has equivalent electrical values of L=1.478mH, C=24.27pF, R=16.6Ω as described in the previous section. The frequency resolution as measured by an HP 34401A frequency counter at resonance was ±0.5 Hz in 840kHz.

5.3 Measurement Results for B/A

The measurement of B/A using TPL was first performed with water at a temperature of 30°C. Water was chosen for its many comparative references found in the literature. A selection of alternate modes leading up to the fundamental resonance of the PZT were locked and B/A was measured for each, acquiring 10000 sample sets of frequency versus pressure per mode. A graphical representation of the results as a function of mode order is given in Fig 5-18.

From this figure it can be seen that B/A measurements beyond mode number 44 deviate from literature accepted values, following a curve similar in shape to that of the transducer admittance. The deviation in B/A is a result of a frequency dependent phase contribution to the measurement. This unwanted phase is a function of mode locality, with modes lying juxtaposed to the fundamental PZT resonance being more affected than those further away. We postulate from our observations that B/A measurement is compromised by 'frequency pulling' in the frequency region surrounding the fundamental resonance. This behaviour will be explored in more detail in the following chapter.

Using Fig 5-18 (as a guideline), we propose a boundary condition for which TPL measurement of B/A is valid. As a general rule we suggest mode locking should occur at modes which

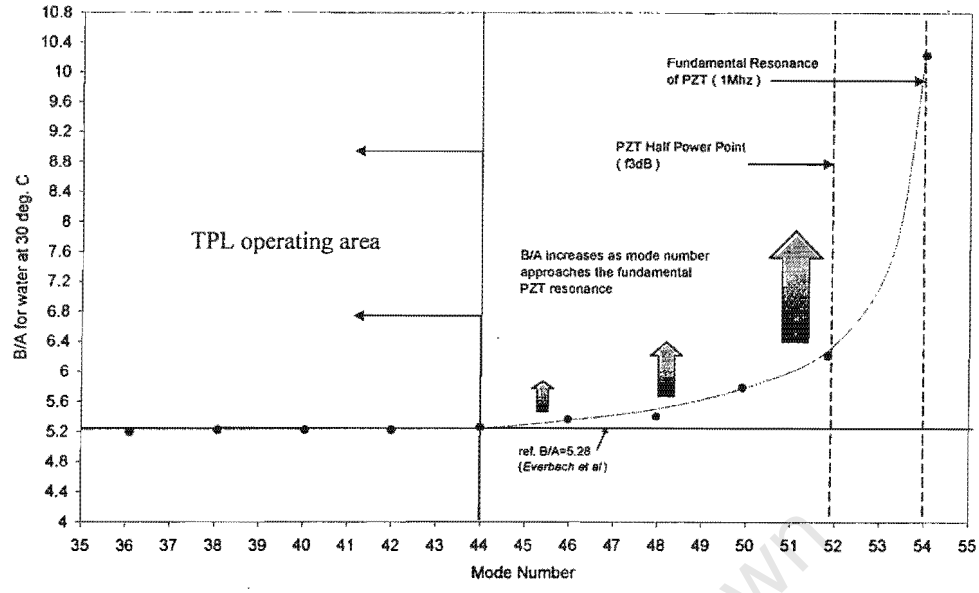

Figure 5-18: Measured values of B/A for water are plotted as a function of mode order. Every data point (depicted here by a circle) represents 10000 sample points, with an uncertainty of less than 1%. The effects of 'frequency pulling' are displayed, with modes closer to the PZT transducer resonance more prominently affected. A reliable operating area for measurement is defined at mode numbers below 44 indicated here by the unshaded region.

lie a period of twice the PZT bandwidth away from the fundamental resonance. This region, shown in Fig 5-18, is defined for modes 44 and below. B/A measurement performed within these boundary limits show results deviating less than 1% from one another.

Apart from water, three test liquids FC43, FC75 and methanol were measured. Each liquid was measured at two independent modes within the boundary limits prescribed. Results show negligible contribution from frequency pulling in-between the modes, with thermal and electrical noise dominating the measurement uncertainty, yet falling within the prescribed 1% tolerance. A typical measurement result for water is described by Figs 4-7 to 4-9 in Chapter 4. Table 5.1 summarises the measured results together with literature reported values. The error indications shown in Table 5.1 are uncertainties pertaining to gradient measurement only and do not include absolute measurement uncertainties.

5.4 Conclusions

The feasibility of measuring B/A using continuous waves is shown in this chapter. A small volume interferometer cell was designed and several practical solutions to design problems

Liquid (30°C)	Density $\rho(kg.m^{-3})$	Velocity $m.s^{-1}$	B/A	Error σ_{gw}	Literature
Distilled Water	995.7	1509.12[30]	5.19	±0.026	5.21 [25]
					5.28 ±0.021 [38]
					5.18 ±0.033 [111]
FC 43	1861	638	13.28	±0.067	12.85 (20°C) [73]
FC 75	1768	567	12.76	±0.048	12.19 (20°C) [73]
Methanol	791	1144	8.97	±0.032	9.62 [25]

Table 5.1: A table of results obtained for different liquids at modes well spaced from the fundamental PZT transducer resonances. Errors included are only uncertainties in the measurement of the gradient df/dp

investigated. A novel mode locking control system was developed to phase lock modes within an interferometer cavity. This technique, labelled Transmission Phase Locking is unique to B/A measurement and was used successfully to trap and track liquid modes within the interferometer cell. Linear control theory was manipulated to incorporate the acoustic interferometer within closed loop calculations, facilitating an easy method for calculating loop components.

Having developed the interferometer and lock-in system, B/A was measured for water at successive modes approaching the PZT fundamental resonance. Preliminary statistical evaluation of the data (some 100000 data points over 10 modes) showed excellent lock-in and phase tracking ability. A plot of B/A as a function of mode order indicated a frequency pulling caused by the PZT resonance. Boundary conditions were defined based on experimentation, to determine a stable operating area for TPL measurement. Using this guideline, B/A was measured for several liquids including two slow sound speed fluorocarbons. Results show good comparison with the literature, with uncertainties in measurement of less than 1%.

In conclusion, we have shown that continuous wave measurement is a viable and accurate alternative to pulsed systems provided boundary conditions are observed. Results of less than 1% are easily achieved using elementary electronics and a simple interferometer system.

Chapter 6

Understanding Tube Resonators

The objective of this study was to develop a simple yet accurate continuous-wave system for measuring B/A isentropically. In partial fulfilment of this, Transmission Phase Locking (T.P.L.) provides a simple and viable alternative to complex pulsed measurement systems. Nevertheless, a limiting factor restricting TPL is its exclusive application to double disc interferometry, and the complexities and problems associated with this approach (highlighted in the previous chapter). With this in mind, a survey of different resonator geometries was conducted, for the purpose of establishing a resonant cell appropriate to continuous wave measurement. A result of this investigation was the uncovering of an acoustic series of loosely coupled modes, present in a liquid filled PZT cylinder. These modes, which appear to be previously unreported, are cylindrical in nature with frequencies which are precisely linear as a function of mode order.

The purpose of this section is to experimentally identify and model the interaction between acoustic and piezoelectric modes, with the purpose of measuring B/A and adopting the PZT tube as a novel cavity resonator. Aspects of admittance measurement are discussed together with equivalent circuit analogies. The acoustic series is examined and an equivalent transmission line model developed. A brief finite element observation of the acoustic series is shown, confirming its origin and geometry. Finally we discuss a novel technique of trapping these modes using a resonant-locked control system thereby facilitating the absolute measure of B/A.

6.1 A Review of Equivalent Circuit Theory

6.1.1 Mason's Equivalent Circuit Model

A piezoelectric (p.e.) transducer can be characterised by modelling the interactive behaviour between electrical and mechanical energy. This can be achieved analytically by manipulating the electromechanical equations of state [72] [3] or experimentally by modelling the piezoelectric behaviour as an equivalent electrical or mechanical circuit. By adopting the latter approach, the task of designing a precise control system for measuring B/A, (as shown in Chapter 5) is greatly simplified because the behaviour of the control 'plant' (the transducer and liquid system) is known and can be substituted as a circuit element for control-loop calculations.

Equivalent circuit modelling has been explored by many authors; however, the behaviour of a piezoelectric response is best described by Warren Mason in the book "Electromechanical Transducers and Wave Filters" [76]. Mason uses a generic transmission line to represent the behaviour of a simple piezoelectric transducer. This transmission line can be converted to a lumped element network under associated loading conditions, resulting in the well known electrical analogue depicted in Fig 6-1.

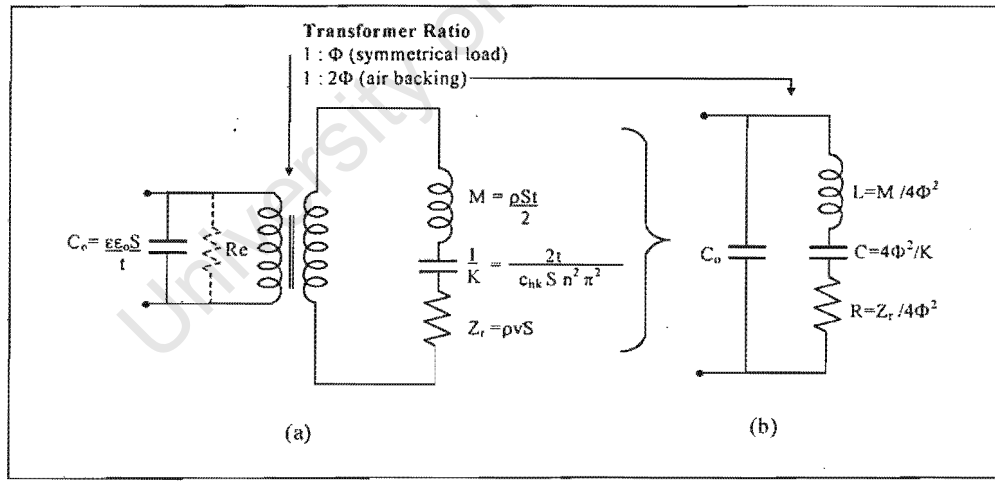

Figure 6-1: Mason's equivalent electromechanical circuit. The ideal transformer couples the electrical to mechanical energy and is transposed to the simplified case using the transformer turn ratios, Φ. These are defined by the loading conditions applied to the system. The variable C_o refers to the electrical capacitance of the piezoelectric transducer. The mechanical analogues of mass, M, compliance, 1/K, and impedance, Zr, are represented by the electrical elements L, C and R.

An examination of Fig 6-1a indicates two circuits isolated from one another by a perfect

transformer. On the primary side of the transformer, the electrical behaviour is represented by the dielectric capacitance in parallel with a resistance[1] representing its dielectric losses. The secondary (or motional) side of the transformer is loaded by the mechanical arm, represented as a series tuned LCR network, analogous to mass, compliance and damping (acoustic impedance). The turns ratio governs the coupling from electrical to mechanical energy and is defined by the loading of the transducer. If the transformer is removed from Fig 6-1a, the motional parameters can be transposed to the primary to represent the simplified electrical circuit shown in Fig 6-1b.

To obtain electrical quantities for the motional arm, a conversion from mechanical to electrical units is required. This can be achieved either by measuring both the physical dimensions and p.e. constants of the transducer and applying the necessary electromechanical equations (see Fig 6-1) [56], or the motional quantities for L,C and R can be derived directly from a plot of the measured admittance or impedance spectrum.

6.1.2 Using Admittance for Equivalent Circuit Prediction

The admittance spectrum is measured by sweeping a unit voltage source, connected to the input, over a predefined frequency range, whilst observing the real and imaginary parts of the current flowing into the network.

By plotting the real part of the admittance or 'conductance' on the abscissa, with the imaginary 'susceptance' on the ordinate, as a function of frequency, we can represent the p.e. behaviour of the transducer as an admittance vector diagram as shown in Fig 6-2.

This vector diagram follows a circle in the complex admittance plane (often referred to as a transadmittance circle [107]); the center of which is vertically offset by an amount equal to the susceptance of the clamped capacitance C_o. This circle characterises a single piezoelectric resonance and has a diameter defined as 1/R which can be measured from the absolute admittance difference $Y_{f_m} - Y_{f_n}$. The dielectric loss conductance G_e determines the tangential offset between the circle and the imaginary axes. The half power points f_{3dB} are shown at an angle $\pi/4$ from the horizontal diameter. The admittance vector diagram provides an intuitive understanding of a piezoelectric response, with each additional circle representing a unique resonance, the size of which is indicative of its magnitude and quality factor.

The admittance transfer function for an isolated p.e. resonance, modelled by Fig 6-1b and

[1]The dielectric loss resistance is in most cases several orders of magnitude larger in impedance than the other circuit elements, therefore it is generally considered infinite and ignored.

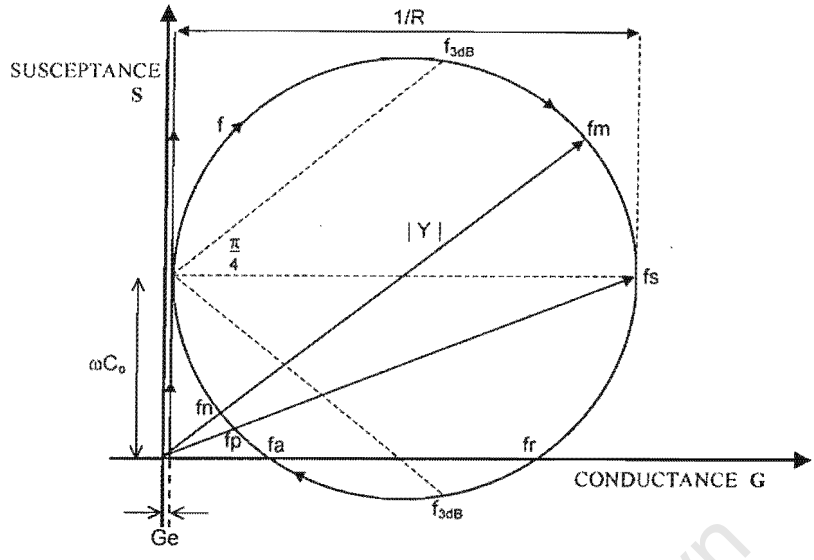

Figure 6-2: An admittance vector diagram for a piezoelectric vibrator [1]. The locus follows a conductive dielectric loss increasing vertically with increased frequency. In the vicinity of a mechanical resonance the locus deviates to follow a motional admittance circle. The maximum and minimum absolute admittance are shown as f_m and f_n, together with the series f_s and parallel f_p mechanical resonances. R indicates the mechanical damping of the resonance.

depicted in Fig 6-2 is described by the following expression:

$$Y = \frac{R}{R^2 + X^2} + j\left[\omega C_o - \frac{X}{R^2 + X^2}\right] \tag{6.1}$$

where $\omega_s = 2\pi f_s$ and the reactance X is given by :

$$X = \omega_s L - \frac{1}{\omega_s C} \tag{6.2}$$

The Absolute Admittance and Conductance Spectrum

Having examined the admittance vector behaviour of a p.e. resonance, we now observe the absolute and complex admittance spectra in order to model this behaviour as an electrical circuit and estimate equivalent circuit parameters[2] [100].

The absolute admittance spectrum (Fig 6-3(a)) can be easily measured using a simple op-amp circuit. It displays both mechanical and electrical resonance behaviour through its local

[2]Although specialised techniques do exist for predicting electrical immittance parameters using vector diagrams and scattering parameters[107] these are beyond the scope of this thesis.

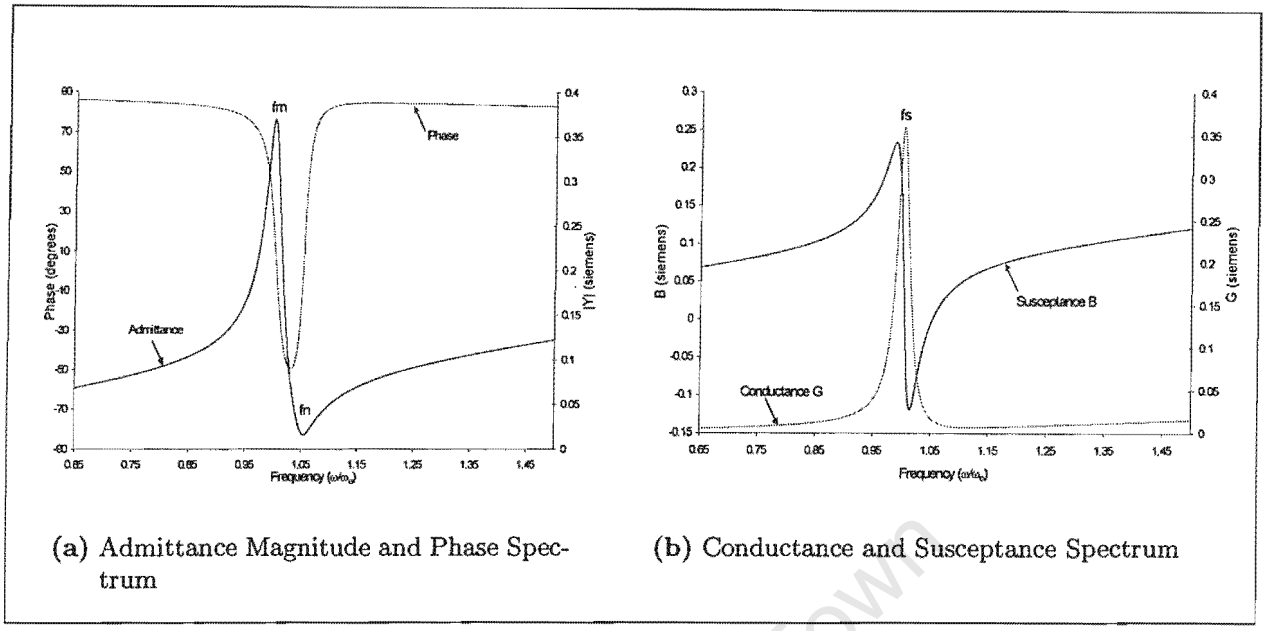

(a) Admittance Magnitude and Phase Spectrum

(b) Conductance and Susceptance Spectrum

Figure 6-3: A comparative plot of the complex and absolute admittance, and phase for a piezoelectric vibrator. The peak of the conductance curve corresponds to the series resonance f_s. The absolute admittance spectrum has both local maxima, f_m and minima, f_n representing both series and parallel resonances. The phase spectrum, described by the arctangent of the susceptance over conductance, reaches a minimum between fr and fa.

maxima and minima. The magnitude plot provides information on the electromechanical coupling of the transducer k_{eff}, which can readily be calculated by:

$$k_{eff} = \sqrt{1 - \frac{f_s^2}{f_p^2}} \simeq \sqrt{1 - \frac{f_m^2}{f_n^2}} \tag{6.3}$$

Although the peak f_m is an indication of the series resonance frequency, it is often more accurate to measure this value from the conductance spectrum as shown in Fig 6-3(b).

Conductance is an indication of the real power radiated by the transducer and its peak f_s corresponds to the mechanical resonance frequency. From the shape of the conductance curve, the 'Q' or quality factor for the series resonance may be measured, with half power points approximately equal in frequency to the local maxima and minima of the susceptance curve.

6.1.3 Equivalent Circuit Calculations

From the admittance curves shown in Fig 6-3 the electrical parameters corresponding to Mason's equivalent circuit can be calculated as follows :

Quality factor

The mechanical quality factor Q_m can be determined [74] [100] by measuring the series resonance f_s and the half power points f_{3dB} of the conductance curve and applying the following equation:

$$Q_m = \frac{f_s}{\Delta f_{3dB}} \tag{6.4}$$

or may be approximated directly from the absolute admittance curve using

$$Q_m \simeq \frac{\omega_m}{2(\omega_n - \omega_m)} \left[\frac{|Y_{fm}|}{|Y_{fn}|}\right] \tag{6.5}$$

Mechanical Arm

Once Q_m is derived, the following set of equations can be used to determine equivalent values for L,C and R

$$L = \frac{Q_m R}{\omega_s} \tag{6.6}$$

$$C = \frac{1}{\omega_s L R} \tag{6.7}$$

$$R = \frac{1}{|Y_{fn}| - |Y_{fm}|} \tag{6.8}$$

where ω_s is the series resonance frequency defined at maximum conductance G_s.

Electrical Arm

Although the electrical capacitance (C_o) can be easily measured using a capacitance bridge, it should be noted that any charge flowing into the transducer will be stored both dielectrically and piezoelectrically. Therefore not only should the measurement of C_o be taken at a frequency well away from any mechanical resonance, but the measured capacitance should be corrected to account for the unclamped piezoelectric strain [1, IRE Standard 1957]. Alternatively, the electromechanical coupling factor, k_{eff} derived earlier with equation 6.3 can be used to determine the clamped electrical capacitance C_o as follows:

$$C_o = C(\frac{1}{k_{eff}^2} - 1) \tag{6.9}$$

Finally the optional dielectric resistance loss R_e may be derived as

$$R_e = \frac{1}{G_s} - R \tag{6.10}$$

6.2 Observing the Resonance Behaviour of a PZT Tube

The theory of modes of vibration of a liquid in a cylindrical cavity is well understood [17]. An analysis closely follows that of electromagnetic [20] and gas cavities, all of which involve the solution of their respective wave equations and boundary conditions. A means of exciting these resonances using a PZT tube was uncovered quite unexpectedly during this research and is examined in detail in the following three admittance studies. The first two studies characterise the behaviour of the tube under empty and water filled conditions. Naturally the acoustic loading effects associated with the water are observed, being typically a flattened response and reduced resonance frequency. The last experiment describes a wetting technique which facilitates the unexpected generation of a series of loosely coupled acoustic modes. These modes, which form an extensive harmonic series, appear in a spectrum where previously none had existed. Their origin and behaviour is examined in detail in the remaining sections of this chapter.

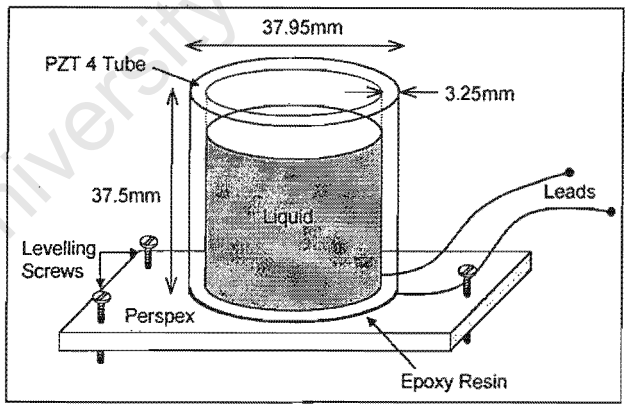

Figure 6-4: A schematic of the cup transducer, showing dimensions of the PZT tube and the experimental setup. Three adjustment screws were used to level the liquid filled structure. The liquid was filled to the brim, however evaporation led to negligible disturbance of the acoustic series.

Each of the following experiments employ the admittance spectrum as a means of observing resonant behaviour. The spectrum is confined to the fundamental resonance frequency, spanning a frequency range from 400kHz to 1Mhz and is measured using a network spectrum

analyser (HP 4195A). A PZT-4 tube was used for this study. This tube was fully electroded on both surfaces and polarised in wall thickness. In order to retain liquid, the tube was glued to a perspex base to form a cup, and leads were soldered to the inside and outside electrodes. Figure 6-4 shows the physical dimensions and construction of the cup setup.

6.2.1 Study 1: PZT Cup - Empty

Figure 6-5 shows a broad band sweep of absolute admittance over the frequency spectrum 400kHz to 1MHz. The spectrum is dominated by the fundamental thickness resonance present at 653.53kHz. Small satellite resonances are present in the spectrum and are marked with an 'x'; however their magnitudes are insignificant in comparison to the fundamental resonance and therefore may be ignored, permitting simple piezoelectric characterisation using Mason's equivalent circuit model. Implementing equation 6.1, the modelled parameters (represented in the equivalent circuit) have been used to generate a comparative plot of admittance magnitude (also shown in Fig 6-5). The circuit model is a good representation of the cup's fundamental resonant behaviour and will be used as a baseline in the following experiments.

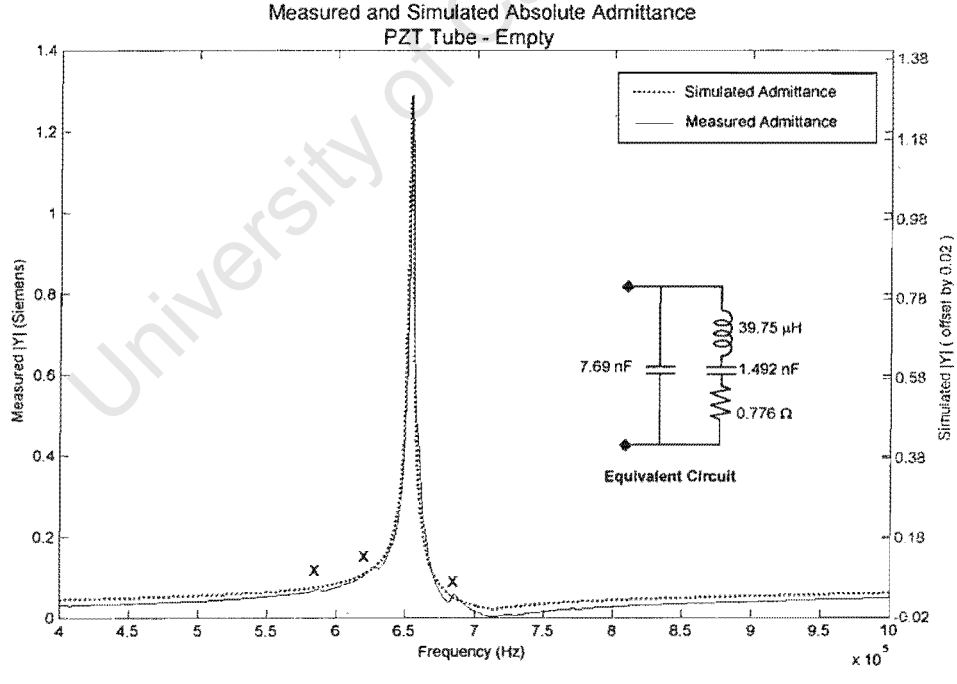

Figure 6-5: A comparison between the measured and simulated absolute admittance spectrum for the PZT cup transducer. Simulated admittance has been vertically offset by 0.02 siemens for comparison purposes. Satellite resonances are marked with an 'x'.

6.2.2 Study 2: PZT Cup - Water Filled

In the second study, the cup transducer was filled with distilled water and levelled using three levelling screws (Fig 6-4). The admittance measurement was repeated over the same frequency interval as before (400kHz to 1Mhz) and the complex spectrum recorded. Figures 6-6 and 6-7 show for comparison the resonant behaviour of the cup transducer before and after the water was added. Damping can be observed in the magnitude plot of Fig 6-5, showing a drop in both admittance magnitude and resonance frequency. This effect is more pronounced in Fig 6-7 where the diameter of the water-loaded motional circle has decreased, reducing conductance accordingly. The remaining spectrum shows no evidence of acoustic activity and the satellite resonances depicted in Fig 6-7 and Fig 6-5 are completely suppressed by the damping. Following the modelling procedure described earlier, the equivalent piezoelectric circuit parameters are derived for the water filled transducer and are displayed comparatively in Table 6.1

Loading	Q_m	f_s hz	f_n hz	k_{eff}	C F (10^{-9})	L H (10^{-5})	R Ω	C_0 F (10^{-9})
Empty	210.3	653536	714605	0.404	1.4926	3.975	0.776	7.69
Water Filled	114.24	651200	711100	0.401	1.532	3.898	1.396	7.99
Change	-96.06 ↓	-2336 ↓	-3503 ↓	-0.003 ↓	-0.039 ↓	-0.077 ↓	+0.620 ↑	+0.3 ↑

Table 6.1: A table comparing the loading effects of water on a PZT tube. The inductance (mechanical mass) is increased causing the mechanical resonance to drop in frequency. The acoustic impedance described by the resistance is increased, whilst the Q has decreased. A measure of the electrical capacitance shows a slight increase indicating an increase in the mechanical capacitance (or compliance); however in comparison with the change in mass, this is negligible. The effect of water loading resembles the loading effects described by Mason.

6.2.3 Study 3 : The Wetting Phenomena

Although acoustic modes within a liquid column are well documented, the previous two experiments show no evidence of their excitation.

An unexpected result appeared after a drop of liquid soap was added to the water column. An acoustic series of resonant piezoelectric responses appeared in the frequency spectrum. This phenomena is displayed in the time lapse admittance series shown in Fig 6-8. It is evident from this series that the acoustic modes are excited by 'wetting' the surface of the PZT tube with the soap liquid. The energy from the thickness resonance is transferred to adjacent acoustic

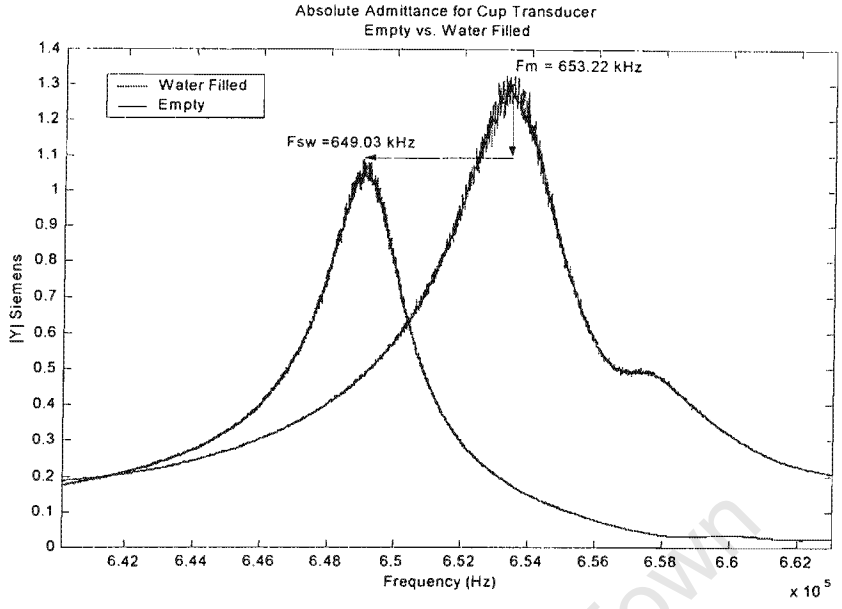

Figure 6-6: A plot of the absolute admittance comparing the resonant behaviour between the empty and the water filled cup. Acoustic damping is observed by the drop in magnitude and shift in resonant frequency.

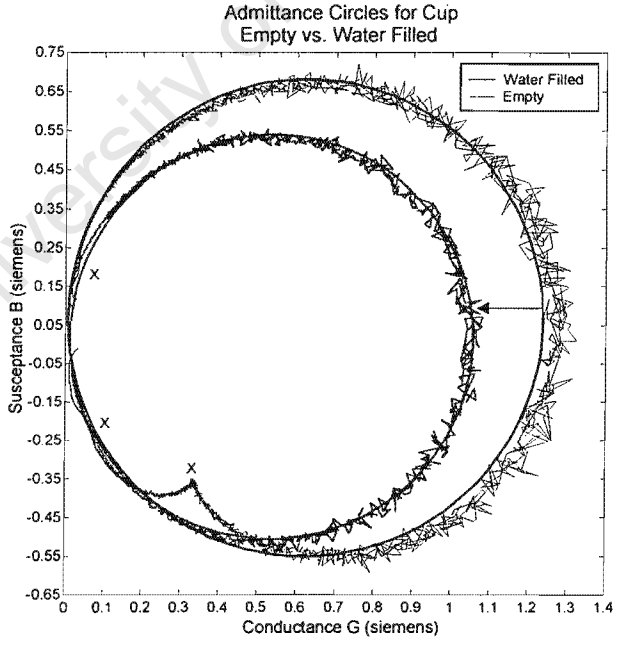

Figure 6-7: An admittance circle showing the loci for the empty and the water filled cup. The 'x's indicate satellite resonances in the empty cylinder, which have been damped by the water in the other locus.

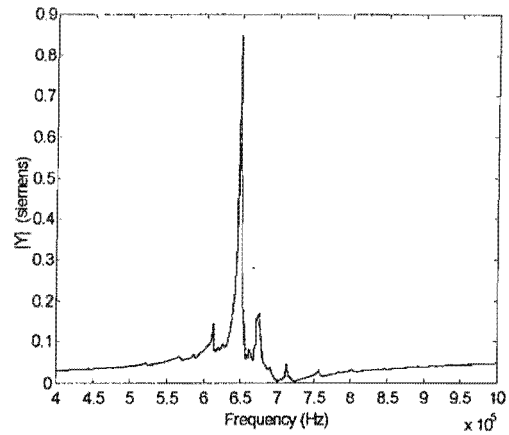

(a) Time = 5 minutes

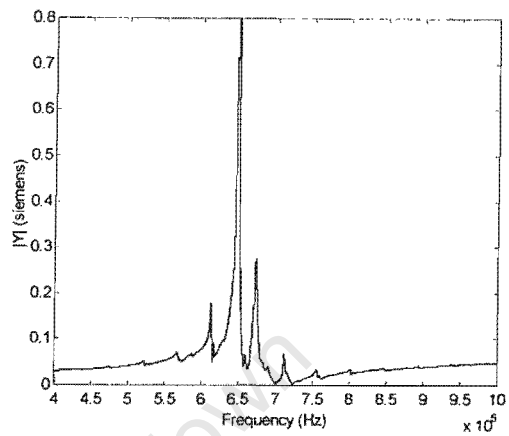

(b) Time = 10 minutes

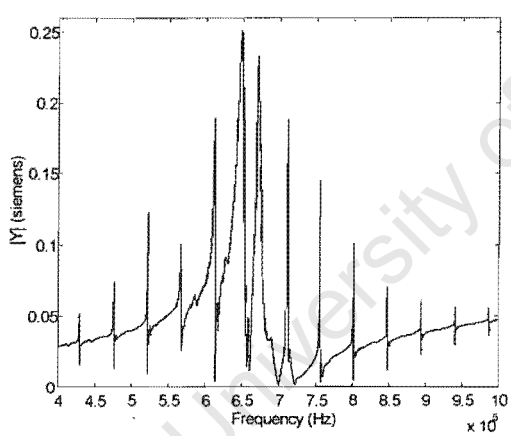

(c) Time = 15 minutes

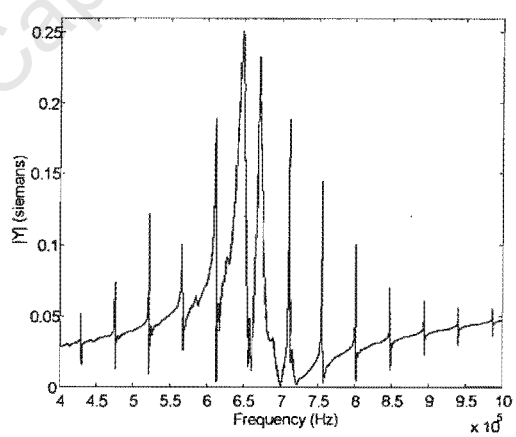

(d) Time = 20 minutes

Figure 6-8: A time sequence capturing the wetting phenomenon associated with a water filled PZT tube. The result following the addition of a drop of liquid soap to the water column is displayed in the set of four absolute admittance plots. The approximate time interval between plots is 5 minutes. The fundamental PZT resonance is damped at the expense of the acoustic resonant series, whose quality factor increases with time. This phenomenon is repeatable if the cylinder is dried for several hours before repeating the experiment.

modes causing a decrease of the fundamental resonant peak.

To further characterise the wetting behaviour the cylinder was emptied, dried and refilled with distilled water. Again the acoustic series was excited (see Fig 6-9(a)), leading us to believe the phenomena is a surface wetting effect. Supplementary studies have shown that the PZT cylinder left to stand dry overnight returned to its 'unwet' state. Wetting was also achieved using a variety of other liquids including carbon tetrachloride, glycerine and fluorocarbon liquids.

6.2.4 Discussion and Conclusions

The modelling of electromechanical acoustic systems as equivalent electrical circuits is well known and proven to be an accurate analogue of the physical system. By deriving equivalent circuit behaviour, control instrumentation (such as that derived in Chapter 4.) can be designed more efficiently rendering a more accurate solution to measuring B/A. Methods for deriving the equivalent circuit of a PZT tube resonator have been presented and initial results for the liquid coupled tube have been reported.

The unexpected wetting phenomenon achieves reproducible excitation of a unique set of acoustic modes. These acoustic modes, with uncharacteristically sharp Q's are harmonically spaced and we postulate may be used to measure B/A effectively (and possibly absolute sound velocity) i.e. an alternative to conventional interferometer resonators and TPL. Their origin however, still needs to be investigated and their admittance characterised in order to derive suitable instrumentation.

6.3 The Acoustic Resonance Series

Figure 6-9 shows admittance magnitude spectra for dissimilar liquids FC75 and water in the PZT cup. Both of these liquids were chosen to analyse and identify the liquid resonant behaviour of the acoustic series uncovered earlier. The unusually slow sound speed of FC75, attributed in part to the fluorine [84] content of its molecules, was used to generate the closely spaced acoustic resonances shown in Fig. 6-9(b). In comparison, water has widely spaced acoustic resonances, allowing us to compare the acoustic behaviour for both liquids in terms of adjacent mode coupling and resonant interaction between the liquid and the PZT cup.

Before analysing individual modes, the resonant frequencies for both liquids were plotted against mode order and a least square regression performed. The results for both liquids are

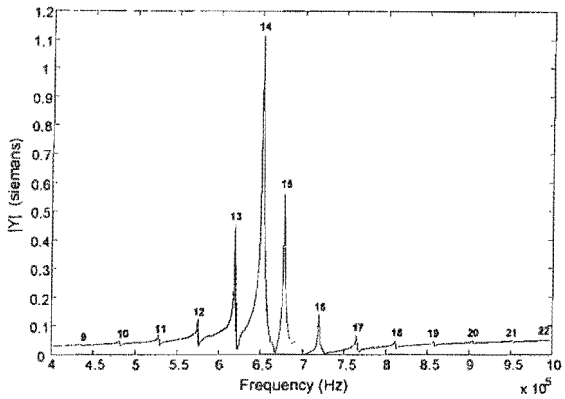

(a) Admittance Spectrum for Water df/dn=±47kHz. This spectrum shows the optimally coupled behaviour of the cup-transducer post wetting. The spectrum is a reproducible measured result.

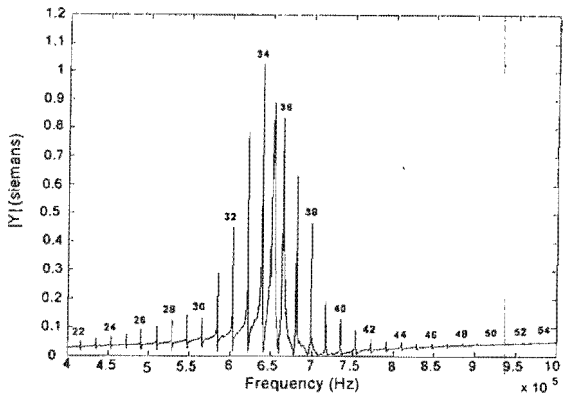

(b) Admittance Spectrum for FC75 df/dn=±17.5kHz.

Figure 6-9: A comparative plot of the absolute admittance spectra for water and FC75. The slow sound speed of FC75 enables more than double the number of acoustic resonances to be examined (modes 22-54) over the same bandwidth as water (modes 9-22).

shown in Figs. 6-10 and 6-11, which display two linear sets of data for each liquid. This artefact is caused by the fundamental PZT resonance, which acts to 'pull' the acoustic spectrum[3] linearly post-resonance resulting in an intercept change of -17.8kHz in FC75 and -19.8kHz in water. It is interesting to note that the gradient for both liquids remains mostly constant with a deviation of +0.3% in FC75 and +1.1% in water

If we examine the acoustics of a cylindrical column, there exist two primary modes of vibration, longitudinal and radial. These modes may be calculated by solving the wave equation for defined boundary conditions determined by the geometry of the liquid column. Blevins [17] provides a generic, numerical solution to this in the form:

$$f_{ijk} = \frac{c}{2\pi}\sqrt{\frac{\lambda_{jk}^2}{R^2} + \frac{i^2\pi^2}{L^2}} \tag{6.11}$$

where R and L are the radius and length of the column and c is the absolute velocity of sound. The terms j and k are the number of nodal diameters and circles respectively, and i

[3]This 'frequency pulling' phenomenon is discussed in further detail in section 6.4.1

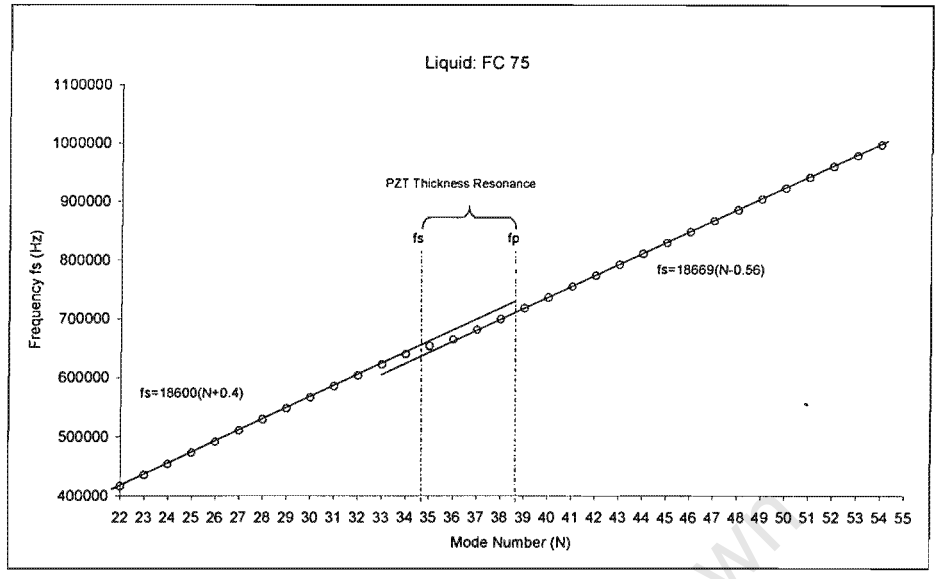

Figure 6-10: A plot of frequency versus mode number for FC75. The PZT series resonance, fs, divides the data between an upper and lower bound, with frequencies above fs being pulled linearly by the coupled PZT resonance. The lower data set corresponds to the theory defined by Blevins[17] with an offset in N of approximately 0.4.

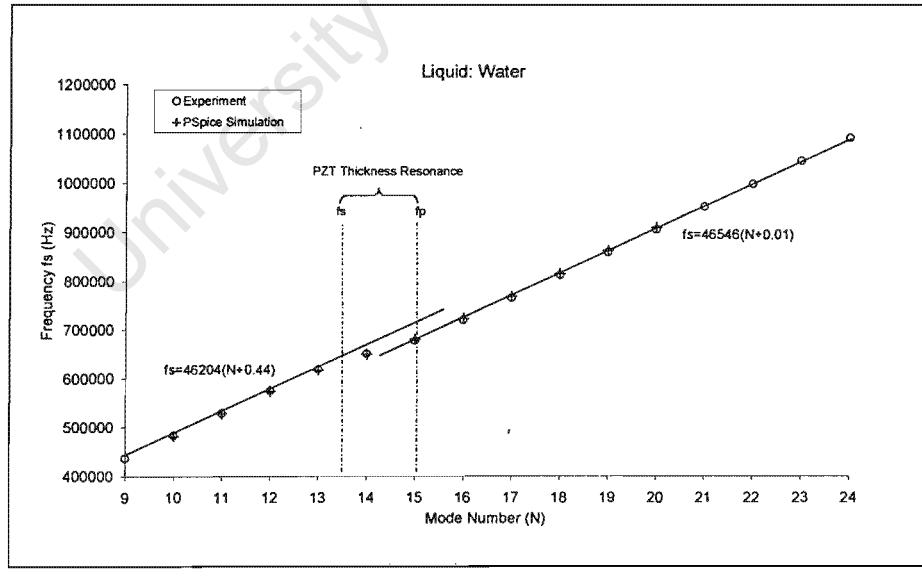

Figure 6-11: A similar plot of resonant frequency versus mode number for water. The data is pulled linearly post resonance in much the same way as FC75. A simulation of the mass coupled mechanical-acoustic model is represented by crosses, showing good comparison between the experiment and simulation.

is the number of axial (or longitudinal) modes. The term λ_{jk} can be approximated[4] under the conditions $i, j = 0$ and k>3 as $\pi(k + 0.25)$.

The dimensions of our PZT cylinder define a condition whereby the radial and longitudinal modes cancel one another [56]. This is observed by the 'clean' thickness resonance present in Fig 6-6, with only a small trace of radial/longitudinal vibration manifesting itself in the vicinity of the thickness resonance (shown in Fig 6-6 as satellites). We can therefore assume that only radial modes propagate in the liquid, causing the expression in equation 6.11 to be reduced to:

$$f_r \simeq \frac{c}{2r}(k + 0.25) \tag{6.12}$$

Returning to Figs 6-10 and 6-11, we notice that the acoustic modes below the PZT resonance approximate equation 6.12 with a gradient almost exactly characterised by $\frac{c}{2r}$ and a constant offset in both liquids of $+0.4(\frac{c}{2r})$. This leads us to believe that the liquid modes present in the spectrum are purely cylindrical in shape. In order to visualise the PZT-liquid interaction and further confirm the liquid mode shape, a finite element analysis was performed on the liquid filled tube transducer using the finite element software ABAQUS [52]. The parametric model developed for this simulation (see Appendix C) was designed as follows :

1. The dimensions given in Fig 6-4 were used for the analysis. Piezoelectric, elastic and dielectric matrices were obtained from the manufacturers.

2. Two sets of quadratic element models were run, using element mesh sizes of 1mm and 0.1mm to confirm convergence. It was found that coarser meshes did not adequately capture the solution to water wavelengths of ±2.3mm at 650kHz.

3. Detailed frequency sampling of 10Hz was necessary to capture the high Q acoustic modes.

4. An oscillating charge excitation of 7 nano-coulombs was used to drive the transducer.

Fig 6-12 shows the pressure profiles for two adjacent water modes n=11 and n=12. These two pressure profiles confirm the cylindrical mode shape, showing no evidence of longitudinal or radial coupling.

[4]For further values of λ_{jk} , consult Blevins[17] or Abramowitz and Stegan[2], Handbook of Mathematical Functions.

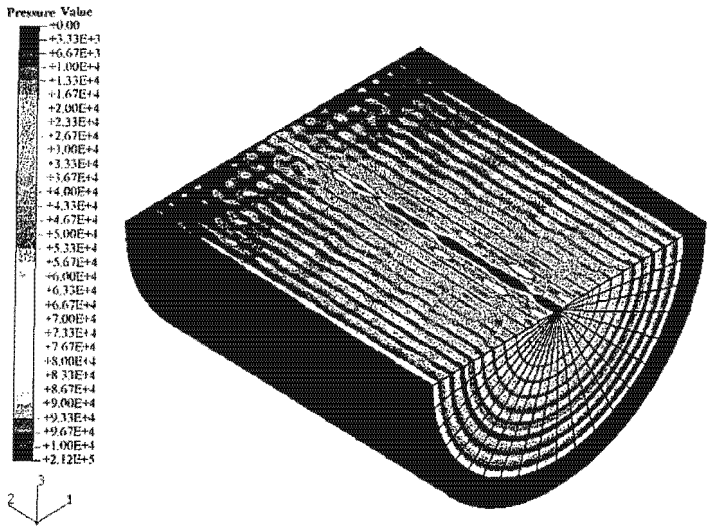

(a) Mode No. 11: Oblique View

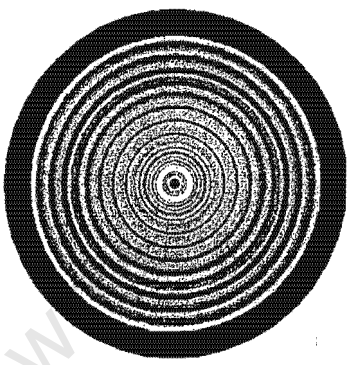

(b) Mode No.11 : Y-axis view

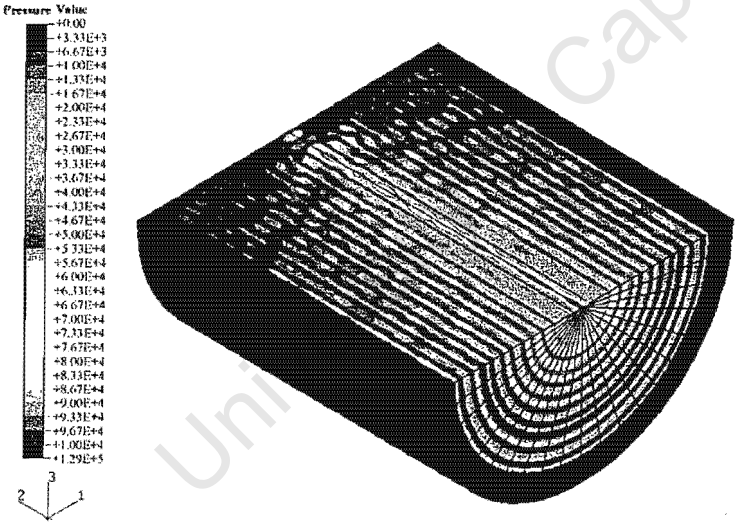

(c) [Pressure profile for water - Mode No.12: Oblique View

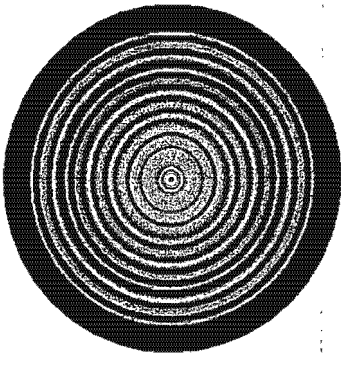

(d) Mode No.12- Y-axis view

Figure 6-12: A cross section plot of the pressure profile for a PZT tube oscillator filled with water (temperature 20°C). Two liquid modes resonant at 528.8kHz (mode 11) and 574.8kHz (mode 12) are plotted for comparison. The distinct cylindrical mode shape is visible in the form of concentric cylinders of constant pressure. A view from the Y-axis clearly shows the nodal circles described in the theory. The dark blue indicates zero pressure, and indicates nodes in the liquid

6.3.1 Applying Equivalent Circuit Parameters to the Resonance Series

Having discussed the origin and mode type of the acoustic resonant series, we now turn our investigation to the behaviour of individual liquid modes, in the hope of understanding the mechanical-acoustic behaviour of the transducer-liquid system. Treating each mode (within the frequency spectrum) as an isolated p.e. response, we are able to apply the modelling equations derived earlier to resolve equivalent circuit parameters for L, C and R. The superposition of these individual responses gives the total frequency characteristic of the system. A result of this modelling procedure is displayed in Figs 6-13 and Fig 6-14 representing the input reactance and conductance associated with each mode.

Inspection of these plots reveals a similar behaviour between susceptance parameters jwC and $1/jwL$ and that of conductance G. Each plot following a similar 'bell shaped' trend, indicating a change in susceptance and conductance for modes approaching the thickness resonance frequency of the PZT cylinder. Similar behaviour is observed in electrical theory when two or more resonant circuits are directly or mutually coupled together. This supports an interesting analogy that the driving (motional) resonance (determined by the PZT) is in fact inductively (or mass) coupled to the series tuned liquid resonance. This analogue would account for the frequency pulling encountered in Figs. 6-11 and 6-10. It would also explain the wetting behaviour observed in Fig 6-8. A more detailed discussion of this will be examined with frequency pulling later on in this chapter.

6.3.2 Conclusions

A summary of findings, characterising the behaviour of the uncovered acoustic series, is given in point form below:

- The acoustic (or liquid) series is cylindrical in shape, with resonant frequencies defined by equation 6.11. The modes are mostly independent of height[5] and spaced $\lambda/2$ apart.
- The piezoelectric cylinder has negligible near-field effects due to its geometry; this can be seen by the harmonic spacing of the acoustic series.
- The acoustic series is excited by a wetting phenomenon which is characterised by adding liquid soap to a column of water. Once wet, the cylinder continues to excite liquid modes,

[5]The liquid level was in all studies filled to the brim of the tube; however, it was noticed that fluctuations in liquid level had almost no effect on the acoustic spectrum.

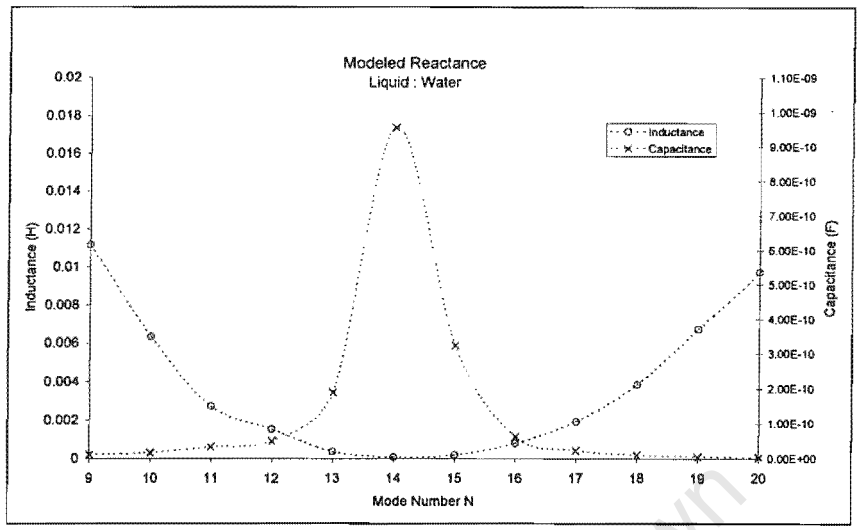

Figure 6-13: Equivalent reactance parameters L and C (representing mass and inverse compliance) are plotted as a function of mode order. These parameters were modelled from experimental measurements. Evidence of PZT coupling is shown by the similar bell shape associated with capacitance and the inverse inductance.

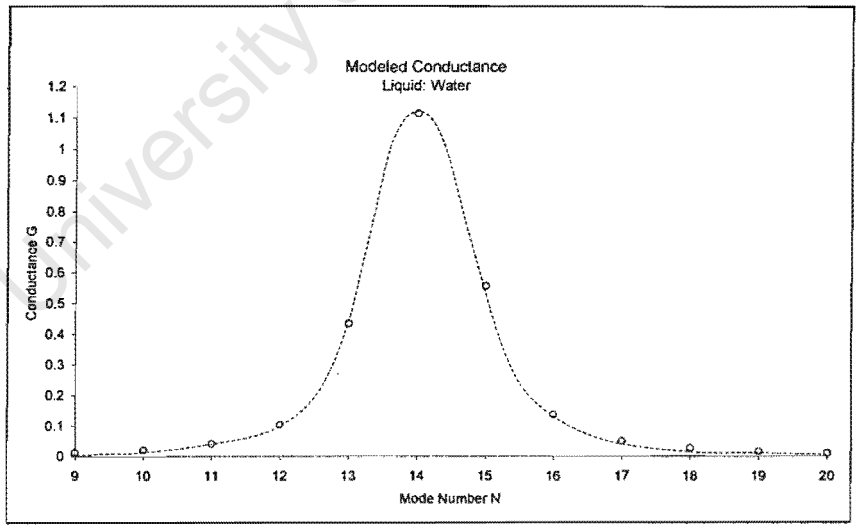

Figure 6-14: The conductance curve shown above for individual modes, represents the power transfer between the PZT (bandwidth between mode 12 - 15) and the liquid. The conductance was modelled from measured results. The bell shape is characteristic of two mutually coupled inductive circuits and supports the model derived for mass coupling.

even when the cylinder is emptied (but not completely dried) and refilled.

- The conductance and reactance curves for the individual resonant modes deviate over the PZT resonance indicating a coupled behaviour typical of resonant coupled electrical circuits.

- An exact change in frequency δf is present for the upper and lower bounds of the defined frequency spectrum (Fig 6-11), however a deviation characterised by frequency pulling is present in the vicinity of the PZT resonance.

- The loose coupling and high Q's of the acoustic spectrum inherently lend themself to c.w. mode locking, creating an ideal basis from which B/A may be measured.

6.4 New Insight into Resonance Modelling

In Chapter 5, we noticed that B/A measurements became distorted for modes locked adjacent to, or in the vicinity of, a PZT thickness resonance. This distortion is a result of "frequency pulling", a term loosely used in previous chapters to describe the coupled reaction between two or more resonant systems, causing a shift in resonance frequency for both systems. The interaction between coupled systems has been well documented, especially within the electrical field where two or more resonant circuits mutually coupled together exhibit signs of pulling. From observations of the liquid filled PZT cup, we notice the same phenomenon of frequency pulling to that observed in interferometry, yet confined to a narrower bandwidth surrounding the PZT resonance. In an attempt to quantify this behaviour, we next investigate frequency pulling and model acoustic coupling.

6.4.1 What is Frequency Pulling ?

When two resonant systems are arranged so that energy can be transferred from one to another, they are said to be coupled. For a coupled system, the individual resonances are shifted or "pulled" in frequency by an amount defined by the impedance and energy coupling associated with each.

A demonstration of frequency pulling is evident in the plots of resonance frequency versus mode order described previously in Figs. 6-10 and 6-11, which show the resonant frequencies of liquid modes pulled linearly in frequency past the PZT fundamental resonance. This behaviour

may be further demonstrated by plotting the change in frequency with mode number, versus mode order such as that shown in Fig 6-15.

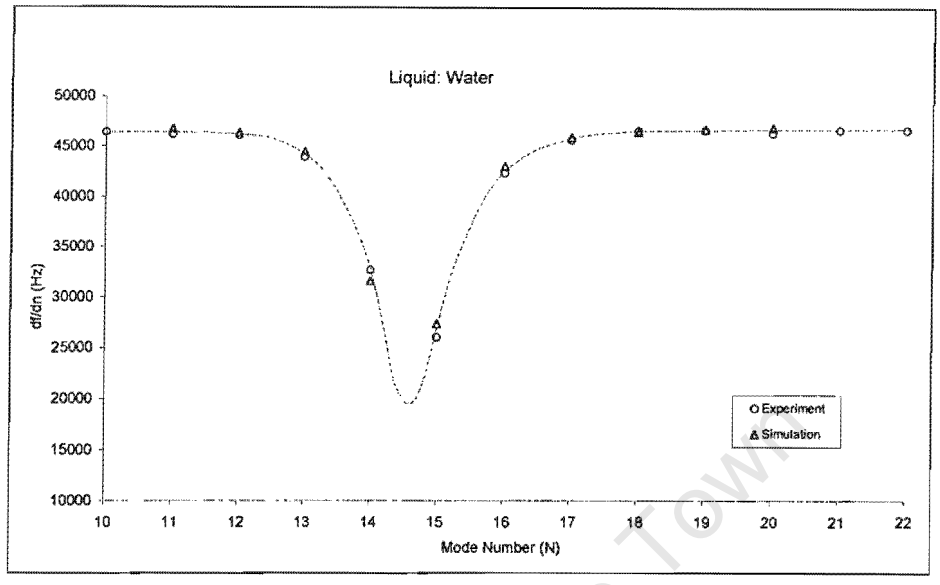

Figure 6-15: A demonstration of frequency pulling observed for experimental values modelled using equivalent circuit theory. The change in frequency with mode number plotted against mode order is shown as a dip in the vicinity of the PZT thickness resonance. Equivalent simulated results are examined in comparison, proving unambiguously the relationship between frequency pulling and mass coupling.

Although a mathematical solution can be derived to quantify this behaviour, it is more intuitive to understand frequency pulling in terms of mutually coupled resonant circuits, a view which will be examined for the remainder of this chapter.

Returning to the subject of measuring B/A; it is imperative that a mode-locked liquid resonance be independent of adjacent frequency pulling (i.e. the mode should not be influenced by the transducer coupling during the pressure jump process). To review this condition, consider two sequential modes located adjacent to a PZT thickness resonance. The nonlinear pulling ascribed to each mode is defined by its locality to the PZT resonance. For a change in sound velocity (such as that caused by an increase in pressure), each mode will experience a corresponding linear change in frequency combined with a mode specific, nonlinear frequency change, determined by the new locality of the modes to the PZT resonance. In order to remove this nonlinearity, the acoustic spectrum over which B/A is measured, should have harmonically spaced acoustic modes (i.e modes unaffected by pulling). Fig 6-15 shows this to be true for most modes except those juxtaposed to the principal PZT resonances (i.e. all modes except 13

- 17).

6.4.2 Mutual Inductive Coupling - A Demonstration of Frequency Pulling

In order to demonstrate frequency pulling, we define ten harmonically spaced water modes (mode numbers 10-19) spanning the fundamental PZT resonance. Each mode is modelled as a separate series tuned LCR circuit with a constant Q of 500 and capacitance determined by the inverse bulk modulus (see Fig 3-1, chapter 3). The frequency interval, defined by equation 6.12, is calculated as 47058Hz. A list of calculated values for each mode is given in table 6.2.

Having derived the acoustic series we now couple each mode to the equivalent circuit for the PZT by implementing mutual inductance (or mass) coupling. Figure 6-16 depicts the equivalent circuit model in terms of an infinite series of liquid modes coupled inductively to the motional inductance of the PZT. The coupling coefficient k represents the energy transfer between the mechanical and acoustic system and is used to calculate the mutual inductance using the equation:

$$M = k\sqrt{L_{pzt}L_{liq}} \tag{6.13}$$

A simulation of three coupling conditions is achieved using PSpice[6], enabling the input admittance to be examined over the frequency spectrum 400kHz to 1MHz. The three conditions are defined as follows :

1. *Weak coupling* (k=0.02): Relatively little energy is transferred from the PZT to the liquid, characteristic of an unwet PZT surface. The admittance spectrum shown in Fig 6-17(a) is dominated by the PZT thickness resonance.

2. *Critical or Optimum Coupling* (k=0.05): Defines the critical energy coupling from the PZT to the liquid. Maximum power is delivered to the acoustic resonant circuits, when the combined coupled resistance of the liquid is equal to the resistance of the PZT (Fig 6-17(b)). This coupling behaviour is the most commonly observed and is assumed as the normal in subsequent analysis

3. *Over coupling* (k=0.08): This situation, although partially evident in Fig 6-8(d), is in most cases physically unrealistic (Fig 6-17(c)).

[6]PSpice is an electrical circuit simulation program developed by Orcad.

Mode No.	L μH	C pF	R Ω	f_{res} Hz
10	237.3377	458.715	1.4386	482352
11	197.0196	458.715	1.3107	529411
12	166.1661	458.715	1.2037	576470
13	142.0309	458.715	1.1128	623529
14	122.7961	458.715	1.0347	670588
15	107.2197	458.715	0.9669	717647
16	94.4295	458.715	0.9074	764706
17	83.7985	458.715	0.8548	811765
18	74.8667	458.715	0.8079	858824
19	67.2904	458.715	0.766	905883

Table 6.2: A table of calculated values for ten equivalent liquid modes spaced approximately 47kHz apart. The modes are calculated with a constant capacitance, determined by the Bulk modulus of water and a Q of 500. Equivalent circuit values for inductance and resistance are calculated using the resonant frequencies defined by equation 6.12. All circuit values are modelled on the dimensions of the PZT-cup transducer (Fig. 6-4).

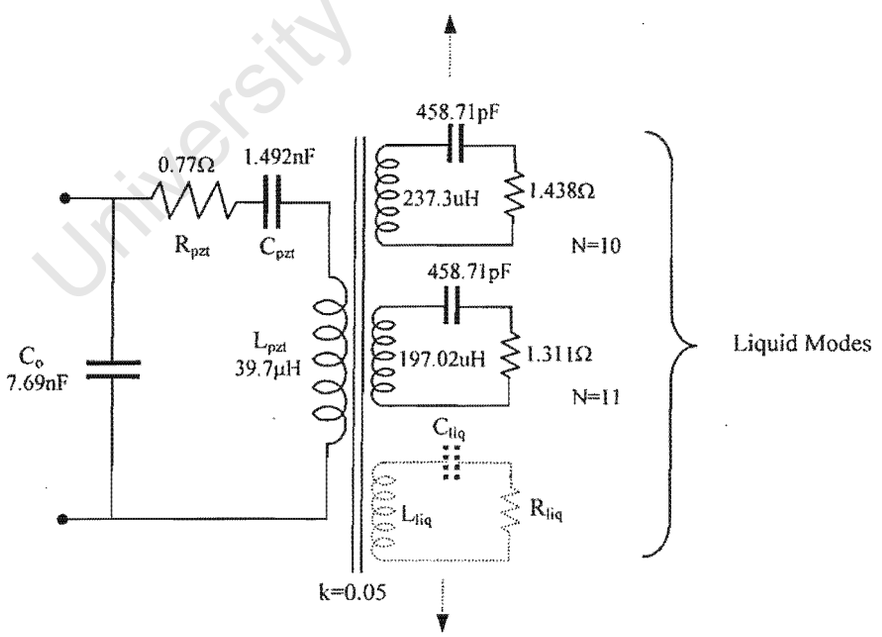

Figure 6-16: An equivalent circuit model showing mutual inductive coupling between the equivalent PZT circuit and individual liquid resonances, defined by the series tuned LCR circuit.

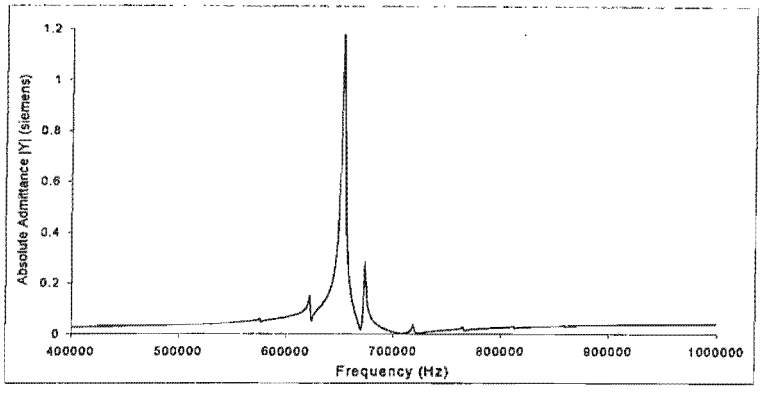

(a) Weak energy coupling, k=0.02.

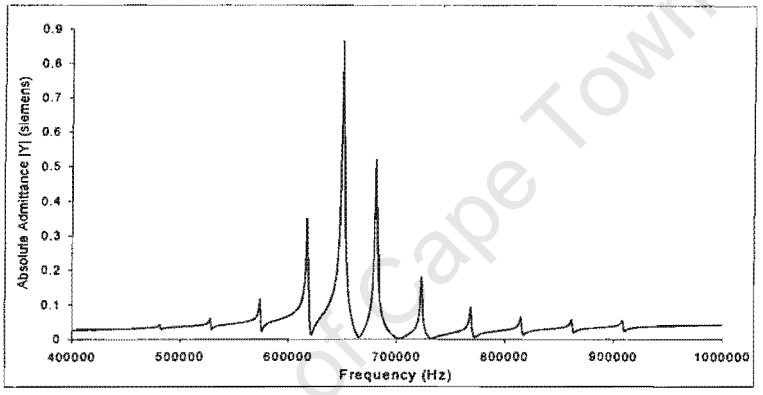

(b) Critical or Optimum coupling, k=0.05. The most commonly observed admittance spectra showing optimum energy coupling between the PZT and the liquid

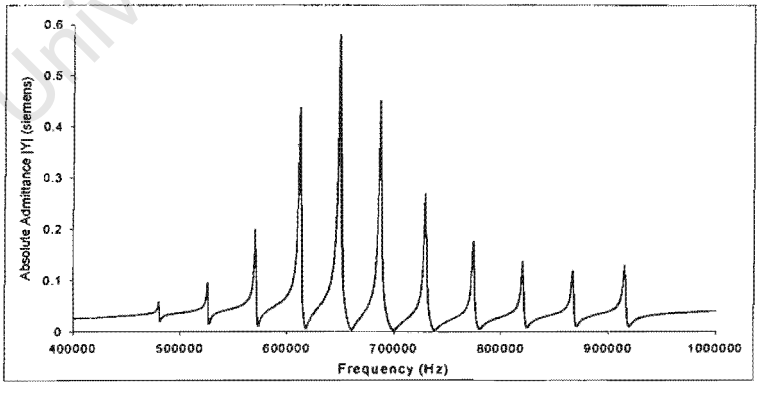

(c) Over coupling, k=0.08.

Figure 6-17: A simulation of absolute input admittance versus frequency for water. Each of the graphs is defined at a different coupling coefficient, enabling three completely different mechanical-liquid interactions to be observed. It is interesting to note the similarity between these simulations and the wetting phenomenon examined earlier.

A more thorough examination of Fig 6-17(b), being the critically coupled admittance, reveals a remarkable similarity to the measured results obtained for water (see Fig 6-9(a)). By using the same modelling procedures as before, individual (simulated) modes are re-modelled as equivalent electrical circuits and displayed in Figs 6-18 and 6-19. A comparison between the simulated (Figs.6-18 and 6-19) and measured (Figs 6-13 and 6-14) results are in general agreement[7] indicating that the coupled model is a reasonable analogue of the PZT-liquid behaviour.

A plot of simulated resonance frequency versus mode order (see Fig 6-20) shows the deviation caused by the PZT resonance and is analogous to the behaviour observed in Fig 6-11, therefore it is safe to assume that the mutually coupled circuits chosen in Fig 6-16 are a valid representation of the PZT-liquid transducer (within a constrained bandwidth).

A theoretical examination of the impedance equations governing the circuit in Fig 6-16 reveals that mutual coupling is determined by the impedance of the resonances and the inductance coupling coefficient k. By transposing the acoustic elements across the transformer, the effective input resistance R_{in} and Reactance X_{in} is given by the expressions :

$$R_{in} = R_{pzt} + \sum_{n=1}^{\infty} \frac{\omega^2 M_n^2 R_n}{Z_n^2} \tag{6.14}$$

$$X_{in} = X_{pzt} - \sum_{n=1}^{\infty} \frac{\omega^2 M_n^2 X_n}{Z_n^2} \tag{6.15}$$

where n represents mode order.

Although this simple demonstration shows the analogy between acoustic systems and electrical circuits, it does not facilitate a robust model under which multiple liquid modes may be coupled to a PZT resonance. In order to resolve this we next investigate a transmission line analysis.

6.4.3 A Transmission Line Analogue

Following Mason [77, Appendix A7.1], a derivation of the equation of motion for an adiabatic plane wave propagating in a viscous medium along the x axis, can be described by:

$$\frac{\rho \partial \dot{\xi}}{\partial t} = \kappa \frac{\partial^2 \xi}{\partial x^2} + (\chi + 2\eta) \frac{\partial^3 \xi}{\partial x^2 \partial t} \tag{6.16}$$

[7]Both simulated and measured functions for L,C and G follow the same shape, confirming the frequency pulling hypothesis. For absolute correlation, the bulk modulus needs to be transposed by the electromechanical turns ratio Φ[77]; this was later achieved with the transmission line model.

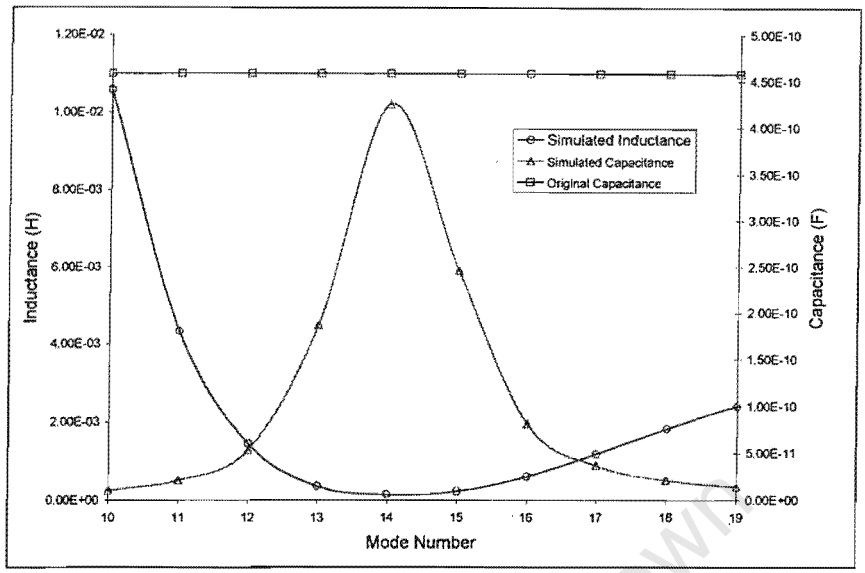

Figure 6-18: A plot of the modelled reactive components L and C versus mode number after the PSpice simulation. It is evident that the capacitance follows the same behaviour as that observed in the experiment, with inductance summed before resonance and subtracted after resonance. This would indicate that the combined Q of the resonant system is increasing with mode order, supporting a transmission line alternative.

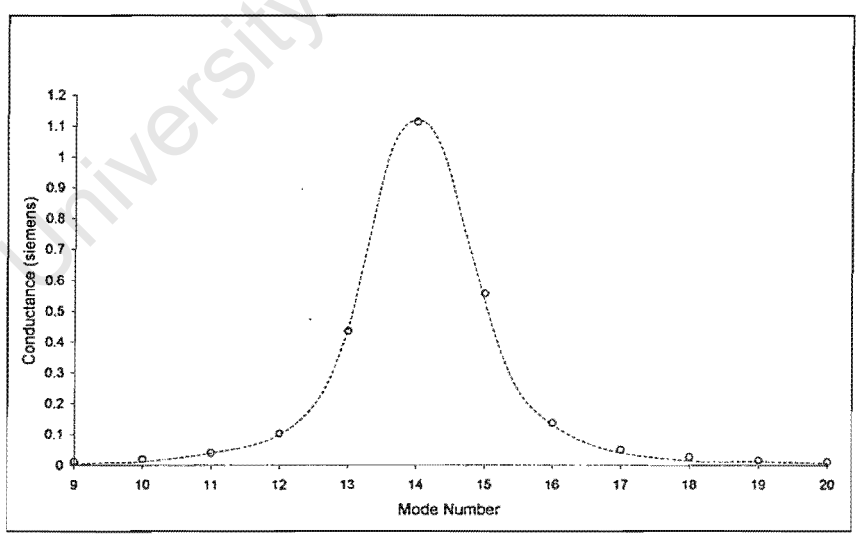

Figure 6-19: A plot of the modelled conductance versus mode number calculated from the results of the PSpice simulation. The bell-shaped curve closely matches that of Fig 6-14 being the modelled conductance determined by experiment. This result conclusively demonstrates power coupling between the PZT and the liquid, with maximum power transfer occurring at mode 14.

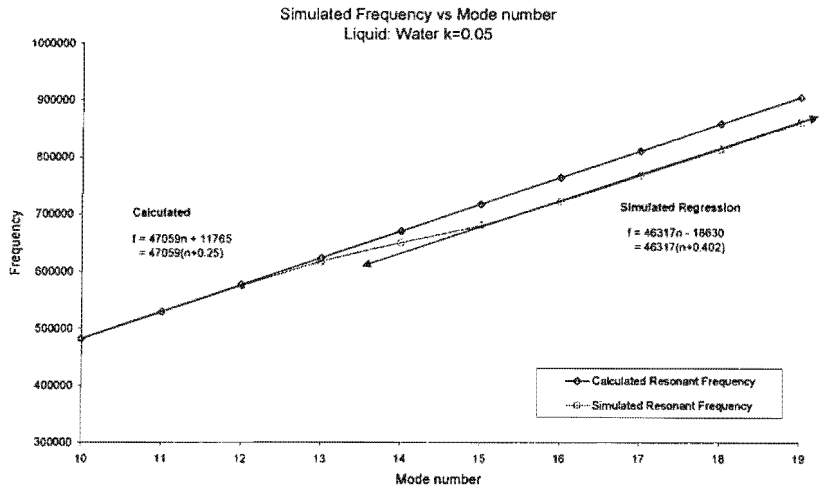

Figure 6-20: A plot of the resonant frequencies for the simulated liquid modes against calculated mode values. Note the identical behaviour to the observed measurements performed on water and FC75 (Fig.6-10 and 6-11). It is also interesting to see that frequency pulling only occurs post PZT resonance.

Assuming simple harmonic motion, equation 6.16 can be further reduced to:

$$\omega^2 \rho \xi + \frac{\partial^2 \xi}{\partial x^2} \{\kappa + j\omega(\chi + 2\eta)\} = 0 \tag{6.17}$$

where χ and η refer to the compressional and shear viscosities, κ the bulk modulus and ξ is the displacement.

A solution to equation 6.17 can be written in the form of input pressure, p, and linear velocity, $\dot{\xi}$ as follows:

$$p = p_r \cosh \Gamma x + \dot{\xi}_r Z_o \sinh \Gamma x \tag{6.18}$$

$$\dot{\xi} = \dot{\xi}_r \cosh \Gamma x + \frac{p_r}{Z_o} \sinh \Gamma x \tag{6.19}$$

Equations 6.18 and 6.19 follow the same solution to the time harmonic transmission-line equations found in electromagnetic wave theory, with pressure and velocity, the acoustic analogues of voltage and current [20]. Following a transmission line approach, which we have found to give a simple representation, we define the constants Γ and Z_o as the *propagation coefficient* and *characteristic impedance* of the acoustic transmission line. Both these quantities are defined

as follows:

$$\Gamma = \frac{\frac{j\omega}{v}}{\sqrt{1+\frac{j\omega(\chi+2\eta)}{\rho v^2}}} \tag{6.20}$$

$$= \alpha + j\beta \simeq \frac{\omega^2}{2\rho v^3}(\chi+2\eta) + \frac{j\omega}{v} \tag{6.21}$$

where ρ is the density, v the velocity of the liquid.

$$Z_o = \rho v\sqrt{1+\frac{j\omega(\chi+2\eta)}{\rho v^2}} \simeq \rho v\left\{1+\frac{j\omega(\chi+2\eta)}{\rho v^2}\right\} \tag{6.22}$$

The propagation coefficient can be described in terms of a real and imaginary components $(\alpha + j\beta)$, more commonly referred to as the *attenuation*[8], α, and *phase*, β, functions of the acoustic line. The characteristic impedance, on the other hand, refers to the ratio of the pressure and velocity at any point x along an infinitely long acoustic line and is in most cases approximated as $Z_o = \rho v$.

If we consider the symmetrical geometry of the cup transducer given by Fig 6-21(a), it is reasonable to assume that the center of the liquid column is a reflector of almost infinite acoustic impedance. With this analogy we can reduce the acoustic problem of the cup transducer to a simple one dimensional transmission line problem, shown in Fig 6-21(b) with the input acoustic impedance defined as

$$Z_a = S\frac{p_a}{\dot{\xi}_a} \tag{6.23}$$

where S is the surface area; and the terminating impedance defined per unit area as

$$Z_r = \frac{p_r}{\dot{\xi}_r} \tag{6.24}$$

Substituting the terminating impedance in equation 6.18 and 6.19 and rewriting we obtain

$$p_a = \dot{\xi}_r(Z_r\cosh\Gamma x + Z_o\sinh\Gamma x) \tag{6.25}$$

$$\dot{\xi}_a = \frac{\dot{\xi}_r}{Z_o}(Z_r\sinh\Gamma x + Z_o\cosh\Gamma x) \tag{6.26}$$

[8]A more classical solution to the attenuation function can be derived by considering Stokes's assumption that a radially expanding liquid has no losses, in which case the combined viscosity is defined as $\chi + 2\eta = \frac{4\eta}{3}$. For a more rigorous analysis of acoustic attenuation, heat conduction and structural relaxation should be considered.

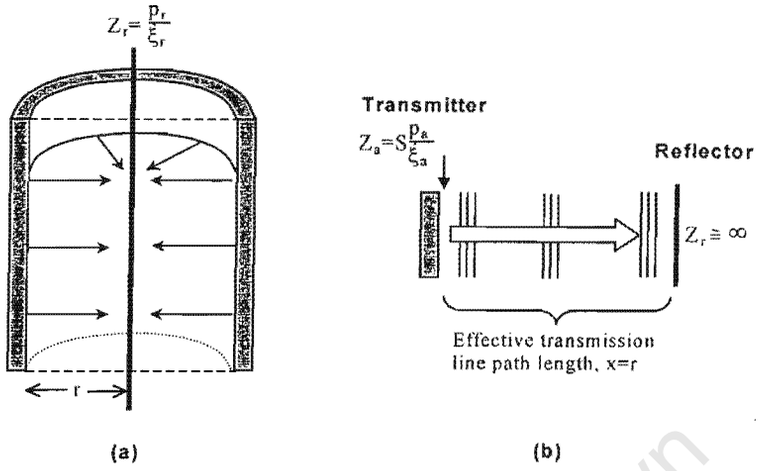

Figure 6-21: A physical schematic showing the convertion of the cylindrical transducer into a one dimensional acoustic transmission line. The solid line in the center of the tube represents the infinite impedance reflector Z_r, whilst the input impedance of the PZT tube is shown as $Z_a = S\frac{p_a}{\xi_a}$. The effective length of the transmission line is determined by the inside radius r of the tube.

which, substituted in equation 6.23 determines the total input acoustic impedance Z_a, for the acoustic transmission line of length x.

$$Z_a = SZ_o \left[\frac{1 + \frac{Z_o}{Z_r} \tanh \Gamma x}{\frac{Z_o}{Z_r} + \tanh \Gamma x} \right] \tag{6.27}$$

Assuming that the terminating impedance is infinite, we can evaluate the input acoustic impedance using the following hyperbolic function.

$$\lim_{Z_r \to \infty} Z_a = SZ_o \coth \Gamma x \tag{6.28}$$

As attenuation is of no critical importance to frequency pulling, nor the frequency behaviour of the transmission line, we assume that the attenuation is negligible i.e. $\Gamma = j\beta$, for a small diameter PZT tube. This allows us to further simplify equation 6.28 (using the identity $\tanh(j\beta l) = j \tan \beta l$) to the more manageable form:

$$X_{liq} = -jSZ_o \cot \beta x \tag{6.29}$$

where X_{liq} refers to the input reactance.

Recalling the numerical solution given by Blevins (Eq 6.12), the resonance frequency for each mode is offset by (n+0.25) which is a function of the cylindrical nature of the wave. Substituting this in Eq 6.29, we gain a revised value for the phase function β

$$\beta = \frac{\pi}{\Delta}\left\{\frac{f}{r} + \frac{\Delta^2}{4\pi}\right\} \tag{6.30}$$

where Δ refers to the frequency interval between modes given by $\Delta = \frac{v}{2r}$, and r is the radius of the cylinder.

Using equation 6.29 as the input reactance of the acoustic transmission line, and defining a resistance to account for viscous effects, we couple the acoustic network in the same way as we did before using a perfect transformer with mutual inductance defined by M. The acoustic network is coupled to the mechanical transmission line as derived by Mason [77] with $X_{pzt} = -2jZ_o \cot\frac{\omega t}{2v_{pzt}}$, and R_{pzt} representing the resistance in the crystal caused by elastic hysteresis, mounting losses and other forms of dissipation. A figure of the transmission line model is given in Fig 6-22.

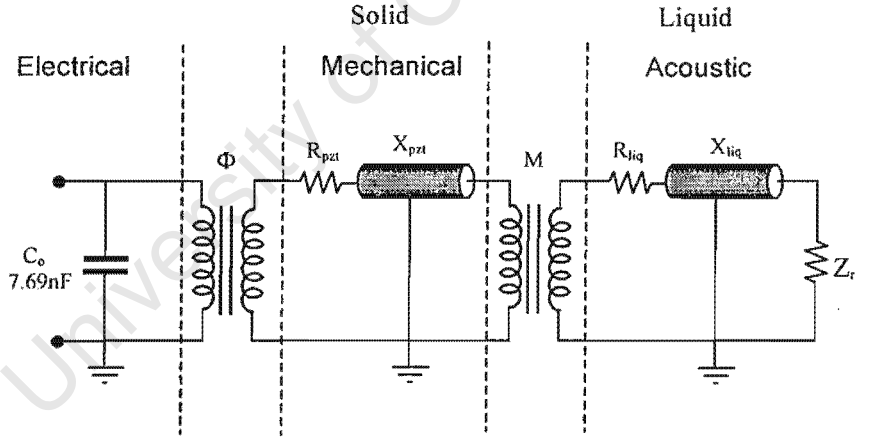

Figure 6-22: A new adaptation of Mason's electromechanical transmission line model is shown as a suitable model for the liquid-cup transducer. The physical and electrical components are isolated from one another by a perfect transformers. The liquid transmission line is terminated by an infinite impedance Z_r and has a series reactance $X_{liq} = -jS\cot\beta x$. The resistance R_{liq} corresponds to viscous effects present in the liquid, whilst the mechanical resistance R_{pzt} represents internal friction and mounting losses. Mason's turns ratio Φ and reactance are calculated as normal.

Using this analogy together with acoustic parameters already determined, we simulate the model using Matlab [78]. Admittance graphs comparing the model with experimentally mea-

sured parameters are given in Fig.6-23.

The acoustic model is in excellent agreement with the experiment, with modes corresponding precisely to the frequency intervals measured. This addendum to Mason's transmission line model, gives an acoustic analytic explanation for the behaviour of the acoustic resonant series present in the liquid filled PZT cup transducer. This resonator and acoustic resonant series will be used to measure B/A in the following chapter.

6.5 Conclusions

In this chapter we have examined the behaviour of a liquid filled PZT tube employed as a cup resonator. This has led to the uncovering of a loosely coupled series of acoustic modes, whose resonant frequencies are precisely linear as a function of mode order, except in the narrow bandwidth surrounding the PZT thickness resonance. These are analogous to a superposition of resonances, coupled to the piezoelectric equivalent circuit which can be simulated with PSpice. The origin and behaviour of this series was rigorously examined and the acoustic behaviour characterised in the form of an equivalent transmission line model. Mason's electro-mechanical model of a PZT transducer, although generic to many PZT systems, does not account for the behaviour of the cup transducer, where aspects of wetting and frequency pulling were observed. To account for this behaviour, Mason's model was adapted by coupling a second 'acoustic' transformer to the mechanical line. The coupling factor of the transformer accounts for both frequency pulling and the wetting phenomenon observed. This analysis is novel and contributes towards understanding tube resonators.

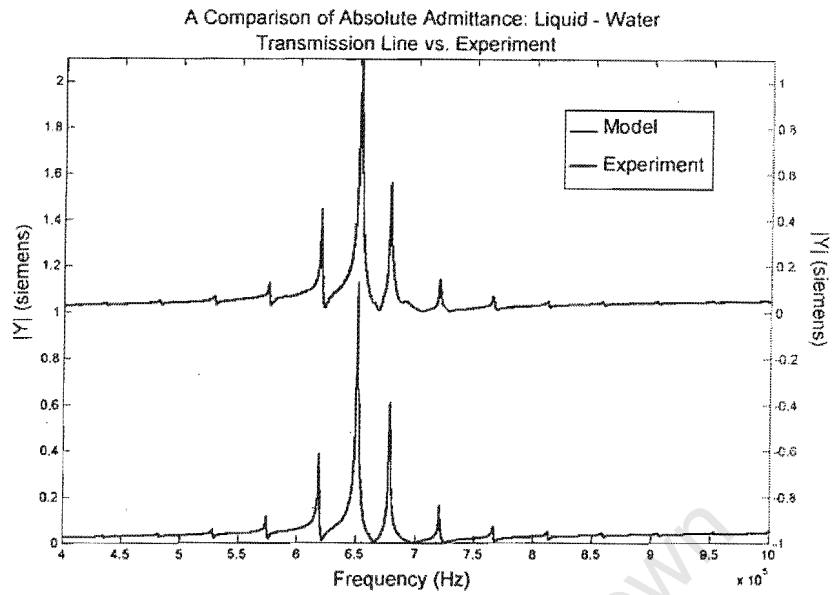

(a) Comparison of Admittance Spectra: Transmission Line model (blue) versus Measured values (green).

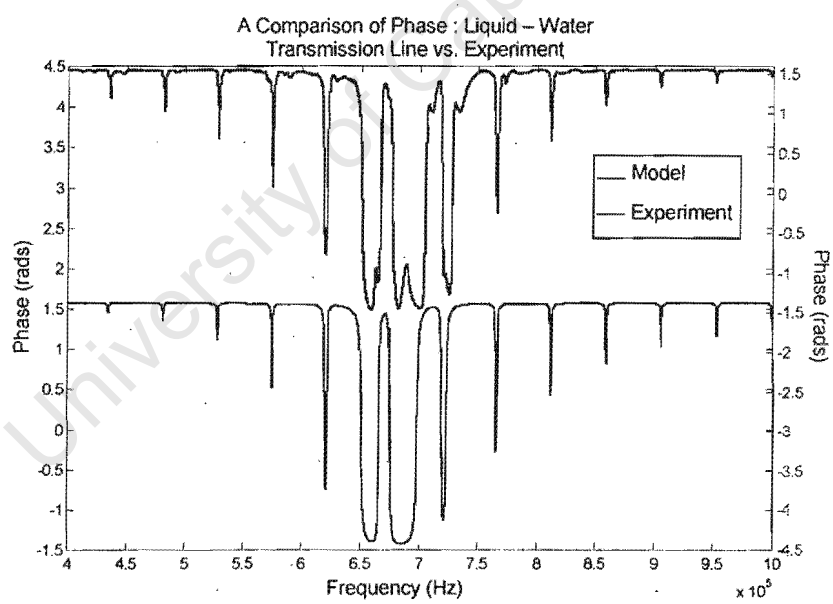

(b) Comparison of Phase Spectra: Transmission Line model (blue) verses Measured phase (green). The distortion in the phase at resonance is from spurious coupled satellite modes.

Figure 6-23: A comparative plot of absolute admittance and phase between the simulated transmission line model and measured results from a network analyser. The simulation is in excellent agreement with the measured results, showing the accuracy with which our model can represent the behaviour of the liquid-filled cup transducer.

Chapter 7

Resonant Phase Locking

The acoustic series uncovered in the previous chapter consists of a sequence of sharp liquid modes which are cylindrical in nature and harmonically spaced in frequency, except for a confined bandwidth (frequency pulling) adjacent to the PZT thickness resonance. These modes are characterised by their loose coupling and high quality factors, providing a favourable basis for continuous wave mode locking. The purpose of this chapter is to utilise the acoustic series using resonant phase locking to measure the nonlinearity parameter B/A isentropically.

We begin by developing a novel cavity resonator and lock-in system capable of trapping any liquid cavity resonance mode within the tube and tracking its phase velocity as a function of frequency. The cavity resonator was designed to both encapsulate and insulate the tube transducer, whilst facilitating the effortless pressurisation of the sample liquid. Forming the heart of the system, the resonant, phase-lock electronics are based on existing phase-lock technology outlined in chapter 5, using the inherently sharp phase gradient accompanying each mode to reach and maintain lock.

Resonant phase locking was used successfully to measure B/A for four sample liquids with a typical accuracy of less than 1%. The result of this method fulfils a primary objective of this study, this being to provide a simple continuous wave alternative to existing pulsed methods capable of accurately measuring B/A.

7.1 Designing a Resonator Cell

The resonator cell was designed to house the cylindrical cavity resonator used in the previous chapter. The geometry of this arrangement can be seen in the photograph and cross sectional schematic of the assembled cell (see Fig 7-1). Here the cavity resonator (a PZT 4 tube) was

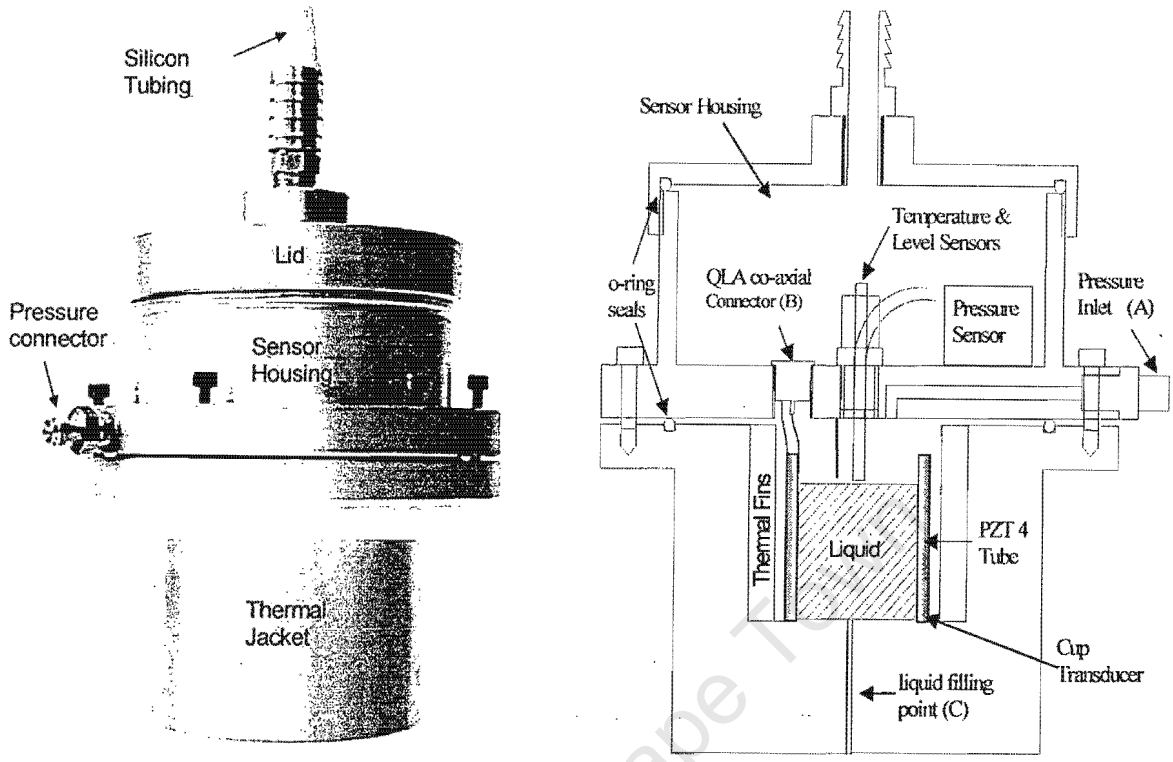

(a) A photograph of the assembled resonator cell

(b) A cross-section schematic of the resonator cell

Figure 7-1: The following two figures show a photograph (a) and schematic (b) of the tube resonator setup. The electronic housing and the thermal jacket, both made from brass, encase the PZT tube which was secured in place by an isobutylene glue, providing a watertight seal whilst minimising mechanical losses. The sample liquid was injected into the cell through a 2mm bored hole (Fig. b - (C)) and pressurised from the outside through a 3mm pressure inlet (Fig. b - (A)). Pressure and water tightness were maintained via o-ring seals.

attached at one end to an isothermal brass jacket to form a cup. The cylinder was affixed with an isobutylene compound which provides a watertight seal, whilst maintaining a weak acoustic coupling to the thermal jacket. The fixing was deliberately kept weak in order to reduce effects of damping typically associated with coupled structures. A second module housing the various temperature, pressure and level sensors fits over the cup transducer. This module, labelled the 'sensor housing', was a watertight capsule containing the various sensors and electrical feed-throughs to the cylindrical cavity. The sensor housing was attached to the thermal jacket using six, 4mm, cap screws, clamping a 3mm o-ring to provide a pressure-tight cylindrical cavity. Threaded onto the sensor housing is a lid, fitted with a silicon tube, which

acts as a watertight electrical feed-through for the various wires and cables. The assembled resonator was held by a perspex stand fitted with three radially spaced (120° apart) levelling screws, ensuring the liquid surface is always perpendicular to the PZT wall.

A detailed discussion for each of the two modules is presented in the undermentioned sections.

7.1.1 The Thermal Jacket

Fig 7-2 shows the brass jacket used to encapsulate the PZT tube. The primary function of the jacket was to house the tube and ensure that the sample liquid was adequately insulated. To achieve this, the dimensions of the jacket were determined using finite element methods (FEM) (ABAQUS - see Appendix C). From a heat transfer point of view, the jacket represents a thermal 'low pass filter' whose time constant is a function of the conductivity of the material and wall thickness. A trade-off exists in calculating this time constant, with the degree of thermal filtering proportional to the thermal inertia and time necessary for the sample liquid to reach isothermal conditions. It was decided therefore, based on the fluctuations measured in the water bath and the isothermal prerequisite defined for measuring B/A, that a 30 second time constant would suffice (see contour plot Appendix C). The base of the jacket was calculated using FEM to be 30mm thick, providing a direct conduction path to the liquid.

Heat conduction and convection lost through the walls of the cylinder were minimised by machining inwardly radiating thermal fins. The fins were designed for a twofold effect to:

- Increase the effective surface area inside the cylindrical cavity. This increases thermal conduction to the air surrounding the tube and traps convection pockets.

- Minimise backside radiation. By creating a series of annular fins along the inside of the thermal cavity, any unwanted acoustic radiation is suppressed.

Once the resonator cell is immersed in the water bath, the sample liquid needs to be injected into the resonator. This was achieved by drilling a 2mm hole into the bottom of the jacket. A liquid level sensor attached to the sensor housing determines the correct height of the liquid, and ensures that the thermometer (a platinum RTD) was immersed to the correct depth - typically 1mm. Fig 7-2 shows an annular groove, used as an electrical conduit for the miniature coaxial cable connecting the transducer to a 'QLA' connector (see Fig 7-1(b) B).

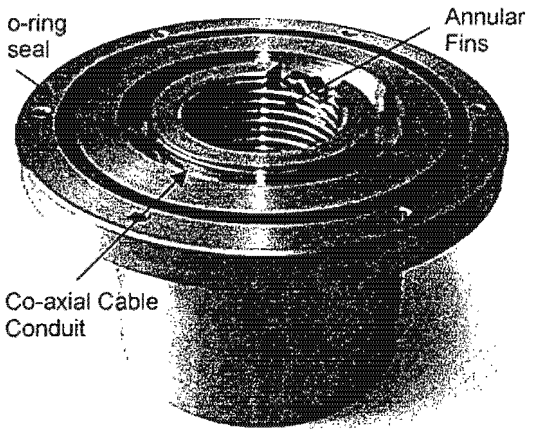

Figure 7-2: A photograph of the cylinder jacket without the PZT tube. The annular groove is a conduit for the miniature coaxial cable connecting the two modules together. The fins are machined as 6mm deep annular ridges, 1.5mm away from the outside of the tube.

7.1.2 Electronic Sensor Housing

Above the thermal jacket, the pressure and temperature sensors are housed in a watertight compartment sealed with a brass lid (see Fig 7-1(a)). The compartment holds a platinum RTD temperature sensor similar to that used in the small volume interferometer cavity. The RTD was calibrated and designed to measure thermal fluctuations of $\pm 0.001°C$ protruding approximately 4mm (1mm liquid depth) inside the cylinder cavity once assembled. The pressure transducer, an MPX 2200PA, is identical to that used in the small volume interferometer; the sensor is a strain gauge device with a single sensing port. The transducer was calibrated (see Appendix D) and fastened to a 4mm copper tube brazed to a hole bored between the two modules. The level sensor was attached to the extending RTD sensor, determining the correct height for the liquid within the tube.

To excite the PZT transducer and minimise cross-talk interference between other sensors, a coaxial feed was necessary. A miniature coaxial cable (3mm in diameter) was used for this purpose, attached to a QLA connector used to earth the resonator cavity and provide an electrical feed-through to the cylinder cavity. A similar coaxial cable was used underneath the sensor housing, between the QLA connector and the PZT. An annular groove in the thermal jacket creates a conduit for this excess cable, allowing the two modules to be taken apart.

The cylindrical cavity was pressurised through an 'L' shaped hole bored into the side of the sensor housing (see Fig 7-1(b)). Since the volume of air inside the resonator is sufficient to

create a 'capacitive' flow effect, the pressurisation time constant of two seconds was determined by the diameter of the helix shaped 'resistance' piping (see chapter 4) and the needle valve.

7.2 Mode Locking Electronics

The acoustic spectrum, uncovered in the previous chapter, is characterised by the sharp quality factors associated with each resonant mode, demonstrating a loosely coupled piezoelectric behaviour. In order to utilise this behaviour in a continuous-wave lock-in system, we re-examine the phase and conductance spectra, for modes preceding the fundamental thickness mode of the PZT[1]. A plot of conductance and phase for five water modes in the frequency interval 400kHz to 650kHz are shown in Fig 7-3.below. The preceding acoustic interval, chosen in

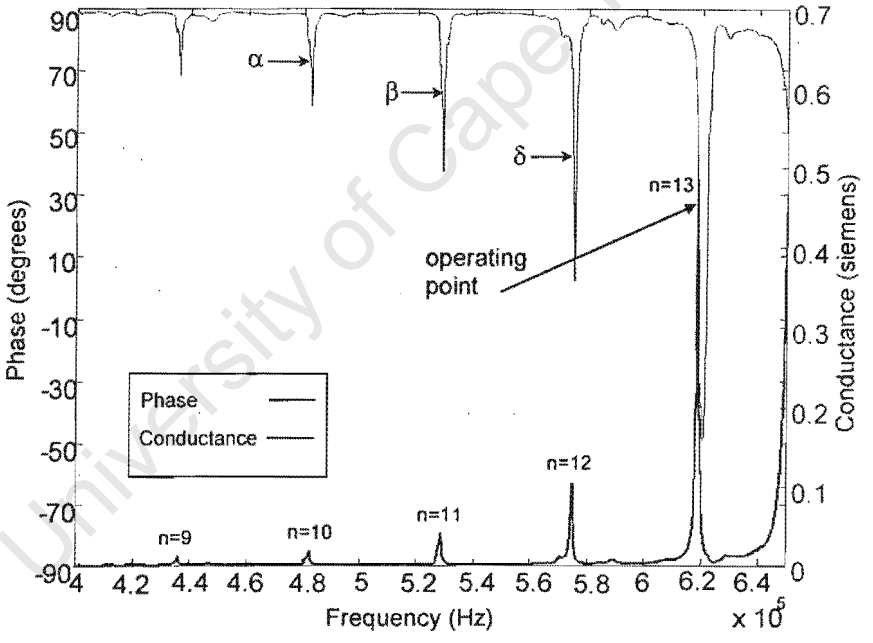

Figure 7-3: A plot of the phase (blue) and conductance (green) spectrum for water modes 9 through 13. From the plot it is evident that each mode is mirrored horizontally by a reciprocal phase dip. By observing the intersection between the conductance peak f_r and phase for mode 13, we notice an operating phase approximately halfway between 90°and the minimum phase dip. The slope $\frac{\partial \phi}{\partial f}$ defines the sensitivity of the loop and determines the closed loop gain.

[1]From Chapter 6 we observe that liquid modes are frequency pulled less before the fundamental PZT resonance. These modes tend to follow the theory provided by Blevins[17], and are therefore used for measuring B/A in this study.

accordance with the acoustic model developed earlier, indicates a liquid series more reliably defined away from the p.e. resonance. It is evident from Fig 7-3 that both the conductance and phase follow equally sharp peaks at each mode, suggesting two principal lock-in techniques applicable, namely:

- A band limited relaxation oscillator
- A resonant phase locked loop

Because phase locking has been shown to be effective and inherently stable in earlier systems, and given that changes in sound velocity are ultimately related as a deviations in phase, we have chosen to investigate resonant phase locking over the relaxation oscillator approach. It should be noted, however, that a self oscillating system should be as effective in measuring B/A, providing particular care is placed on frequency dependent phase contributions typically introduced by loop filters, which could lead to erroneous values for B/A.

7.2.1 Resonant Phase Locking

Resonant Phase Locking (RPL) is a term chosen for the following implementation of continuous wave mode locking. In contrast to Transmission Phase Locking, resonant phase locking uses the oscillating current flowing through the transducer as the phase feedback, locking the transducer at a point where the voltage and current are in quadrature (90° apart). Observing figure 7-3 reveals the capacitive behaviour of the PZT dominating the phase spectrum. Acoustic modes are characterised by the sharp dip in phase occurring at each conductance peak. In order to phase lock any particular mode, a slight phase injection in the form of a voltage offset is applied to the loop, causing the loop to lock at the liquid resonance. To further demonstrate this concept, we show Figs 7-4(b) and 7-4(a) representing the output of the phase detector ($\cos\phi$) and the phase relationship between two resonances of various magnitudes in an admittance vector diagram. The phase offset from quadrature between each of the two liquid modes is given by the symbols α, β, and δ and is shown in terms of the output from the phase detector. By subtracting this voltage (or phase offset), the loop will lock at the desired liquid mode. Applying the phase lock principles outlined in chapter 5, we develop the resonant phase locked loop shown in Fig 7-5. The current is simply measured as a voltage across a 1.8Ω resistor placed in series with the tube. The resistance was chosen sufficiently small so as not to appreciably reduce the acoustic resonance, yet large enough to ensure a reasonable signal to noise ratio.

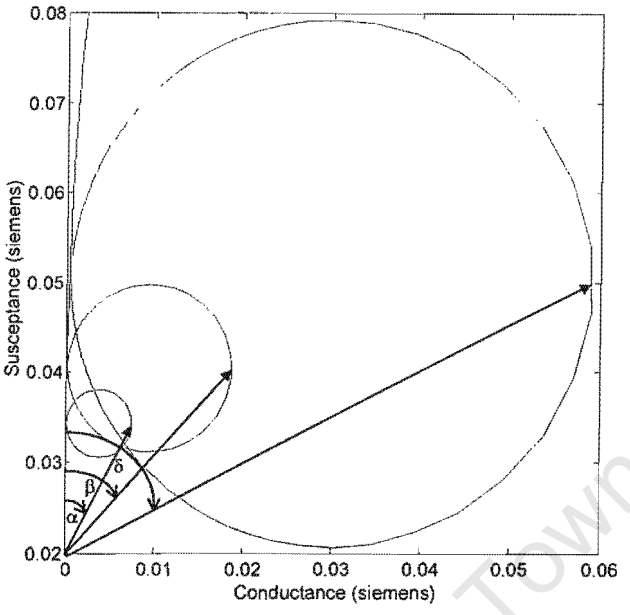

(a) A vector plot showing the deviation in phase for water modes 10 through 12

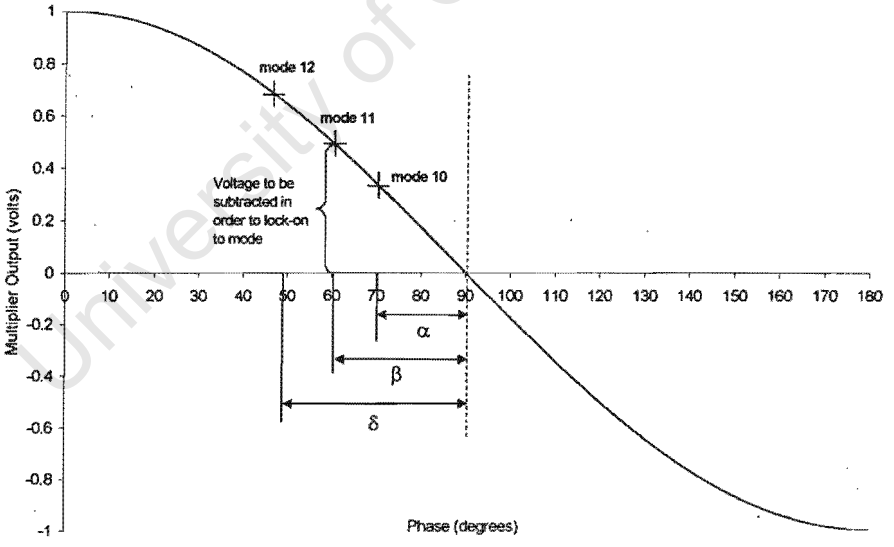

(b) A plot of voltage as a function of phase for an analogue phase detector

Figure 7-4: The following two figures show the relationship between phase, resonant frequency and multiplier output. The vector plot displays three circles, defining water modes 10 through 12. The phase for each mode is represented by the symbols α β and δ, which are plotted in terms of the DC multiplier output for the phase detector. The voltage offset needs to be subtracted by a reference voltage in order for the system to lock onto each mode.

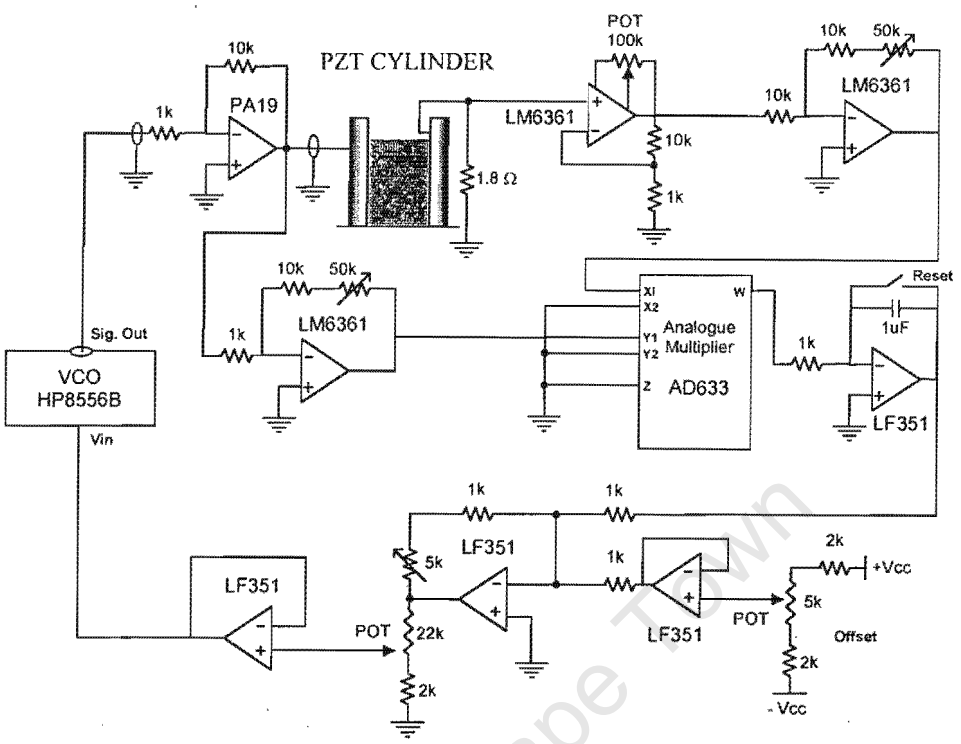

Figure 7-5: A circuit diagram of the Resonant Phase Locked Loop. The current from the transducer is sensed using a 1.8Ω resistor and compared in phase to the driving voltage. An offset using an opamp summer, enables the loop to lock anywhere between 10° and 170°. A reset switch is located in parallel with the integrating capacitance in the event the loop loses lock.

The loop itself is similar in function to the circuit designed for TPL, except the closed loop gain is controlled by the coupled transducer-liquid behaviour (modelled in chapter 6). The high Q of the acoustic series causes large loop gain at each mode, improving the signal to noise ratio and providing a highly stable lock condition. The phase offset shown in Fig 7-4(b), is subtracted by summing a reference voltage determined by a simple potential divider, creating a circuit capable of locking any liquid mode preceding the PZT resonance.

The circuit in Fig 7-5 produced a highly stable mode locking condition with tracking stability of a few parts in 10^7, an order of magnitude more stable than previous interferometer systems.

7.3 B/A Measurement using Resonant Phase Locking

The resonant phase locked loop and resonator cell described in this chapter were used to measure B/A for four test liquids at 30°C (see Table 7.1).

This measurement procedure was slightly different to TPL and was achieved thus:

1. Firstly the acoustic cavity was placed inside the empty temperature bath and the stand was adjusted so that the liquid and wall of the tube were normal to one another. This was achieved by using a centre bubble spirit level placed directly on top of the PZT tube.[2]

2. Water was then added and the temperature controller set for the desired operating temperature.

3. Once the setpoint temperature was reached, the sample liquid was injected into the cup transducer through the base of the resonator.

4. Output from the level sensor was monitored to ensure that the liquid reached the correct height, enabling the temperature sensor to be immersed to a defined depth of 1mm.

5. Lock-in electronics were enabled, trapping a predetermined liquid mode within the resonator cavity, and the system was then left to stabilise for one to two hours.

6. Thermal stability for the loop was monitored by both a temperature sensor (RTD) and (even more effectively) frequency tracking of sound velocity.

7. When thermal fluctuations of less than $\pm 0.001°C$ were observed, the measurement procedure was initiated as set out in Chapter 4.

The pressure circuit used in RPL is slightly different to TPL as there is no need for an intermediate pressure liquid (such as silicon oil). The system was designed to be pressurised within a two second time period. The time constant, τ, for this process was experimentally determined using a needle valve and helix shaped pressure constriction (see Chapter 4). A single iteration is plotted in Fig 7-6(a) showing the pressure profile inside the cavity with time. The corresponding change in sound velocity, is recorded through frequency and is plotted for the depressurisation process in Fig 7-6(b) as a function of time. Plotting frequency versus phase and applying the statistical techniques laid out earlier, we report results in Table 7.1. Again it should be noted that absolute measurement error of temperature and density are not included in this table.

It is interesting to compare the absolute values calculated for TPL and RPL, as their B/A values were determined to be within 1.2% of each other. The measurement accuracy for RPL, as would be expected, is slightly better than TPL because of the nonlinear loop response defined

[2]To ensure the surface of the tube was glued normal to the base of the thermal jacket, both base and tube surface were leveled using a center bubble spirit level.

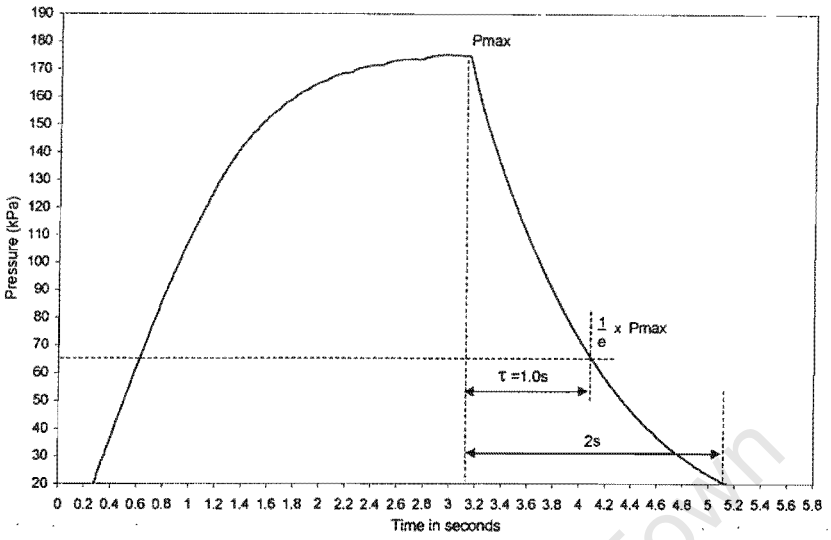

(a) A plot of the pressure variation as a function of time within the resonator cavity

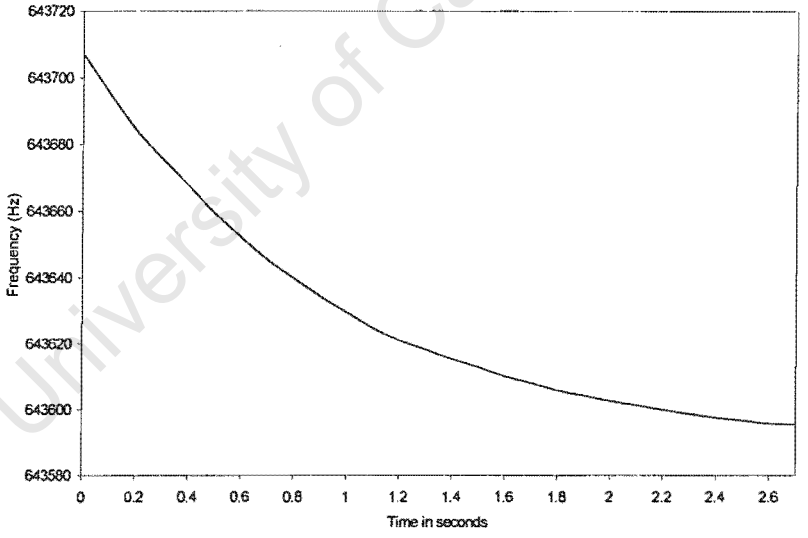

(b) Frequency tracking with time for a pressure drop of 180kPa.

Figure 7-6: The two figures above illustrate the depressurisation and frequency logging process for RPL. The resonator cavity is first pressurised to 180 kPa at which time the loop is locked to 643.7kHz. The resonator is then vented to the atmosphere through a pressure constriction circuit designed with a time constant of 1 second. The frequency logging procedure is done within a 2 second time window capturing a 170 kPa pressure drop for analysis.

Liquid *30°C*	**Velocity** *m/s*	**Density** kg/m^3	**B/A**	**Literature** *(B/A)*
Water	1509.12	995.7	5.13 ± 0.020	5.18 [111]
FC 43	638	1861	13.19 ± 0.023	12.85 [73]
FC75	567	1768	12.83 ± 0.021	12.19 [73]
CCl_4	1519	1002	8.34 ± 0.04	8.7 [11]

Table 7.1: A Table of measured values for B/A compared with those from the literature. Note the error in B/A is the uncertainty in gradient measurement df/dp only and does not include absolute measurement uncertainties

by the characteristically sharp phase gradients of the acoustic series. Measurement uncertainty for this method was calculated to be 0.48%. A sample plot of frequency versus pressure for a typical iteration is shown in Fig 7-7. Each sample run requires 100 measurement iterations, with an estimate of the average correlation coefficient for the gradient determined to be 0.9997. B/A results for the two slow sound speed fluorocarbons were satisfactory having a standard deviation of 0.02.

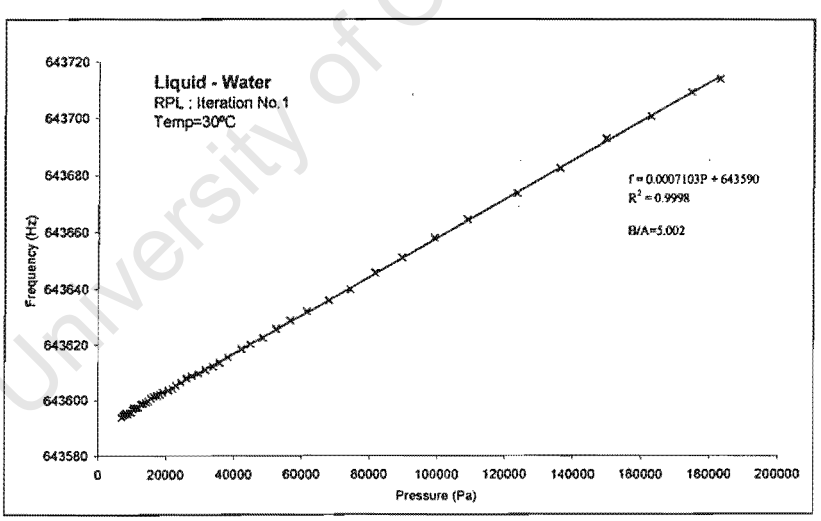

Figure 7-7: Frequency plotted as a function of pressure for water mode 13.

The results of these experiments are in good agreement with those found in the literature. Measured uncertainty for RPL based on a conservative statistical approach indicates that its accuracy in most cases exceeds that of pulsed techniques.

7.4 Conclusions

The resonant phase locked loop uses the sharp phase peaks caused by acoustic excitation to adequately determine and demonstrate the nonlinearity parameter B/A in several testing liquids. The system is far more stable than traditional interferometer cells and has a conservative error in measurement of less than 0.5%. The resonant phase locked loop provides a generic alternative to measuring B/A using continuous wave mode locking. The piezoelectric cylinder provides an ideal vessel to measure B/A as the size can be reduced to hold extremely small biological samples. Furthermore, the tube cavity provides a means of measuring the infinitesimal sound velocity of a liquid, with the only calibration being that of the diameter. Aside from the publications generated by this text, this work on B/A Resonant Phase Locking, is unique and represents a novel contribution to the field, especially small volume *in vitro* experimentation.

The limitations of RPL are determined by the physical size of the transducer. As the walls of the transducer become thinner, the higher the fundamental resonant frequency and as the diameter of the tube becomes smaller, the further apart the liquid modes will be spaced and liquid will be more difficult to remove. However the benefit of RPL over other small volume techniques such as SAM (scanning acoustic microscopy) is that the bulk measurement is made of the sample volume not just a localised measurement, which is more advantageous for measuring B/A of nonhomogenius biological preparations.

Chapter 8

Summary and Conclusions

The preceding chapters have described an investigation into the viability of implementing a continuous wave (c.w.) system for *in vitro* measurement of the nonlinearity parameter B/A. We have compared this technique with traditional pulsed B/A locked systems. The outcome of this investigation has led to two unique mode locking solutions each employing control electronics which are either simpler or superior to existing pulsed systems. The goal of measuring B/A using c.w. technology was achieved by first understanding the relevant problems associated with c.w. methods and solving these problems through novel electronic synthesis and design methodology. Furthermore, we have chosen to study the resonant behaviour of transducer coupled systems in an endeavour to unravel the complex relationship between phase and sound velocity, and to separate transducer characteristics from liquid behaviour. The salient points of this study are summarised in this chapter. They are reviewed in terms of the original work that has been performed and the ability with which continuous wave mode locking can successfully be used as a substitute for measuring B/A.

8.1 Contributions and Originality

The following list reports, in specific terms, the original work that constitutes the bulk of this thesis:

1. A novel continuous wave system was developed to trap liquid modes within an interferometer cavity. The design uses elementary analogue electronics to phase lock the driving voltage to the received voltage maintaining quadrature between each. This real-time approach to measuring B/A enables phase velocity to be accurately tracked throughout the

isentropic measurement process. Labelled 'Transmission Phase Locking', or TPL, this type of control system is the first implementation of c.w. mode locking for the purpose of measuring B/A [28].

2. Following similar designs [71, pgs 67-72] [37, pgs 75-81], various interferometer cavities were investigated resulting in the design of a small volume interferometer. Aspects of the design process and peripheral instrumentation were reviewed and practical solutions to several design problems were presented. The interferometer cell designed for this study was specific to continuous wave measurement and was used successfully to measure B/A for several liquids using TPL.

3. A theoretical foundation for TPL was developed using linear control theory. This theory is the first to be used in measuring B/A. A mathematical model for the closed loop system was formulated to include the resonance behaviour of the interferometer cavity under a confined operating bandwidth. Having defined the closed loop transfer function, control theory was applied to calculate the necessary loop filter characteristics to ensure a stable and absolute tracking of phase (or sound velocity within the interferometer cavity). This theory is central to the optimal design of TPL.

4. B/A was measured using four test liquids, including the two slow sound speed fluorocarbons FC43 and FC75. The fluorocarbon liquids, having the highest value for B/A of any inorganic liquid, were chosen to test the stability and tracking capabilities of the TPL loop. Results for B/A indicated good correlation with existing published values, however further observation revealed measurement uncertainties for liquid modes locked adjacent to or in the near vicinity of the fundamental PZT resonance. Although the technique for TPL requires only a single mode to be locked, further investigation of this phenomenon was necessary. A literature review revealed an uncertainty in the harmonic spacing of modes within an interferometer cavity. Although correction functions have been reported using mathematical derivations for absolute velocity measurement, it was suspected that the phenomenon was similar to 'frequency pulling' typically encountered in coupled electrical systems.

5. An investigation of various transducer geometries led to the unexpected excitation of a set of loosely coupled acoustic modes present within a liquid filled PZT tube. These modes were uncovered by implementing a wetting technique applied to the inside of the tube.

The acoustic series appears to be unreported in the literature and is therefore considered an original contribution to the field of acoustics [10].

6. The acoustic series was investigated in detail by analysing the electrical characteristics of admittance and phase. Equivalent circuit models were derived for each of the liquid modes present within a confined bandwidth. It was found that due to the extremely sharp quality factors of the individual modes and substantially loose piezoelectric coupling, the series was mostly harmonic; proving ideal for continuous wave measurement of B/A. A study of frequency pulling was confirmed using a lumped element analogy simulated using PSpice. This behaviour is the first to be reported, conclusively defining the coupled interaction between transducer and liquid resonance series.

7. Finite element methods (FEM) were used to investigate the resonant behaviour of the liquid-filled cup transducer. A cross-section contour plot of pressure revealed a cylindrical shape to the resonant series indicating a purely cylindrical transducer coupling. It was found that the liquid modes could only be generated using an extremely fine mesh of quadratic liquid element, with an element size of less than 0.25λ.

8. Experimental changes of liquid height within the PZT tube had relatively little effect on the acoustic spectrum, confirming the results obtained in the FEM examination and indicating a possible piezoelectric cancellation between longitudinal and radial modes for the observed tube geometry.

9. Adopting the well-understood theory of electrical and acoustic transmission lines, a new acoustic transmission line model was developed for the PZT tube. This model provides a necessary extension to Mason's original electro-mechanical circuit, enabling the mechanical-acoustic behaviour to be represented by an infinitely terminated transmission line circuit. The theory for this model includes an understanding of the observed wetting phenomenon caused by the mutual inductance of an independently coupled 'acoustic' transformer. This second transformer is essential in defining the mutually coupled behaviour between the liquid resonant series and the PZT resonant series. Using the newly derived model, frequency pulling can be explained and simulated, defining boundary conditions for which modes may be used to determine B/A. A comparison between experimental and simulated results show an excellent agreement.

10. A novel cavity resonator was designed to encapsulate the PZT tube so that liquid modes

could be exploited for measuring B/A. The cavity was constructed from brass and designed using FEM to enforce the prerequisites of isentropic phase measurement. The resonator was designed to house various sensors enabling the pressure, velocity and level of the liquid to be measured. In comparison with existing interferometer cells, the cavity resonator proves superior. The construction of the cell is relatively simple without the need for pressure diaphragms, and secondary pressure vessels. Also new liquids can be injected and removed from the cell *in situ* without the need for disassembly as with many interferometer systems.

11. A unique resonant phase locked loop (RPL) was designed to trap acoustic modes within the cavity resonator. The loop uses the novel idea of quadrature phase locking the transducer's driving voltage with current. The characteristic gradient of phase versus frequency defined by the cavity resonator, is used by the loop to track the resonance frequency of a liquid mode. During a change in sound velocity the loop experiences a similar change in phase which is immediately compensated for by feedback. In addition the loop experiences a nonlinear reduction in gain (and signal to noise ratio), which inherently forces the loop to seek a more stable operating point, returning the loop to its locked position. Nonlinear loop gain control is unique to the transducer filled cavity and is more stable than existing pulsed phase locked methods. This method has been reported in the literature by the present author [29].

12. B/A was successfully measured for the four test liquids and once again showed remarkable accuracy, comparing favourably with existing literature reports. Accuracies of typically 0.5% are frequently observed for RPL, classing it as one of the most accurate methods available for measuring B/A.

8.2 Advantages of Using Continuous Wave Methods

In this study we have shown conclusively that continuous wave methods are a viable and accurate low-cost technique for measuring the nonlinearity parameter B/A in liquids. Summarised below we list the benefits of c.w. systems over traditional pulsed systems.

- The c.w. measurement of B/A designed primarily for isentropic phase measurement, can easily be extended to the thermodynamic method, providing a replacement module for existing pulsed technology.

- The resonator cavity designed to encapsulate the transducer tube is simpler in function than interferometer cells typically used in pulsed systems. The cavity can be easily dismantled for cleaning purposes and facilitates *in situ* refilling and draining of the sample liquid. In comparison, interferometer cells are more tedious and time consuming in their application to measuring B/A.

- Many small volume interferometer cells suffer from problems associated with cross talk, diffraction and ringing between pulsed pairs, making it extremely difficult for edge detection and B/A measurement. The need for small volume acoustic cells is a requirement imposed by small yield biochemical samples. In response to this, continuous wave resonant locking is an ideal solution, with small volume PZT tubes readily available[1], and RPL impervious to cross talk and other coupling problems unique to pulsed systems.

- Measuring B/A using pulsed technology usually requires complex sample-and-hold microprocessor systems [37, pgs 85-86] which are often limited in bandwidth, accuracy and application. Such systems are either commercially manufactured or require extensive knowledge of electronics. As the primary goal and purpose of this study we have removed the complex nature of measuring B/A typically imposed by pulsed systems. The simplicity of c.w. measurement allows RPL instrumentation to be designed with relatively little knowledge of instrumentation electronics.

- In comparison with existing pulsed systems we have shown that continuous wave phase locking is inherently more stable than similar pulsed systems. The reason for this can be ascribed to the inherent noise rejection associated with phase lock systems, locking the phase to a point corresponding to acoustic resonance thereby inherently retaining the strongest signal to noise ratio.

- Table 8.1 draws a comparison between previously used pulsed methods and continuous wave methods used in this study (viz. TPL and RPL). Each measurement has been defined for water at 30°C. It is immediately apparent that continuous wave methods compare more than favourably in both accuracy and value with pulsed methods. From the table, the measurement uncertainty ($\frac{df}{dp}$ in water) for TPL is determined at 0.5%, whilst RPL is determined at 0.39% - a result exceedingly more accurate than similar reported pulsed systems. B/A values are shown to be similar to those of Zhang [111] yet

[1]Small volume PZT tubes are used as mechanical actuators in many scanning tunnelling microscopes.[104]

slightly less than those measured by Beyer [25] and Everbach [38]. The deviation in B/A can be attributed to thermal fluctuations present within the sample liquid. Since thermal insulation of the sample liquid was originally designed for a B/A accuracy of 1%, these fluctuations are within tolerance. Absolute measurement of temperature and density have contributed to the uncertainty in measurement and are shown here as σ_a.($\pm$1% for water). Since these measurements do not form the basis of this thesis, their uncertainty has been added separately. Relevant significant figures for the measurement of gradient have been added for comparison of the two techniques.

- Each continuous wave method was designed as a convergence on the method of maximum accuracy over existing pulsed methods with RPL being the more suited based on simplicity in method and construction and accuracy in measurement.

Water *Author*	**Temp.** *(°C)*	**Density** *kg/m³*	**Sound Velocity** *m/s*	**B/A** $\pm\sigma_g$ ($\sigma_a = \pm 0.05$)
Everbach [38]	30	995.7±0.1	1508.8±0.1	5.28 ±0.021
Zhang [111]	30			5.18 ±0.033
Beyer [25]	30	996	1509.26	5.21
TPL (This work)	30	995.7	1509.127±0.015 [30]	5.19 ±0.026 ($+\sigma_a$)
RPL [29]	30	995.7	1509.127±0.015 [30]	5.13 ±0.020 ($+\sigma_a$)

Table 8.1: A comparison between pulsed and continuous wave methods for measuring B/A in water at 30°C. Note absolute measurement uncertainty of the system has been added as σ_a

While the investigation of continuous wave measurement was aimed at improving existing techniques of the isentropic phase method, it can be easily adapted to measure B/A using the thermodynamic method. Phase lock methods integrating acoustic resonance behaviour are not only applicable to B/A design but may have relevance to many similar types of acoustic lock-in systems. The resonant behaviour and acoustic modelling can be applied to a variety of transducer instrumentation, with 'frequency pulling' providing an explanation to variable frequency velocimetry calculations. The results presented in this study are in the process of being disseminated through the scientific literature, and will hopefully reach an audience to whom they will prove most useful.

Chapter 9

Future Work

Continuous wave technology can be explored in many different aspects and the previously discussed chapters do not account for every newly-revealed possibility. Some of the directions in which aspects of this research can proceed are described in the following sections.

9.1 Admittance and Power Locking Techniques

We have chosen in this study to focus primarily on phase locking techniques to trap liquid modes within acoustic cavities. As an alternative to phase locking, a form of amplitude or admittance locking can be considered. The concept behind admittance locking is to use the amplitude of the admittance curve as a feedback mechanism to providing a frequency variable system capable of locking onto any admittance peak or local maxima. This admittance locked loop is based on the principle of maximum power transfer between the transducer and the liquid. This occurs when the current flowing through the transducer is kept at a maximum i.e. at resonance. To achieve this we require a hill climbing circuit, a block diagram of which is displayed in Fig 9-1.

The block diagram shows an RMS to DC converter which is used to derive the average magnitude of the transducer current. A 50% duty-cycle dither signal is used to modulate the VCO driving frequency. This dither generates a small modulation in the transducer drive current because the driving frequency dithers at two points above and below the average transducer driving frequency. These points operate at two different admittance values, essentially measuring the slope of the admittance curve over the dither frequency bandwidth. The magnitude of the transducer current is detected by the RMS-DC converter and includes a small signal due to the dither oscillation. The dither oscillation is used to synchronously detect this small

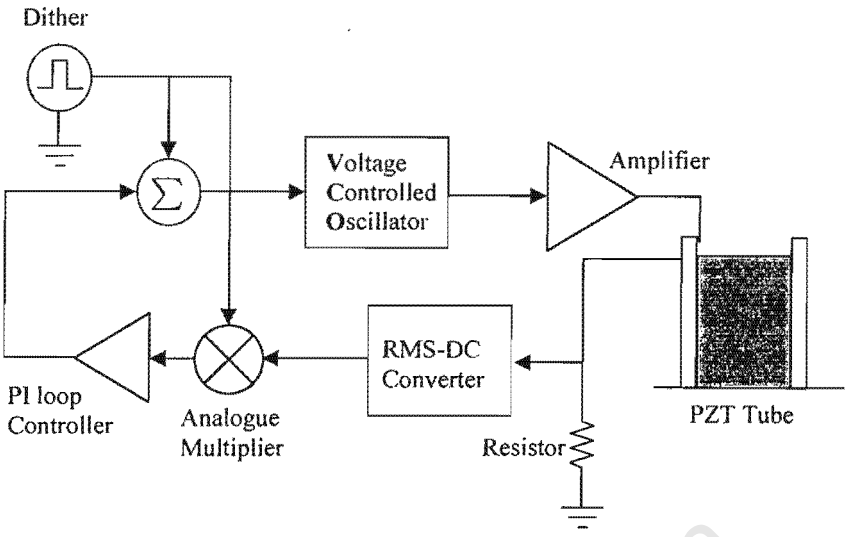

Figure 9-1: A Block diagram of the potential admittance locked loop. The transducer is represented here as a PZT tube, and is driven by a voltage source (represented here as a standard amplifier). The current through the transducer is an indication of the admittance and is measured through a series resistor. A DC voltage equivalent to the mean RMS value of the current is derived from an RMS to DC converter. This voltage is multiplied with the dither signal, which is also used to dither the input to the VCO. The multiplier output is proportional to $\frac{\partial Y}{\partial f}$,where Y is the admittance and f is the frequency. The loop is stabilised and controlled using a PI loop filter, using the gradient information to adjust the input level of the VCO, tracking the peak of the admittance.

signal (i.e. it demodulates it). The resulting output of the demodulator represents a slope of the admittance curve $\frac{\partial Y}{\partial f}$. A PI controller moves the VCO setpoint in the direction of the local admittance maxima. The circuit establishes the direction in which to move the operating frequency by detecting the current level at the extremities of the dither frequency excursion, which are ideally above and below the operating frequency.

Although this interesting circuit is a more complex alternative for B/A measurement and mode locking in general, it would be interesting to observe the effects of frequency pulling on amplitude locked acoustic modes. This type of mode locking system has been successfully used in power applications and is discussed in the literature [85].

9.2 Self Oscillating Systems

Another alternative to mode locking is the self oscillating circuit. These circuits are the principle behind many relaxation oscillators and are commonly used in frequency instrumentation

and timing circuits. Figure 9-2 shows a typical block diagram for a self oscillator needed to track phase velocity.

The block diagram shows the current through the PZT being sensed by a resistor in much the same way as admittance locking. This signal is then fed into a high gain amplifier, and band limited using a band pass filter. This ensures that the system oscillates at the desired mode. The signal is then fed through a variable phase (or time) delay circuit causing the driving signal to be at the correct resonant phase with the current. The phase delay is adjusted until a maximum oscillating signal is present at the resistor, ensuring the loop is locked at resonance. The large signal gains and inherent noise in the circuit cause the system to begin oscillating with maximum signal to noise ratio defined at resonance.

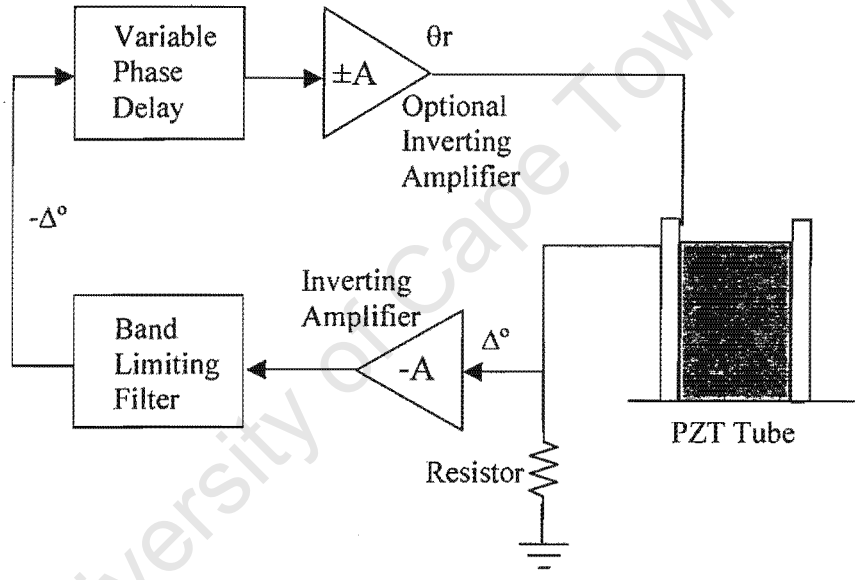

Figure 9-2: A block diagram showing the functional elements of a self oscillator designed for measuring B/A. The current through the transducer is sensed using a resistor and then fed through a phase independent band pass filter. This is used to ensure the loop oscillates at the desired acoustic resonance. The signal is then shifted in phase using a variable time delay, causing the output signal to be in phase with the driving signal at resonance.

Any change in sound velocity causes the resonance frequency of the system to change so that maximum signal is retained. This change in oscillating frequency is then used as a measure of differential velocity. The principle difficulty behind implementing such a system is to ensure that there is no frequency dependent phase contribution from the two filters. This will lead to incorrect values for B/A as shown in Chapter 3. The self oscillating circuit is however (in principle) optimal for mode locking and tracking.

9.3 Measuring B/A in Contrast Agents Using Pump Waves

During the course of this study, progress in the field of diagnostic ultrasound has increased significantly, with many new echo contrast agents being synthesized [59] [4]. In conventional angioplasty procedures, commercially available contrast agents are injected intravenously into the patient. These agents such as Levovist®[1] and SonoVue®[2] produce preformed coated microbubbles which are readily carried by the blood to the heart enabling opacification of both left and right cardiac cavities. Using echocardiography, the contrast between the blood being dominated by low acoustic impedance bubbles and the surrounding high impedance tissue becomes clearly visible and facilitates the assessment of myocardial perfusion [4].

The problem with this non invasive technique of observing blood flow and cardiac passages is that the microbubbles are destroyed by higher powered acoustic imaging. Many contrast systems deliberately 'flush' the contrast agent by applying increased acoustic power to the transducers; this has been shown to cause cavitation of the microbubbles with possible damage to blood cells [27] and the surrounding tissue [23].

The acoustic nonlinearity parameter B/A has been shown to be an excellent characterisation of bubbly media [64] and can therefore be used to measure the behaviour of microbubble derivative systems. The problem with measuring a contrast agent *in vitro* using the isentropic phase or thermodynamic methods is that the excess pressure is too large for the bubbles to survive. As an alternative technique we propose an amplitude modulated, resonant phase-locked loop. This loop will use small oscillatory pump waves supplied by the modulated signal to the transducer. The carrier wave will be used in conventional RPL as an extremely sensitive means of detecting changes in phase velocity caused by the small oscillatory changes in volume pressure. The two oscillatory signals defining sound velocity and pressure can be plotted against one another to determine a real-time value for B/A, which may be monitored with increased amplitude. This technique should accurately define the acoustic pressure necessary for microbubble collapse and characterise the liquid in terms of B/A.

9.4 Conclusions

This study has married together phase locking and continuous wave mode locking in a successful bid to measure B/A in a simple and accurate fashion. It is hoped that this study will be used

[1]Schering AG, Berlin Germany
[2]Bracco SpA, Milan, Italy

as a blueprint to encourage researchers unfamiliar with electronics to design and develop an accurate c.w. measurement instrument for measuring B/A. In the course of this study we have endeavoured to solve some of the many questions surrounding coupled piezoelectric systems. In so doing, we have given rise to further unanswered questions, which remain an exciting challenge for future research.

Bibliography

[1] The piezoelectric vibrator: Definitions and methods of measurement. *IRE Standards on Piezoelectric Crystals*, pages 353–358, 1957.

[2] M. Abramowitz and I. Stegan. *Handbook of Mathematical Functions.* Dover Publications, New York, 1970.

[3] N.T. Adelman and Y. Stavsky. Axisymmetric vibrations of radially polarized piezoelectric ceramic cylinders. *J. of Sound and Vibration*, 38(2):245–254, 1975.

[4] L. Agati, S. Funaro, G. Veneroso, C. Volponi, F. De Maio, M. Madonna, and F. Fedele. Non-invasive assessment of myocardial perfusion by intravenous contrast echocardiography: State of the art. *Ital Heart*, 2:403–407, 2001.

[5] R. Apfel. Prediction of tissue composition from ultrasonic measurements and mixture rules. *J. Acoust. Soc. Am.*, 79(1):148–152, 1986.

[6] J. Banchet and J.D. Cheeke. Measurement of the acoustic nonlinearity parameter B/A in solvents: Dependence on chain length and sound velocity. *J. Acoust. Soc. Am.*, 108(6):2754–2758, 2000.

[7] A.J. Barlow and E. Yazgan. Phase change method for the measurement of ultrasonic wave velocity and a determination of the speed of sound in water. *Brit. J. Appl. Phys.*, 17:807–819, 1966.

[8] J.F.W. Bell. Satellite resonances in ultrasonic interferometry. *Proc. Physical Society B*, LXIII:958–964, 1950.

[9] J.F.W. Bell. Private communications, 1996.

[10] J.F.W. Bell and J.R. Davies. A cavity for liquid velocity measurement. *Ultrasonics International*, July 1999. (Abstracts).

[11] R. Beyer. Parameter of nonlinearity in fluids. *J. Acoust. Soc. Am.*, 32(6):719–721, 1960.

[12] R. Beyer. *Nonlinear Acoustics in Fluids.* Van Nostrand Reinhold Co., Berkshire, England, 1984.

[13] R. Beyer. *Nonlinear Acoustics.* Acoustical Society of America, 1997.

[14] L. Bjørnø. Acoustic nonlinearity of bubbly liquids. *Applied Sci. Research*, 38:291–296, 1982.

[15] L. Bjørnø and P. Lewin. *Measurements of Nonlinear Acoustic Parameters in Tissue.* CRC, Boca Raton, 1986.

[16] D. Blackstock. Connection between the Fay and Fubini solutions for plane sound waves of finite amplitude. *J. Acoust. Soc. Am.*, 39(6):1019–1026, 1965.

[17] Robert D. Blevins. *Formulas for Natural Frequency and Mode Shape.* Van Nostrand Reinhold Co., New York, 1979.

[18] F.E. Borgnis. Theory of the acoustic interferometer for plane waves. *Acustica*, 7:151–175, 1957.

[19] N. Cedrone and D. Curran. Electronic pulse method for measuring the velocity of sound in liquids and solids. *J. Acoust. Soc. Am.*, 26(6):963–966, 1954.

[20] D.K. Cheng. *Field and Waves : Electromagnetics.* Addison-Wesley, New York, second edition, 1991.

[21] Ciba-Geigy. Thermosetting ceramic adhesive Araldite AT-1.

[22] W. Cobb. Finite amplitude method for the determination of the acoustic nonlinearity parameter B/A. *J. Acoust. Soc. Am.*, 73(5):1525–1531, 1983.

[23] A. Coleman, T. Kodama, M. Choi, T. Adams, and J. Saunders. The cavitation threshold of human tissue exposed to 0.2 Mhz pulsed ultrasound: Preliminary measurements based on a study of clinical lithotripsy. *Ultrasound in Med. and Biol.*, 21(3):405–417, 1995.

[24] J. Colladon and J. Sturm. Memoir on the compression of liquids. *Ann. Chim. Phys.*, 36:225–257, 1827.

[25] A. Coppens, R. Beyer, M. Seiden, J. Donohue, F. Guepin, R. Hodson, and C. Townsend. Parameter of nonlinearity in fluids II. *J. Acoust. Soc. Am.*, 38:797–804, 1965.

[26] CSIR, P.O. Box 395, Pretoria, South Africa.

[27] S. Daniels, T. Kodama, and D. Pierce. Damage to red blood cells induced by acoustic cavitation. *Ultrasound in Med. and Biol.*, 21(1):105–111, 1995.

[28] J. Davies. Determination of the acoustic nonlinearity parameter B/A using a phase locked ultrasonic interferometer. *J. Acoust. Soc. Am.*, 103(5):3080–3081, 1998.

[29] J. Davies, J. Tapson, and B. Mortimer. A novel phase locked cavity resonator for B/A measurements in fluids. *Ultrasonics*, 38:284–291, 2000.

[30] V. Del Grosso and C. Mader. Speed of sound in pure water. *J. Acoust. Soc. Am.*, 52(5):1442–1446, 1972.

[31] J.J. Dosch, D.J. Inman, and E. Garcia. A self-sensing piezoelectric actuator for collocated control. *J. of Intell. Mater. Syst. and Struct.*, 3:166–185, 1992.

[32] S. Earnshaw. *Phil. Trans. Roy. Soc.*, 150:133, 1860.

[33] W. F. Egan. *Phase-Lock Basics.* John Wiley and Sons, New York, 1998.

[34] F. Eggers. Ultrasonic velocity and attenuation measurements in liquids with resonators extending the MHz frequency range. *Acustica*, 76:231–240, 1992.

[35] F. Eggers and U. Kaatze. Broad-band ultrasonic measurement techniques for liquids. *Meas. Sci. Technol.*, 7:1–19, 1996.

[36] F. Eggers, U. Kaatze, K. H. Richmann, and T. Telgmann. New plano-concave ultrasonic resonator cells for absorption and velocity measurement in liquids below 1Mhz. *Meas. Sci. Technol.*, 5:1131–1138, 1994.

[37] E.C. Everbach. *Tissue Composition Determination Via Measurement of the Acoustic Nonlinearity Parameter.* PhD thesis, Yale University, New Haven, CT., 1989.

[38] E.C. Everbach. An interferometric technique for B/A measurement. *J. Acoust. Soc. Am.*, 98(6):3428–3438, 1995.

[39] E.C. Everbach and R.E. Apfel. Enhanced nonlinearity in a bubbly liquid considered as a mixture. *J. Acoust. Soc. Am.*, 83(S1):S109, 1988.

[40] R. Fay. Plane sound waves of finite amplitude. *J. Acoust. Soc. Am.*, 3:222–241, 1931.

[41] E. Fubini-Ghiron. Anomalies in the propagation of an acoustic wave of large amplitude. *Alta Freq*, 4:532–581, 1935. Translated by Robert Beyer.

[42] K. Fujii and R. Masui. Accurate measurements of the sound velocity in pure water by combining a coherent phase-detection technique and a variable path-length interferometer. *J. Acoust. Soc. Am.*, 93(1):276–282, 1993.

[43] F.M. Gardner. *Phaselock Techniques.* John Wiley and Sons, New York, 1979.

[44] X. Gong, Z. Zhu, T. Shi, and J. Huang. Determination of the acoustic nonlinearity parameter in biological media using FAIS and ITD methods. *J. Acoust. Soc. Am.*, 86(1):1–5, 1989.

[45] M. Greenspan and C. E. Tschiegg. Sing-around ultrasonic velocimeter for liquids. *Rev. Sci. Instr.*, 28(11):897–901, 1957.

[46] M. Hagelberg, G. Holton, and S. Kao. Calculation of B/A for water from measurements of ultrasonic velocity versus temperature and pressure to 10000kg/cm^2. *J. Acoust. Soc. Am.*, 41(3):564–567, 1966.

[47] B. Hartmann. Potential energy effects on the sound speed in liquids. *J. Acoust. Soc. Am.*, 65:1392–1396, 1979.

[48] E. Heidemann. Ultraschallforschung. *De Gruyter*, 1939.

[49] E. Heidemann and K. Zankel. The study of ultrasonic waveform by optical methods. *Acustica*, 11:213–223, 1961.

[50] R Helsel. *Visual Programming with HPVEE.* Prentice Hall, New Jersey, second edition, 1997.

[51] K. Heremans, F. Ceuterick, and J. Rijkenberg. High pressure jump apparatus. *Rev. Sci. Instrum.*, 51(2):252–253, 1980.

[52] HKS, 1080 Main St., Pawtucket, Rhode Island. *ABAQUS.*

[53] J.P. Holman. *Heat Transfer.* McGraw-Hill, New York, 1997.

[54] P. Horowitz and W. Hill. *The Art of Electronics.* Cambridge, 2nd edition, 1989.

[55] J.C. Hubbard. The acoustic resonator interferometer: I. The acoustic system and its equivalent electrical network. *Physical Rev.*, 38:1011–1019, 1931.

[56] T.F. Hueter and R.H. Bolt. *Sonics.* John Wiley and Sons, New York, 1955.

[57] F. Ingenito and B. Cook. Theoretical investigation of the integrated optical effect produced by sound fields radiating from plane pistons. *J. Acoust. Soc. Am.*, 45(3):572–577, 1969.

[58] P. Jiang, E.C. Everbach, and R. Apfel. Applications of mixture laws for predicting the composition of tissue phantoms. *Ultrasound Med. in Biol.*, 17(8):829–838, 1991.

[59] F. Jung. Microbubbles and the microcirculation. *Adv. in Cardiac Echo-Contrast*, 5(3):86, 1997.

[60] H. Kashkooli, P. Dolan, and C. Smith. Measurement of the acoustic nonlinearity parameter in water, methanol, liquid nitrogen, and liquid helium-II by two different methods: A comparison. *J. Acoust. Soc. Am.*, 82(6):2086–2089, 1987.

[61] S. Kato, H. Nomura, and Y. Miyahara. Cylindrical resonator technique for ultrasonic absorption measurement and its application to cellulose acetate-cyclohexanone system. *Polymer J.*, 11:455–461, 1979.

[62] L. Kinsler, A. Fry, A. Coppens, and J. Sanders. *Fundamentals of Acoustics.* John Wiley and Sons, New York, 1982.

[63] W. Knoche and G. Wiese. An improved apparatus for pressure-jump relaxation measurements. *Chem. Instrum.*, 5:91–98, 1974.

[64] Y.A. Kobelev and A.M. Sutin. Difference-frequency sound generation in a liquid containing bubbles of different sizes. *Sov. Phys. Acoust.*, 26(6):485–487, 1980.

[65] S. K. Kor and U. S. Tandon. Scattering of sound by sound from beyer's (B/A) parameters. *Acustica*, 28:129–130, 1973.

[66] P.E. Krasnooshkin. On supersonic waves in cylindrical tubes and the theory of the acoustic interferometer. *Physical Rev.*, 65(5 and 6):190–195, 1944.

[67] V. Krassilnikov, V. Shklovkaya-Kordy, and L. Zarembo. On the propagation of ultrasonic waves of finite amplitude in liquids. *J. Acoust. Soc. Am.*, 29(5):642–647, 1957.

[68] A. Kundt and O. Lehmann. Über longitudinale schwingungen und klangfiguren in cylindrischen flüssigkeitssäulen. *Poggendorff's Ann. Phys. Chem.*, 153:1–12, 1874.

[69] L.M. Kustov, V.E. Nazarov, and A.M. Sutin. Nonlinear sound scattering by a bubble layer. *Phys. Acoust.*, 32(6):500–503, 1986.

[70] K. Lautscham, F. Wente, W. Schrader, and U. Kaatze. High resolution and small volume automatic ultrasonic velocimeter for liquids. *Meas. Sci. Technol.*, 11:1432–1439, 2000.

[71] W. Law. *Measurement of the Nonlinearity Parameter B/A in Biological Materials Using the Finite Amplitude and Thermodynamic Method.* PhD thesis, University of Illinois, Urbana-Champaign, 1984.

[72] V.N. Lazutkin and Yu.V. Tsyganov. Axisymmetric modes and electrical impedance of radially polarized piezoelectric ceramic rings. *Sov. Physics*, 17(3):330–334, 1972.

[73] W. Madigosky, I. Rosenbaum, and R. Lucas. Sound velocities and B/A in fluorocarbon fluids and in several low density solids. *J. Acoust. Soc. Am.*, 69(6):1639–1643, 1981.

[74] G.E. Martin. Determination of equivalent-circuit constants of piezoelectric resonators of moderately low Q by absolute-admittance measurement. *J. Acoust. Soc. Am.*, 26(3):413–420, 1954.

[75] W. Mason and R. Thurston. *Physical Acoustics - Principles and Methods*, volume VIII. Academic Press, New York and London, 1971.

[76] W. P. Mason. *Electromechanical Transducers and Wave Filters.* Van Nostrand, Princeton, New Jersey, 1934.

[77] W.P. Mason. *Piezoelectric Crystals and their Applications to Ultrasonics.* Van Nostrand, Princeton, New Jersey, 1950.

[78] Mathworks, 3 Apple Hill Drive, Natick, MA, USA. *Matlab.*

[79] H. McSkimin. Variations of the ultrasonic pulse-superposition method for increasing the sensitivity of delay-time measurements. *J. Acoust. Soc. Am.*, 37(5):864–871, 1965.

[80] R.L. Melcher and D.I. Bolef. *Phys. Rev.*, 178:864, 1969.

[81] G.L. Miller and E.R. Wagner. Resonant phase shift technique for the measurement of small changes in grounded capacitors. *Rev. Sci. Instrum.*, 61(4):1267–1272, 1990.

[82] E. A. Moelwyn-Hughes. *Physical Chemistry*, volume 7. Pergamon Press, Oxford, 1961.

[83] M. Moffet, P. Westervelt, and R. Beyer. Large-amplitude pulse propagation - a transient effect. *J. Acoust. Soc. Am.*, 47(5):1473–1474, 1970.

[84] B. Mortimer. *Liquid Wave Focusing and the Production of Pulsed Jets.* PhD thesis, University of Witwatersrand, Jhb, South Africa, 1997.

[85] B. Mortimer, T. Du Bruyn, J. Davies, and J. Tapson. High power resonant tracking amplifier using admittance locking. *Ultrasonics*, 39:257–261, 2001.

[86] T. Muir and E. Carstensen. Prediction of nonlinear acoustical effects at biomedical frequencies and intensities. *Ultrasound in Med. and Biol.*, 6:345–357, 1980.

[87] K. Negishi, T. Takagi, and H. Ozawa. Observation of phase advance due to diffraction of ultrasonic pulse. *J. Acoust. Soc. Jpn.*, E(1980):151, 1980.

[88] K. Negita and H. Takao. Superposed pulse echo overlap method for ultrasonic sound velocity measurement. *Rev. Sci. Instrum.*, 60(11):3519–3521, 1989.

[89] K. Ogata. *Modern Control Engineering.* Prentice-Hall, Englewood Cliffs, N.J., 1990.

[90] E. Papadakis. Ultrasonic phase velocity by the pulse-echo-overlap method incorporating diffraction phase correction. *J. Acoust. Soc. Am.*, 42(5):1045–1051, 1967.

[91] R. Pethrick. The swept frequency acoustic resonant interferometer: Measurement of acoustic dispersion parameters in low megahertz frequency range. *J. of Phys. E: Scientific Instr.*, 5:571–574, 1972.

[92] PI Ceramics, Polytec-Platz, 1-7 D-76337 Waldbronn, Germany.

[93] A. Pierce. *Acoustics.* McGraw-Hill (reprinted by Acoustical Society of America), New York, 1981.

[94] S. Poisson. Memoir on the theory of sound. *J. Ec. Poltech.*, 7:364–370, 1808.

[95] I. Rudnick. On the attenuation of finite amplitude waves in liquids. *J. Acoust. Soc. Am.*, 30(6):564–567, 1958.

[96] R. Ryan, A. Lutsch, and R. Beyer. Measurement of the distortion of finite ultrasonic waves in liquids by a pulse method. *J. Acoust. Soc. Am.*, 34(1):31–35, 1962.

[97] F. Sanders. Diffraction of light by ultrasonic waves. *Nature*, 138:285, 1936. (Letters to the editor).

[98] C. Sehgal, R. Bahn, and J. Greenleaf. Measurement of the acoustic nonlinearity parameter B/A in human tissue by a thermodynamic method. *J. Acoust. Soc. Am.*, 76(4):1023–1029, 1984.

[99] Federal Standard. Telecommunications: Glossary of telecommunication terms. *1037C*, 1996.

[100] D. Stansfield. *Underwater Electroacoustic Transducers.* Bath University Press, 1990.

[101] G. Stokes. On the difficulty in the theory of sound. *Philos. Mag.*, 33:349–356, 1848.

[102] F.G. Stremler. *Introduction to Communication Systems.* Addison-Wesley, New York, third edition, 1990.

[103] J. Strutt (Lord Rayleigh). *The Theory of Sound*, volume 1 and 2. Macmillan and co., New York, second edition, 1894.

[104] J. Tapson. *A Wide-Area Scanning Tunneling Microscope Configured for Metallurgical Research.* PhD thesis, University of Cape Town, 1994.

[105] J.R. Taylor. *An Introduction to Error Analysis.* University Science Books, California, 1982.

[106] Temperature Controls, 5d Maitland Park, Voortrekker Rd, Bellville, South Africa.

[107] R.N. Thurston and A.D. Pierce. *Ultrasonic Measurement Methods*, volume XIX. Academic Press, 1990.

[108] D.H. Wolaver. *Phase-Lock Loop Circuit Design.* Prentice Hall, Englewood Cliffs, New Jersey, 1991.

[109] W.T. Yost and J.H. Cantrell. Fundamental aspects of pulse phase-locked loop technology-based methods for measurement of ultrasonic velocity. *J. Acoust. Soc. Am.*, 91(3):1456–1468, 1992.

[110] J. Zhang. *Influences of Biological Structural Features on the Acoustic Nonlinearity Parameter B/A*. PhD thesis, University of Illinois, Urbana-Champaign, 1990.

[111] J. Zhang and F. Dunn. A small volume thermodynamic system for B/A measurement. *J. Acoust. Soc. Am.*, 89(1):73–79, 1991.

[112] Z. Zhu, M. Roos, W. Cobb, and K. Jensen. Determination of the acoustic nonlinearity parameter B/A from phase measurements. *J. Acoust. Soc. Am.*, 74(5):1518–1521, 1983.

Appendix A

Calculations and Derivations

A.1 Derivation of the Compressibility of a Fluid

From the Taylor expansion in Chapter 1 (Eq 1.3), we obtain definitions for $A = \rho_0 c_0$ and $B = \rho_0^2 \left(\frac{\partial^2 P}{\partial \rho^2}\right)$, resulting in the following expression for the nonlinearity parameter B/A:

$$\frac{B}{A} = \frac{\rho_0^2 \left(\frac{\partial^2 P}{\partial \rho^2}\right)_S}{\rho_0 c_0} = \frac{\rho_0}{c_0^2}\left[\frac{\partial^2 P}{\partial \rho^2}\right]_S = \frac{\rho_0}{c_0^2}\left[\frac{\partial}{\partial \rho}(c_0^2)\right]_S \tag{A.1}$$

Remembering $c^2 = \frac{\partial P}{\partial \rho}$,and defining γ as the *compressibility* of the fluid we obtain

$$\frac{B}{A} = \frac{1}{c_0^2}\left[\frac{\partial(\rho c_0^2)}{\partial \rho} - c_0^2\right]_S = \frac{1}{c_0^2}\left[\frac{\partial\left(\frac{1}{\gamma}\right)}{\partial \rho}\right]_S - 1 \tag{A.2}$$

$$= \left[\frac{\partial\left(\frac{1}{\gamma}\right)}{\partial P}\right]_S - 1 \tag{A.3}$$

A.2 Heat Loss During the Pressure Jump Process

Equation 1.14 describes B/A in terms of an isentropic change in sound velocity with pressure. Using this equation to measure B/A requires a technique that ensures minimal entropy loss. This pre-requisite is practically achieved by holding the sample liquid at a constant temperature and ensuring an isothermal pressure jump by performing the measurement over a short time frame. The length of this frame can be calculated using a lumped heat capacity approach as follows:

Consider the small volume interferometer (see Chapter 5) filled with a volume of water V, at a measurement temperature T_s. The water volume, having a certain thermal capacitance, will lose energy during a typical depressurisation. This decrease in internal energy Q_t [53] [110] can be described by:

$$Q_t = -\rho C_p V(\Delta T_s) \tag{A.4}$$

where ρ is the density, C_p the specific heat capacity and ΔT_s the change in temperature of the water.

Assuming this energy is transferred by conductance and that the heat-transfer rate per unit area is proportional to the normal temperature gradient across the cylindrical interferometer shell, we may calculate the heat transfer rate q using Fourier's law[53] of heat conduction as follows:

$$q = \frac{dQ_t}{dt} = -k_t A \frac{dT_s}{dr} \tag{A.5}$$

where k is the thermal conductivity of the cylinder, A is the inside surface area and r the radius of the cylinder. Solving for boundary conditions ΔT_s across the cylinder thickness $(r_i - r_o)$ we obtain:

$$\frac{dQ_t}{dt} = \frac{2\pi k_t l \Delta T_s}{\ln(\frac{r_o}{r_i})} \tag{A.6}$$

for a length l between the transducers.

Using equations A.4 and A.6, we can calculate the absolute ratio of heat flow during any time period $\Delta t \simeq dt$, to the total heat loss as follows:

$$\left|\frac{\Delta Q_t}{Q_t}\right| = \frac{2\pi k_t l \Delta t}{\rho C_p V \ln(\frac{r_o}{r_i})} \tag{A.7}$$

Using the following values for water and perspex[1] and substituting into equation A.7

$k_t = 0.18$ W/m·°C

$l = 4$ cm

$\rho = 995.7$ kg/m^3

$V = 7.25$ cm^3

[1]chemical name: polymethylmethacrylate

$r_i = 7.6$ mm

$r_o = 11.6$ mm

$C_p = 4179$ J/kg·°C

$\Delta t = 2$ s

we obtain $\left|\frac{\Delta Q}{Q}\right| = 7.085 \times 10^{-3}$, which means that 0.7% of heat is transferred from the water to the surrounding silicon oil during a 2 second depressurisation. This is a good approximation of an isentropic process and will have marginal effect on the measurement of B/A.

A.2.1 Heat Contribution by the Transducer

Although applying energy to a transducer will cause it to heat up, it is a consequence of a continuous wave system that it operates at thermal equilibrium in a temperature controlled environment. This 'steady state' condition was ensured by allowing the entire system (in both RPL and TPL) to reach thermal equilibrium once power had been applied to the transducer. With this assumption, and the fact that the entire measurement procedure was achieved during a 2 second time frame enables us to safely assume quasi-isentropic conditions for B/A measurement. The electrical power applied to the transducers never exceeded 1 watt in any of the measurements.

Appendix B

Selected Electronic Schematics

B.1 Pressure Transducer Electronics

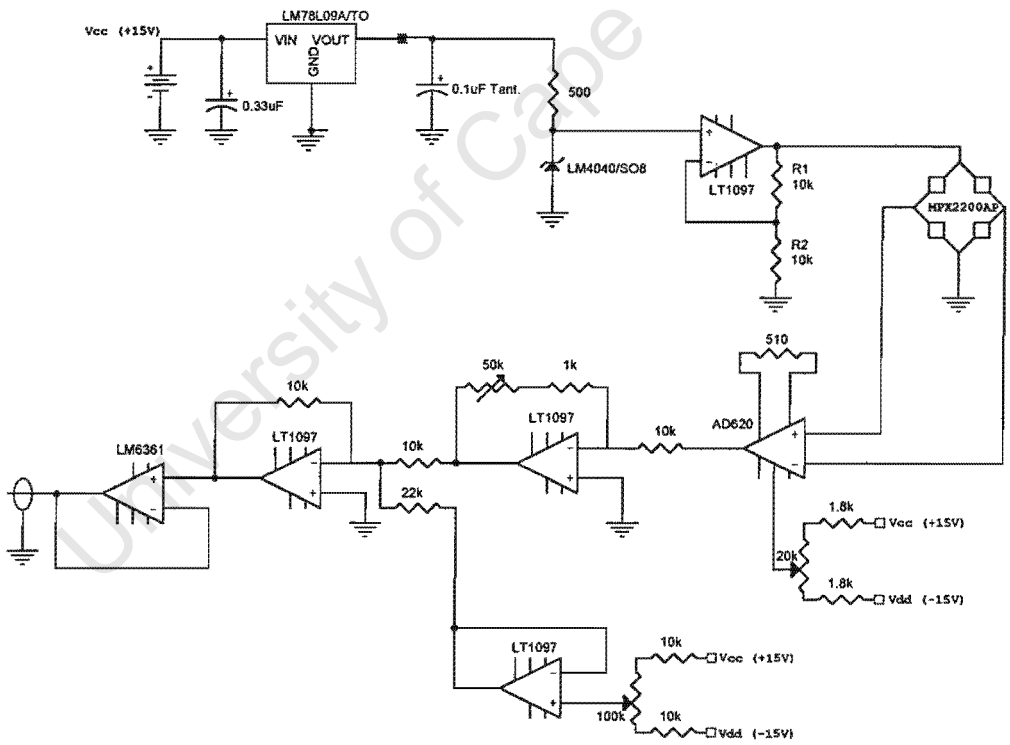

Figure B-1: A circuit diagram for signal conditioning and driving the MPX2200AP pressure sensor. A double voltage regulator circuit is used to reduce voltage ripple and noise. The first regulator is a standard LM78L09 followed by a reverse biased presision LM4040 zener diode regulater. Together these circuits produce a highly stable 10 volt DC supply to the strain gauge bridge of the MPX2200AP. Standard offset and gain opamps are used for basic signal calibration and processing.

B.2 Valve Control Circuit and Power Supply

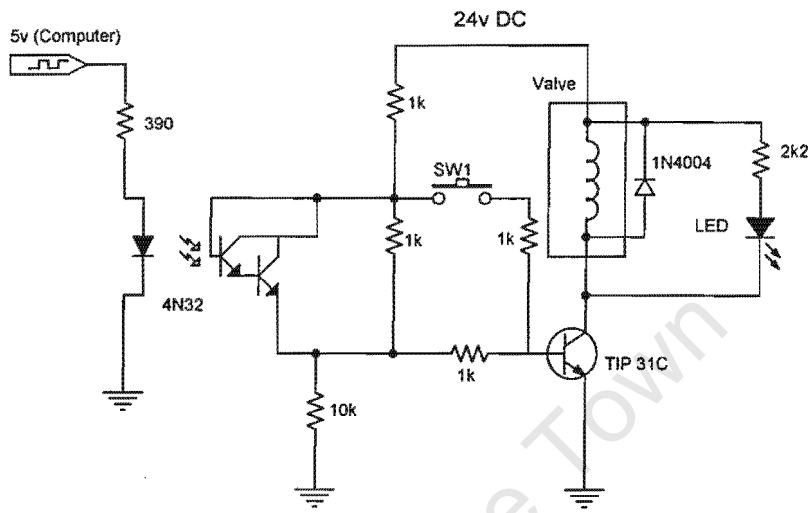

Figure B-2: This is a simple electric-valve driving circuit. An opto-isolator (4N32) is used to seperate the computer output voltage (5v) from the solenoid driving voltage (24v DC). An LED is included as a visual indicator for when the valve is opened. The push-button (SW1) is used as a manual overide to force the valve open.

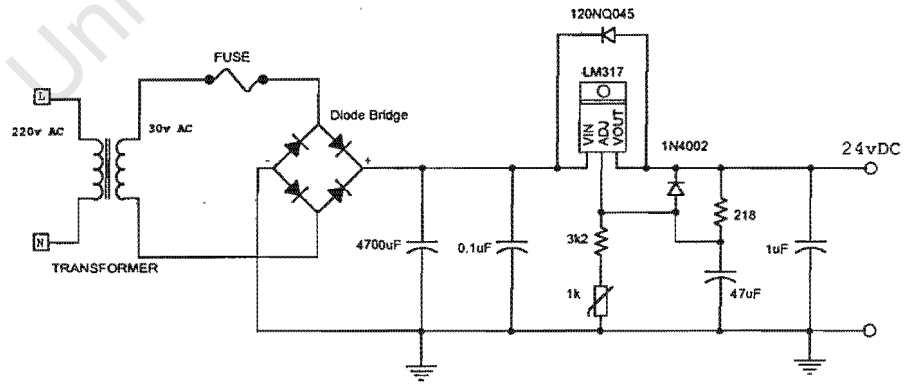

Figure B-3: A standard 24V DC power supply circuit is used to drive the electric-valve pair.

B.3 Automatic Gain Control Circuit

The AGC circuit shown below (Fig. B-4) uses the VCA610 as a variable gain opamp, driving the voltage reference pin from a negative feedback circuit. The time constant, defined by the integrator capacitance and resistance determines the closed loop bandwidth for the AGC loop. As this circuit is used as a control feature inside the TPL loop, it is important to design the time constant to be an order of magnitude faster than the loop it is controlling. If this is not done, the bandwidth characteristics of the AGC loop constrict the bandwidth of the TPL loop, resulting in nonlinear cycle slipping effects.

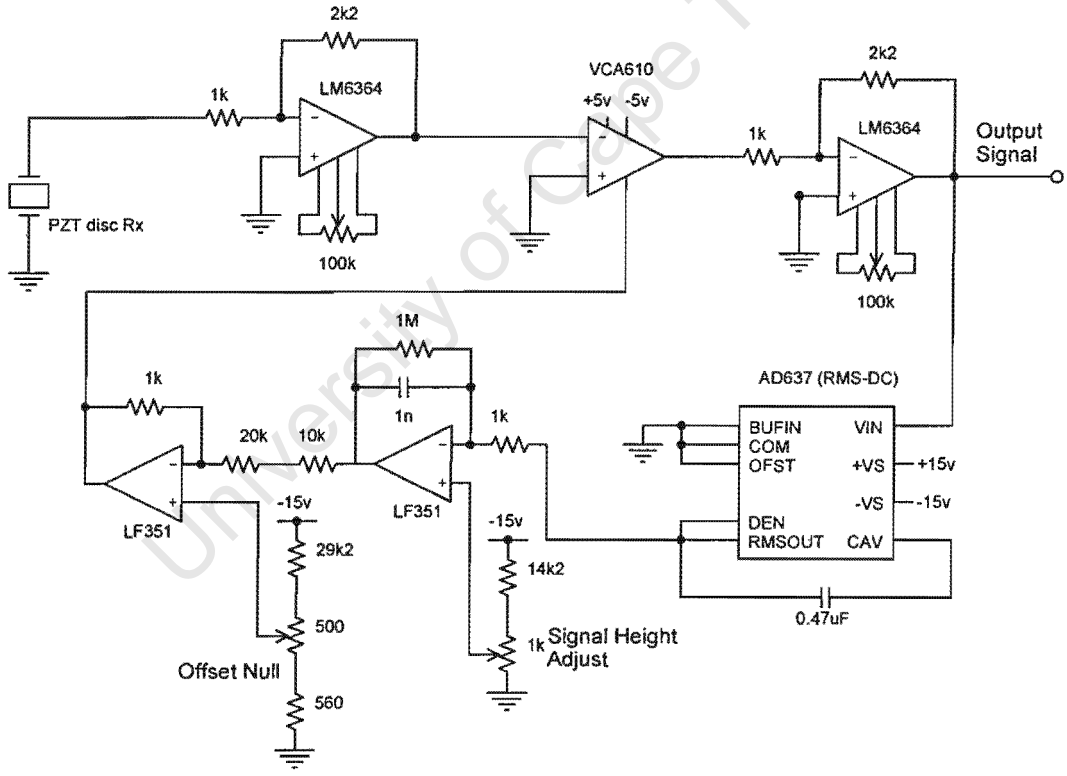

Figure B-4: A circuit diagram using the VCA610 as an automatic gain controller. The RMS value of the input signal is measured by an RMS to DC converter(AD637) and used in feedback to adjust the gain of the VCA610. Signal offsets and amplitude adjustments are made through two potentiometers in the feedback path.

B.4 Digital Transmission Phase Locked Loop

Digital transmission phase locking works in much the same way as its analogue counterpart. Phase is measured between the driving and receiving transducers and compared using a digital phase detector. The output from the phase detector is then filtered and used as a negative feedback source to drive the VCO.

The fundamental difference from the analogue loop is that both measured signals are sinusoidal and need to be first converted to a square wave before phase can be measured. This requires a zero crossing detector in the form of a comparator. Weak signals resulting from antinodes in the interferometer cavity have low SNR and often hinder digital conversion adding signal jitter and phase offsets in the process. However, once the signal conversion is accomplished, phase detection is elementary, with a variety of phase detectors present on a single chip (74HC4046). Loop filter values are calculated in the same way as TPL (see Chapter 5).

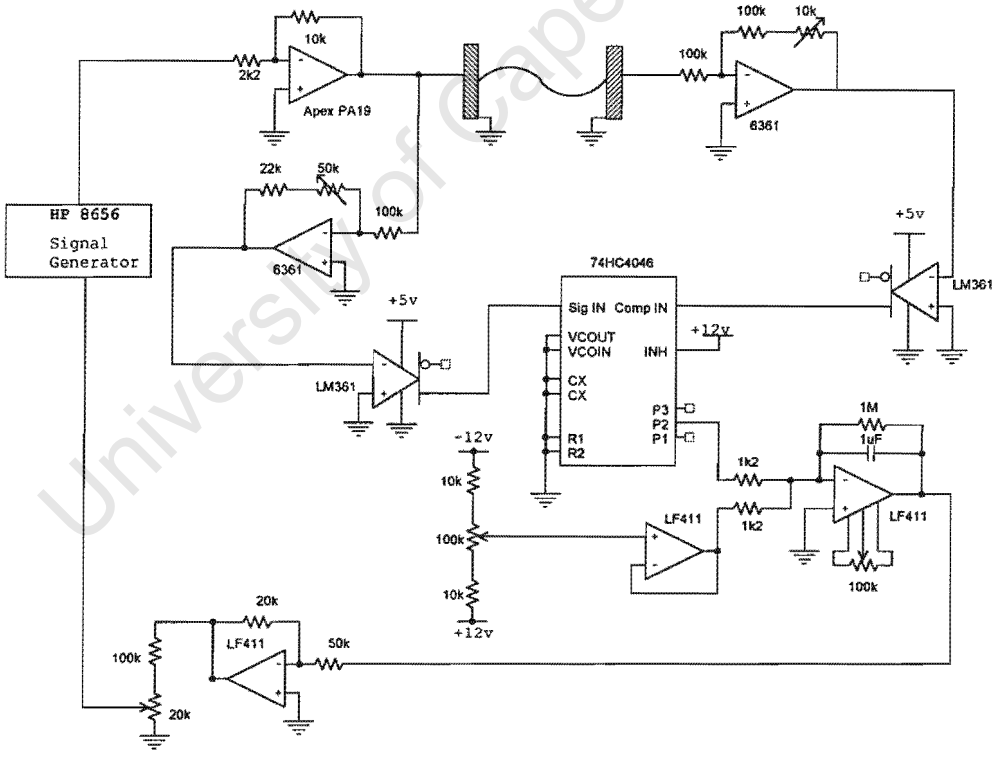

Figure B-5: The above circuit is a typical DTPL loop, without the AGC. Square wave conversion is achieved using a high speed comparator (LM361) and phase is detected using the 74HC4046. Offsets and integrator values are calculted as per usual. It should be noted that low pass filters were often required in the received path and were duplicated in the transmit path for phase subtraction, however B/A measurements are compromised to some degree by this action.

B.5 Temperature Controller

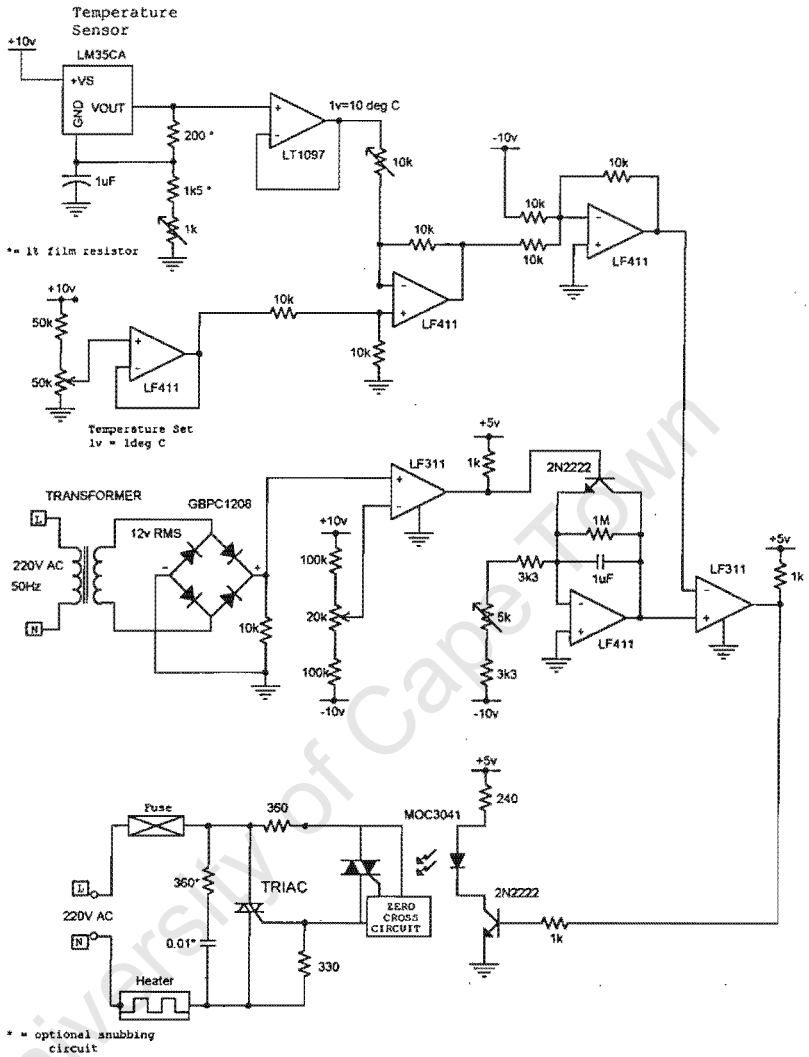

Figure B-6: The temperature control circuit, drawn above, uses pulse width modulation in a temperature feedback loop ensuring the measured and setpoint temperatures are always the same. To do this, pulses are formed by comparing the temperature difference with a ramp waveform, generated from a 50Hz main supply. The pulses are used to modulate the main supply by firing a diac-triac circuit. An optional snubber circuit is included as a means of reducing harmonics from the triac.

Appendix C

ABAQUS Journals and Results

C.1 Abaqus Parametric Input Deck for a PZT Tube Filled with Water.

```
*heading
    Axis symmetric PZT cylinder, filled with water
    od 37.95mm id 31.45mm height 37.5mm
    material PZT 4 - poling radial
    Charge excitation - 7nC
    *preprint, model=no, echo=no, history=no, parsubstitution=yes, parvalues=yes
    **_____
    **parameter definitions
    **_____
    *parameter
    #_____#
    #piezo 'physical' parameters i.e. dimensions in meters!
    #_____#
    pzt_ro = 0.03795/2
    pzt_ri = 0.03145/2
    pzt_ht = 0.0375
    #_____#
    # H2O mesh details
    #
```

```
# h20_elmt1 >> number of elements in radial direction
# h20_elmt2 >> number of elements in vertical direction
#-----------------------------------#
h2o_elmt1 = 16
h2o_elmt2 = 38
elset_h2o = 'water'
nset_h2o_freesurface = 'h2o_free'
#-----------------------------------#
# interface mesh details
#-----------------------------------#
elset_intf= 'interface'
#-----------------------------------#
# piezo mesh details
#
# pzt_elmt1 >> number of element through radial thickness of piezo
#-----------------------------------#
pzt_elmt1 = 3
elset_pzt = 'piezo'
nset_electrode_neg = 'neg'
nset_electrode_pos = 'pos'
node_num_ref_pos = 1000000
nset_ref_pos = 'ns_ref'
#-----------------------------------#
# vertical springs > to simulate epoxy bonding to perspex
#-----------------------------------#
elmt_num_sprg = 1000000
sprg_elmt_stiff= 1.
elset_sprg = 'sprg_dof2'
#-----------------------------------#
# eigenanalysis frequency extraction
#-----------------------------------#
num_eigenvalues = 5
max_frequency_Hz= 750.e3
```

```
shift_point_sqHz= (700.e3)**2
#-----------------------------------#
# steady state frequency harmonic analysis
#-----------------------------------#
start_freq = 500.e3
end_freq = 800.e3
freq_resolution = 10000.
excitation_charge = 7e-9
divisions = int((end_freq-start_freq)/freq_resolution)
#*****************************************#
# Parametric Calculations
#*****************************************#
# h2o mesh details
#-----------------------------------#
node_num_h2o1 = 2*(h2o_elmt1)+1
# h2o + piezo nodes defined!
node_num_pzt1 = (2*pzt_elmt1)+node_num_h2o1
offset_nnum2 = node_num_pzt1+10
offset_nnum2_x2 = 2*offset_nnum2
divisions_h2o2 = 2*(h2o_elmt2)
offset_nnum2_total = offset_nnum2*divisions_h2o2
# master h2o element, node numbering
h2o_node1=1
h2o_node2=3
h2o_node3=offset_nnum2_x2+3
h2o_node4=offset_nnum2_x2+1
h2o_node5=2
h2o_node6=offset_nnum2+3
h2o_node7=offset_nnum2_x2+2
h2o_node8=offset_nnum2+1
# water free surface
node_num_h2o_free1=1+offset_nnum2_total
node_num_h2o_free2=node_num_h2o1+offset_nnum2_total
```

```
#-------------------------------#
# interface mesh details
#-------------------------------#
elmt_num_intf = h2o_elmt1+1
# master interface element, node numbering
intf_node1=node_num_h2o1
intf_node2=node_num_h2o1+offset_nnum2
intf_node3=node_num_h2o1+offset_nnum2_x2
#-------------------------------#
# piezo mesh details
#-------------------------------#
elmt_num_pzt = h2o_elmt1+2
# master piezo element, node numbering
pzt_node1=node_num_h2o1
pzt_node2=node_num_h2o1+2
pzt_node3=node_num_h2o1+offset_nnum2_x2+2
pzt_node4=node_num_h2o1+offset_nnum2_x2
pzt_node5=node_num_h2o1+1
pzt_node6=node_num_h2o1+offset_nnum2+2
pzt_node7=node_num_h2o1+offset_nnum2_x2+1
pzt_node8=node_num_h2o1+offset_nnum2
# electrode node number
neg2 = node_num_h2o1+offset_nnum2_total
pos2 = node_num_pzt1+offset_nnum2_total
#-------------------------------#
# spring mesh details
#-------------------------------#
sprg_elmt_total= 2*pzt_elmt1+1
# end!
#**-----------------------------
#** node generation
#**-----------------------------
*node, nset=bot_h2o
```

1, 0., 0., 0.

<node_num_h2o1>, <pzt_ri>, 0., 0.

*ngen, nset=bot_h2o

1, <node_num_h2o1>, 1

** piezo definition

*node, nset=bot_pzt

<node_num_pzt1>, <pzt_ro>, 0., 0.

*ngen, nset=bot_pzt

<node_num_h2o1>, <node_num_pzt1>, 1

** define bottom edge node set

*nset, nset=bot

bot_h2o, bot_pzt

** copy bottom edge node set to make top edge

*ncopy, shift, old set=bot, new set=top, multiple=1, change number=<offset_nnum2_total>

0., <pzt_ht>, 0.

0., 0., 0., 0., 0., 1.0, 0.0

** fill between edges

*nfill, nset=face1

bot, top, <divisions_h2o2>, <offset_nnum2>

**_____

** water element & material definitions, dof=8

**_____

*element, type=acax8, elset=<elset_h2o>

1, <h2o_node1>,<h2o_node2>,<h2o_node3>,<h2o_node4>,

<h2o_node5>,<h2o_node6>,<h2o_node7>,<h2o_node8>

*elgen, elset=<elset_h2o>

1, <h2o_elmt1>,2,1, <h2o_elmt2>,<offset_nnum2_x2>,<offset_nnum2>

*solid section,elset=<elset_h2o>, material=water

*material, name=water

*acoustic medium, bulk modulus

2.18e9

*density

1000.

** definitions of node sets 4 water free surface

*nset, nset=<nset_h2o_freesurface>, generate

<node_num_h2o_free1>,<node_num_h2o_free2>,1

**_____

** interface element & material definitions

**_____

*element, type=asi3a, elset=<elset_intf>

<elmt_num_intf>, <intf_node1>,<intf_node2>,<intf_node3>

*elgen, elset=<elset_intf>

<elmt_num_intf>, <h2o_elmt2>,<offset_nnum2_x2>,<offset_nnum2>

*interface, elset=<elset_intf>

**_____

** piezo element & material definitions

**_____

*element, type=cax8e, elset=<elset_pzt>

<elmt_num_pzt>, <pzt_node1>,<pzt_node2>,<pzt_node3>,<pzt_node4>,

<pzt_node5>,<pzt_node6>,<pzt_node7>,<pzt_node8>

*elgen, elset=<elset_pzt>

<elmt_num_pzt>, <pzt_elmt1>,2,1, <h2o_elmt2>,<offset_nnum2_x2>,<offset_nnum2>

*solid section,elset=<elset_pzt>, material=pzt4_p1

*material, name=pzt4_p1

*elastic, type=ortho

13.90e10,7.428e10,11.54e10,7.784e10,7.428e10,13.90e10,2.564e10,2.564e10,

2.564e10

*piezoelectric, type=s

15.08,-5.207,-5.207,0.,0.,0.,0.,0.

0.,12.710,0.,0.,0.,0.,0.,0.,

12.710,0.

*dielectric, type=aniso

5.872e-9,0.,6.752e-9,0.,0.,6.752e-9

*density

7550.

** definitions of node sets 4 electrodes

*nset, nset=<nset_electrode_neg>, generate

<node_num_h2o1>,<neg2>,<offset_nnum2>

*nset, nset=<nset_electrode_pos>, generate

<node_num_pzt1>,<pos2>,<offset_nnum2>

** tie pos+ electrode to common node <node_num_ref_pos>

*node, nset=<nset_ref_pos>

<node_num_ref_pos>, 0.025,0.019,0.

*equation

2

<nset_electrode_pos>,9,1.0, <node_num_ref_pos>,9,-1.0

**_____

** vertical (dof2) spring support elements on lower piezo edge & material definitions

**_____

*element, type=spring1, elset=<elset_sprg>

<elmt_num_sprg>, <node_num_h2o1>

*spring, elset=<elset_sprg>

2

<sprg_elmt_stiff>

**_____

** step

**_____

*step,perturbation

harmonic frequency analysis

*steady state dynamic, direct

<start_freq>,<end_freq>,<divisions>,1,1

*boundary, op=new

<nset_electrode_neg>, 9,,

<nset_h2o_freesurface>, 8,,

*cecharge

<node_num_ref_pos>, , <excitation_charge>

*restart, write, f=0

*monitor, node=<node_num_ref_pos>, dof=9

*node file, f=1, nset=<nset_ref_pos>

RCHG, PHCHG, EPOT, PHPOT

*node file, f=1, nset=<nset_electrode_neg>

POR,PPOR

*el print, f=0

*node print,f=0

*end step

C.2 Thermal Analysis - PZT Tube Acoustic Resonator

C.2.1 Axisymmetric Input Deck - Sine Oscillating Thermal Boundary

*heading

Thermal Analysis of PZT container

*preprint, echo=no, model=yes, history=yes

*node

1,0.0,0.0

83,0.041,0.0

132001,0.0,0.066

132083,0.041,0.066

132139,0.069,0.066

112139,0.069,0.056

*ngen,nset=n_bot

1,83,1

*ngen,nset=n_top

132001,132083,1

*ngen,nset=out_lip

112139,132139,1000

*nfill,nset=n_block

n_bot,n_top,132,1000

*nset,nset=in_lip,generate

112083,132083,1000

*nfill,nset=n_lip

in_lip,out_lip,56,1

*nset,nset=ns_all

```
n_lip,n_block
*nset,nset=out_wall,generate
83,112083,1000
*nset,nset=bot_lip,generate
112083,112139,1
*nset,nset=ns_edge
n_bot,out_wall,bot_lip,out_lip
**_____
*element,type=dcax8
1,1,3,2003,2001,2,1003,2002,1001
2501,50001,50003,52003,52001,50002,51003,52002,51001
2517,50033,50035,52035,52033,50034,51035,52034,51033
2520,50039,50041,52041,52039,50040,51041,52040,51039
2522,50043,50045,52045,52043,50044,51045,52044,51043
5642,112083,112085,114085,114083,112084,113085,114084,113083
6301,126001,126003,128003,128001,126002,127003,128002,127001
*elgen,elset=br_bot
1,41,2,1,25,2000,100
*elgen,elset=br_wall
2522,20,2,1,41,2000,100
*elgen,elset=br_lip
5642,28,2,1,10,2000,100
*elset,elset=e_brass
br_bot,br_wall,br_lip
*elgen,elset=e_h2o
2501,16,2,1,38,2000,100
*elgen,elset=e_pzt
2517,3,2,1,38,2000,100
*elgen,elset=he_wall
2520,2,2,1,41,2000,100
*elgen,elset=he_top
6301,19,2,1,3,2000,100
*elset,elset=e_helium
```

```
he_top,he_wall
*elset,elset=e_all
e_helium,e_brass,e_pzt,e_h2o
**_____
*solid section,elset=e_pzt,material=pzt
*material,name=pzt
*density
5450.0
*specific heat
420.0
*conductivity,type=iso
2.1
** min. time step > (5450*420)/(6*2.1)*(1.0e-3)^2
** min. time step > 181.67millisec
**_____
*solid section,elset=e_brass,material=brass
*material,name=brass
*density
8522.0
*specific heat
385.0
*conductivity,type=iso
111.0
** min. time step > (8522*385)/(6*111)*(1.0e-3)^2
** min. time step > 4.92millisec
**_____
*solid section,elset=e_h2o,material=water
*material,name=water
*density
994.9
*specific heat
4174.0
*conductivity,type=iso
```

```
0.623
** min. time step > (994.90*4174)/(6*0.623)*(1.0e-3)^2
** min. time step > 1.11sec
**_____
*solid section,elset=e_helium,material=helium
*material,name=helium
*density
0.1328
*specific heat
5200.
*conductivity,type=iso
0.14
** min. time step > (0.1328*5200)/(6*0.14)*(1.0e-3)^2
** min. time step > 82.21millisec
**_____
*initial conditions, type=temperature
ns_all,30.0
**_____
*amplitude,name=sine,definition=periodic, value=absolute
1, 0.6283, 0.0, 30.
0.1, 0.0
**_____
*step, inc=5000
*heat transfer,end=period
1.0,40,1.0e-06,500, ,
*boundary,amplitude=sine
ns_edge,11,11,
*restart,write,f=1
*monitor, dof=11, node=132001
*node file,f=1,nset=ns_all
*el print,f=0
*node print,f=0
*end step
```

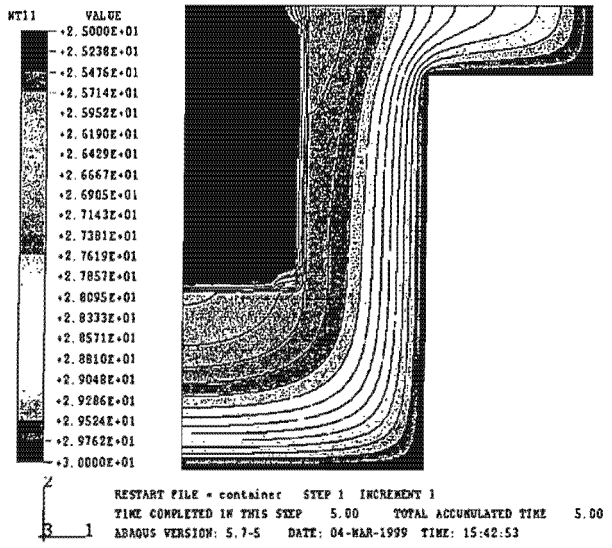

(a) Time = 5 seconds

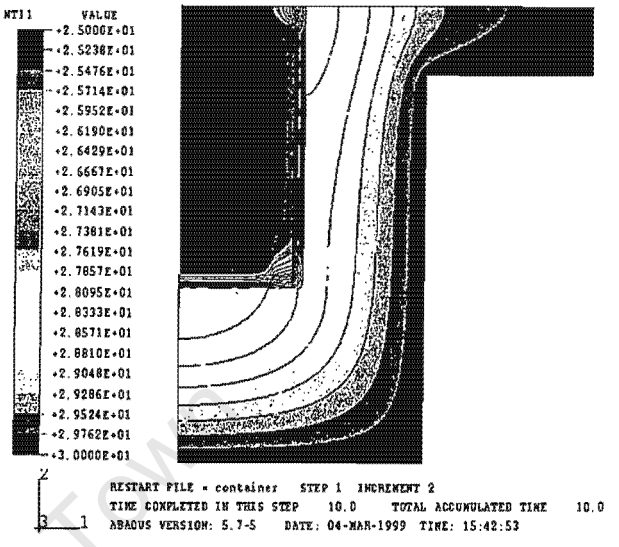

(b) Time = 10 seconds

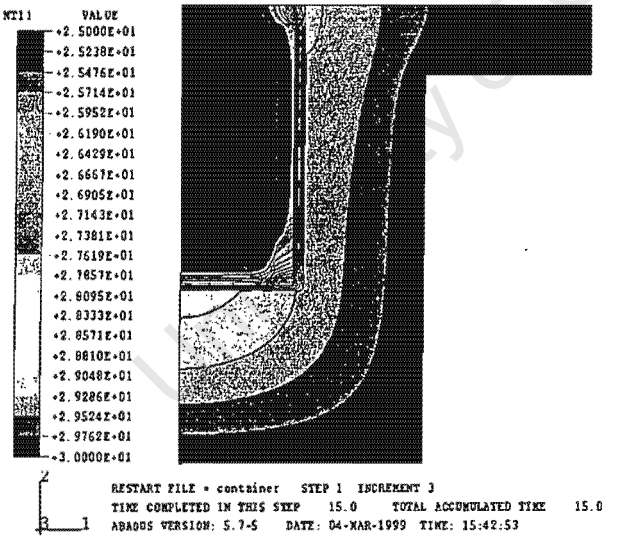

(c) Time = 15 seconds

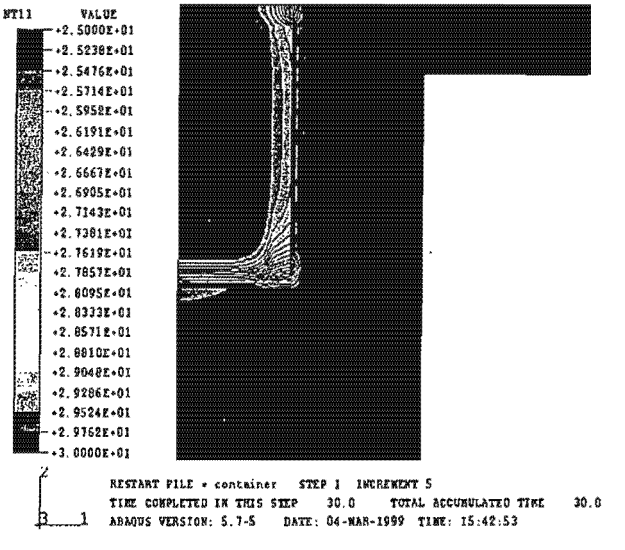

(d) Time = 30 seconds

Figure C-1: A time sequence capturing the thermal contours in an axisymmetric brass jacket. The time is stepped in increments of 5 seconds. Note that after 30 seconds the brass reaches a constant temperature thus defining the thermal time constant and low pass filter characteristics of the jacket.

Appendix D

Calibration and Measured Results

D.1 MPX 2200 Calibration Curve

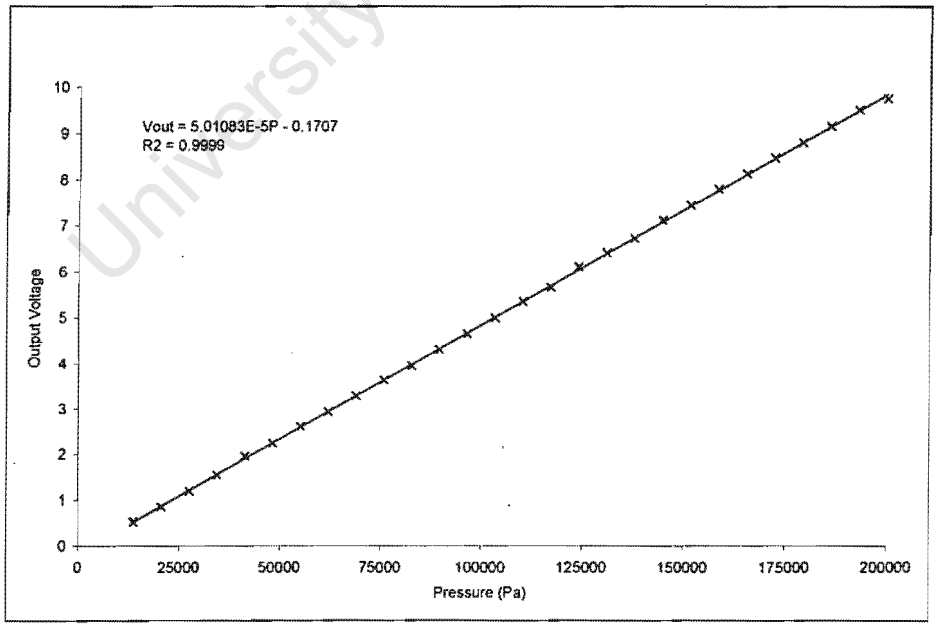

Figure D-1: Calibration curve for the MPX2200AP pressure transducer.

D.2 A Review of Measured B/A Results

Liquid	Temp (°C)	B/A	Referance
Distilled Water	20	5.0	Beyer[13]
	25	5.11	Zhu [112]
	30	5.31	Law[71]
	30	5.13	Davies[29]
D_2O	30	5.01	Zhang[111]
Methanol	20	9.61	Coppens [25]
	30	9.64	Coppens
		8.6	Banchet[6]
Ethanol	20	10.52	Coppens
	30	10.57	Coppens
FC43	20	12.85	Madigosky [73]
	30	13.19	Davies
FC75	20	12.19	Madigosky
	30	12.83	Davies
CCl_4	25	8.7	Beyer
	25	7.85	Zhu
Benzene	20	9.0	Beyer
	25	6.5	
(4% H_2O)	25	8.58	Zhu et al, 1983
		8.84	Sehgal et al, 1984
	30	9.0	Beyer, 1974
		9.4	Law et al, 1985
		9.08	Sehgal et al, 1984
Nitro benzene	30	9.9	Beyer, 1974
Toluene	20	5.6	Beyer, 1960
	25	7.9	Beyer, 1960
	30	8.929	Kor et al[65]
Chlorobenzene	30	9.33	Coppens et al, 1966
n-Propanol	20	10.69	Coppens et al, 1966
	30	10.71	Coppens et al, 1966
n-Butanol	20	10.69	Coppens et al, 1966
	30	10.72	Coppens et al, 1966
Benzyl Alcohol	30	10.19	Coppens et al, 1966
Ethylene Glycol	25	9.88	Zhu
	26	9.6	Gong et al[44]
	30	9.93	Law et al, 1985
	30	9.7	Beyer, 1974

Continued on next page ...

Liquid	Temp (°C)	B/A	Referance
Diethylamine	30	10.3	Coppens et al, 1966
Ethyl Formate	30	9.8	Beyer, 1974
Heptane	30	10.0	Beyer, 1974
Hexane	25	9.81	Zhu et al
	30	9.9	Beyer, 1974
Cyclohexane	30	10.1	Beyer, 1974
Chloroform	25	8.2	Beyer, 1960
Methyl Acetate	30	9.7	Beyer, 1974
Glycerol	20	8.77	Sehgal et al, 1984
(4% H_2O)	25	8.58	Zhu et al, 1983
	25	8.84	Sehgal et al, 1984
	30	9.0	Beyer, 1974
	30	9.4	Law et al, 1985
	30	9.08	Sehgal et al, 1984
Carbon Bisulfide	25	6.2	Beyer, 1960 [11]
Acetone	20	9.23	
Nitro benzene	30	9.9	Beyer, 1974
Toluene	20	5.6	Beyer, 1960
	25	7.9	Beyer, 1960
	30	8.929	Kor et al[65]
Ethylene Glycol	26	9.6	Gong et al

Table D.1: A consolodation of measured B/A values for one-component liquids